
Monitoring Homology Search during DNA Double-Strand Break Repair *in vivo*

DISSERTATION DER FAKULTÄT FÜR BIOLOGIE
DER LUDWIG-MAXIMILIANS-UNIVERSITÄT MÜNCHEN



vorgelegt von
Jörg Renkawitz, M.Sc. Biochemie

Juni 2013

EIDESSTATTLICHE ERKLÄRUNG

Hiermit erkläre ich an Eides statt, dass ich die vorliegende Dissertation selbstständig und ohne unerlaubte Hilfe angefertigt habe. Ich habe weder anderweitig versucht, eine Dissertation einzureichen oder eine Doktorprüfung durchzuführen, noch habe ich diese Dissertation oder Teile derselben einer anderen Prüfungskommission vorgelegt.

München, den.....

.....

(Unterschrift)

Promotionsgesuch eingereicht am: 27.06.2013

Datum der mündlichen Prüfung: 12.09.2013

Erster Gutachter: Prof. Dr. Stefan Jentsch

Zweiter Gutachter: Prof. Dr. Peter Becker

Die vorliegende Arbeit wurde zwischen Dezember 2008 und Juni 2013 unter der Anleitung von Prof. Dr. Stefan Jentsch am Max-Planck-Institut für Biochemie in Martinsried durchgeführt.

Wesentliche Teile dieser Arbeit sind in den folgenden Publikationen veröffentlicht und zusammengefasst:

Renkawitz, J., Lademann, C.A., Kalocsay, M., and Jentsch, S. Monitoring homology search during DNA double-strand break repair in vivo. *Mol. Cell* **50**, 261-272, 2013

Renkawitz, J., Lademann, C.A., and Jentsch, S. γ H2AX spreading linked to homology search. *Cell Cycle*. Editorial feature, in press.

Renkawitz, J., Lademann, C.A., and Jentsch, S. Mechanisms and principles of homology search during recombination. *Nat. Rev. Mol. Cell Biol.* Commissioned review in preparation.

Table of Contents

1 SUMMARY	3
2 INTRODUCTION.....	4
2.1 HOMOLOGOUS RECOMBINATION	5
2.2 <i>SACCHAROMYCES CEREVISIAE</i> REPRESENTS A MODEL ORGANISM TO STUDY HOMOLOGOUS RECOMBINATION	7
2.3 THE RECOMBINASE RAD51	10
2.4 REGULATION OF HOMOLOGOUS RECOMBINATION	12
2.5 HOMOLOGY SEARCH	15
3 AIMS OF THIS STUDY.....	19
4 RESULTS	20
4.1 HOMOLOGY SEARCH CAN BE MONITORED <i>IN VIVO</i> BY RAD51 CHIP.....	20
4.1.1 <i>Broad Distribution of Rad51 ChIP Signals upon a Single DSB.....</i>	20
4.1.2 <i>DSB-distant Rad51 ChIP Signals are Specific.....</i>	23
4.1.3 <i>DSB-distant Rad51 ChIP Signals Depend on Rad52 and Rad55/Rad57 ..</i>	25
4.1.4 <i>DSB-distant Rad51 ChIP Signals are a General Phenomenon upon Single DSBs in Saccharomyces Cerevisiae.....</i>	26
4.1.5 <i>DSB-distant Rad51 ChIP Signals Exceed the Area of Resection.....</i>	28
4.1.6 <i>DSB-distant Rad51 ChIP Signals are Indicative of Recombination Competence</i>	32
4.1.7 <i>DSB-distant Rad51 ChIP Signals are Traceable during Active Repair..</i>	36
4.1.8 <i>DSB-distant Rad51 ChIP Signals Depend on a DNA-Binding Site of Rad51.....</i>	39
4.2 NUCLEAR ORGANIZATION INFLUENCES HOMOLOGY SEARCH.....	41
4.2.1 <i>The RE element can Guide Homology Search in trans</i>	41
4.2.2 <i>Centromeres can Guide Homology Search in trans.....</i>	45
4.2.3 <i>Homology Search upon Single DSBs in Proximity of Different Nuclear Landmarks.....</i>	49
4.3 COMPONENTS AND REQUIREMENTS OF HOMOLOGY SEARCH	53
4.3.1 <i>Role of the Single-Strand Binding Protein RPA during Homology Search.</i>	53
4.3.2 <i>Efficient Homology Search Requires Rad54.....</i>	56
4.3.3 <i>Phosphorylation of Histone 2A Follows Homology Search.....</i>	58
5 DISCUSSION.....	64
5.1 MONITORING HOMOLOGY SEARCH <i>IN VIVO</i>	64
5.2 CONFLICTING MODELS FOR HOMOLOGY SEARCH	66
5.3 HOMOLOGY SEARCH IS INFLUENCED BY THE NUCLEAR ORGANIZATION.....	68
5.4 REVISITING EARLIER DATA IN VIEW OF HOMOLOGY SEARCH BEING INFLUENCED BY NUCLEAR ORGANIZATION	72
5.5 FACILITATED 3D/1D HOMOLOGY SEARCH MODEL	74
6 MATERIALS AND METHODS	78
6.1 MICROBIOLOGY	78
6.1.1 <i>Escherichia Coli Techniques.....</i>	78
6.1.2 <i>Saccharomyces Cerevisiae Techniques.....</i>	79
6.2 MOLECULAR BIOLOGICAL TECHNIQUES	84
6.2.1 <i>Polymerase Chain Reaction (PCR).....</i>	84
6.2.2 <i>Molecular Cloning</i>	86

6.3	BIOCHEMISTRY AND CELL BIOLOGY TECHNIQUES	87
6.3.1	<i>Protein Methods</i>	87
6.3.2	<i>Induction of Single DSBs in vivo</i>	89
6.3.3	<i>Chromatin-Immunoprecipitations (ChIP)</i>	89
6.3.4	<i>ChIP-on-chip Analysis</i>	92
6.4	COMPUTER-AIDED ANALYSIS	93
6.5	STATISTICAL ANALYSIS	93
7	REFERENCES	94
8	ABBREVIATIONS	103
9	FIGURE INDEX	104
10	ACKNOWLEDGEMENTS	106
11	CURRICULUM VITAE	107

1 Summary

Homologous recombination (HR) is essential for the repair of DNA double-strand breaks (DSB) and thus pivotal for genome integrity. HR relies on the usage of an intact homologous donor sequence to repair the DSB and has been extensively investigated for decades. Nevertheless, how homology search – the crucial exploration of the genome for the intact homologous donor sequence – functions in the context of the crowded nuclear environment remained largely enigmatic.

This study visualizes homology search for the first time *in vivo*, using chromatin immunoprecipitation (ChIP) of the recombinase Rad51 in *S. cerevisiae*. Rad51 forms a nucleoprotein filament at the DSB, which assists in the recognition of the homologous donor sequence during homology search. Due to a high ChIP efficiency and genome-wide analysis by tiling arrays (ChIP-chip) Rad51 could not only be detected in the nucleoprotein filament at the DSB, but also at very DSB-distant locations. We demonstrate by several lines of evidence that these DSB-distant Rad51 signals reflect homology search. By taking advantage of this approach, we show that homology search preferentially probes on the broken chromosome with an increasing efficiency toward the DSB. Moreover, homology search is influenced by the nuclear organization. This became apparent by the finding that homology search can be efficiently guided to a far-distant chromosomal location by an intrachromosomal loop in the yeast mating-type system, and by the observation that homology search can be efficiently guided to all centromeres upon a centromere-proximal DSB. In addition, by investigating the molecular requirements of homology search, we discovered a homology search-promoting role of the translocase Rad54 and found that the histone phosphorylation γ H2A follows homology search.

In summary, this study describes for the first time an approach to monitor homology search *in vivo*, and reveals that homology search is influenced by chromosomal architecture and nuclear organization.

2 Introduction

Cells are constantly challenged by DNA damage, either due to endogenous cellular processes such as replication¹ or transcription², or exogenous incidents such as radiation or exposure to mutagenic chemicals³. In order to preserve the genetically inherited information, cells developed elaborated mechanisms to repair the DNA damage. Prominent types of DNA damages include base substitutions, interstrand cross-links, micro-insertions or -deletions and DNA double-strand breaks (DSBs)⁴. DSBs are considered to be one of the most toxic types of DNA damage as their inaccurate repair can lead to mutations and chromosomal rearrangements⁴, and hence potentially to cancer⁵ and aging⁶. On the other hand, directed DSBs and their controlled repair provide the basis for physiological processes like meiosis⁷ and immunoglobulin rearrangements⁸.

Two major pathways repair DSBs, namely nonhomologous end joining (NHEJ) and homologous recombination (HR)⁹. Which of the two pathways is used, depends mainly on the cell-cycle phase, the structure of the broken DNA ends, and proteins binding to the broken DNA ends^{9,10}. NHEJ occurs preferentially in the G1 cell-cycle phase and is based on ligation of the broken DNA ends¹¹. Notably, NHEJ can result in mutagenic deletions or insertions¹². In contrast, HR relies on an intact homologous donor sequence to repair the DSB¹³ and is thus generally considered to be error-free, despite also being slightly mutagenic^{14,15}.

2.1 Homologous Recombination

Homologous recombination (HR) has been intensively studied for decades and numerous components of its mechanism have been elucidated and implicated in diseases such as cancer⁴. Initially, a DSB is recognized and bound by the MRX complex (MRN complex in higher eukaryotes^{*}), which subsequently serves as a recruitment platform for other proteins and initiates 5'-3' resection together with Sae2¹⁶ (Figure 1). The initial short-range resection turns into sustained long-range resection by a set of different factors, including the nucleases Exo1 and Dna2, the helicase Sgs1¹⁷⁻¹⁹, and chromatin remodeling enzymes mediating accessibility to chromatinized DNA²⁰ (Figure 1).

Sustained 5'-3' resection results in long tracks of single-stranded DNA (ssDNA), which are directly bound by the ssDNA-binding protein RPA (replication protein A), a heterotrimeric protein complex that eliminates secondary ssDNA structures²¹. Subsequently, RPA is replaced – at least partially²² - by the recombinase Rad51 (Figure 1). Rad51 forms dynamic nucleoprotein filaments on ssDNA and is regulated by a multitude of Rad51 mediators. Once the Rad51 nucleoprotein filament is formed, it is thought to perform the search for homologous donor sequences to enable error-free repair of the DSB-bearing sequence^{13,23,24}. In the majority of cases, the homologous donor sequence used for repair is located on the sister chromatid, making HR the favored pathway during the G2 cell cycle phase²⁵. Nevertheless, HR can also use non-allelic homologous donor sequences on the same or other chromosomes (ectopic recombination)²³. Once the intact homologous donor sequence has been found and recognized by DNA base-pairing, a joint-molecule between the intact and the DSB-bearing homologous sequence is formed by the establishment of a D-loop (displaced strand) structure (Figure 1).

* As *S. cerevisiae* has been extensively used to study DSB repair, *S. cerevisiae* pathways, gene and protein names constitute the basis of this thesis for simplicity; yet, well known homologs and additional pathways are highlighted.

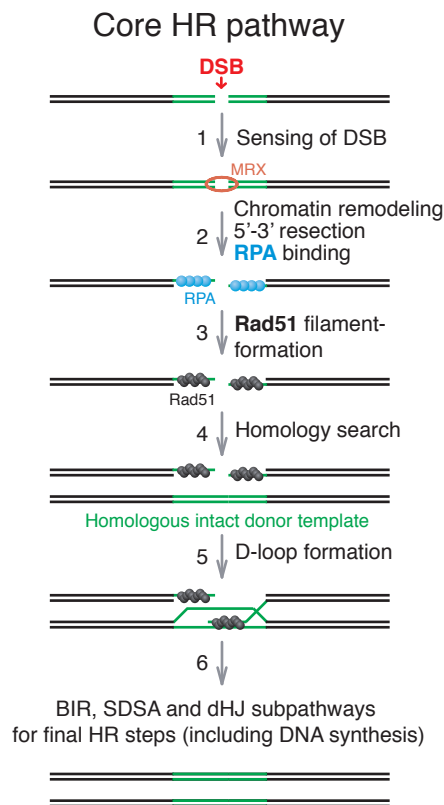


Figure 1. The core pathway of homologous recombination.

(1) The core pathway of homologous recombination (HR) starts with binding of the MRX complex to the DNA double-strand break (DSB).

(2) Mre11, a subunit of the MRX complex, initiates resection, which also requires chromatin remodeling and additional factors for continuous resection. The emerging single-stranded DNA (ssDNA) is rapidly coated by the single-strand binding protein RPA.

(3) RPA is subsequently replaced by the recombinase Rad51, which forms a filament on ssDNA.

(4) Then, the DSB has to get into direct spatial proximity of the intact homologous donor sequence, a process called homology search.

(5) If the DSB and the intact homologous donor sequence are in direct spatial proximity, the Rad51 filament (on the DSB-associated ssDNA) can invade the double-stranded donor sequence, forming a displacement loop (D-loop).

(6) This initial D-loop structure represents the branching point for different HR subpathways, namely BIR (break-induced replication), SDSA (synthesis-dependent strand annealing) and dHJ (double-Holliday junction)¹³. All subpathways finally use DNA synthesis on the intact homologous donor sequence to restore the genetic information at the DSB.

Size, structure and subunit compositions of proteins are arbitrary.

From this intermediate DNA structure the three sub-pathways of HR are branching, namely “break-induced replication (BIR)”, “synthesis-dependent strand annealing (SDSA)” and “double Holliday junction (dHJ)”¹³. The initially formed D-loop structure is thought to contain only one of the two broken ends, and can represent the starting point for replication in the BIR sub-pathway²⁶. If the second broken end is also present in the D-loop structure, the SDSA sub-pathway is favored. SDSA is the main sub-pathway in somatic cells and avoids crossovers, whereas the third sub-pathway dHJ favors crossovers during meiotic recombination¹³.

All these subpathways share a common feature, namely the use of homologous donor sequences to synthesize the 3' end of the broken chromosome²⁷ catalyzed by polymerase δ , thereby restoring the genetic information (Figure 1).

2.2 *Saccharomyces Cerevisiae* Represents a Model Organism to Study Homologous Recombination

Historically, major early findings about homologous recombination were obtained using the budding yeast *S. cerevisiae* as a model organism²⁸. One of the key findings was that the programmed switching of the mating-type genes involve the specific induction of a DSB²⁹, created by the site-specific HO endonuclease³⁰. Subsequently, the gene encoding for HO endonuclease was placed under an inducible promoter, thus opening the possibility to study the formation and subsequent repair of a single specifically induced DSB³¹. *S. cerevisiae* and its mating-type (MAT) system thus became the favored model organism to study the basic functions of homologous recombination and DSB repair^{28,32,33}. Because of the numerous advantages of the MAT system, this system was also used in this thesis, and the following paragraphs introduce the mating-type system and its general and special features.

Like other fungi, *S. cerevisiae* can switch the mating-type (determined by two different *MAT* alleles (*MAT α* and *MATa*)), which physiologically happens in haploids in some cells of a colony³³. Upon switching, the cell can mate with a cell of the opposing mating-type, forming a diploid cell (*MATa/MAT α*) (Figure 2A). This diploid state is thought to enable evolutionary advantages, such as spore formation under nutritionally limiting conditions and genetic exchange during meiotic recombination³³. On the molecular level, the two mating-type defining *MAT* alleles (*MAT α* and *MATa*) contain shared and unshared sequences (Figure 2B). Shared sequences include the recognition sequence of the site-specific HO endonuclease, which initiates the programmed mating-switching by generating a DSB in *MAT*. Unshared sequences contain mating-type-defining promoters and genes, located in a region designated *Ya* (in *MAT α* cells) and *Ya* (in *MATa* cells) (Figure 2B). Mating-type specific genes encode for proteins that mainly act as transcriptional activators or repressors³³.

Notably, next to the *MAT* locus, *S. cerevisiae* contains two other mating-type related loci on the very same chromosome (chromosome III), called *HML* and *HMR* (Figure 2C). *HML* and *HMR* are located on the opposite ends of the chromosome and comprise silenced mating-type information (either for *MAT α* (*HML*) or *MATa* (*HMR*)), thereby providing homologous donor sequences to repair the HO endonuclease induced DSB in the *MAT locus* by homologous recombination.

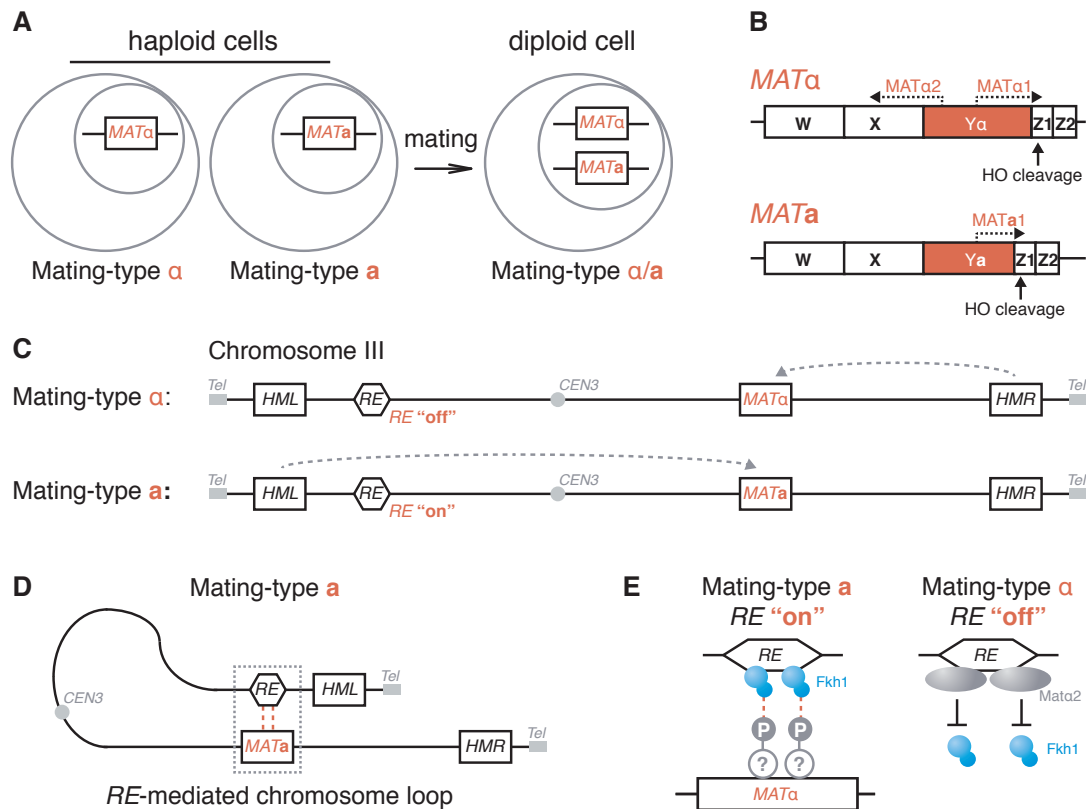


Figure 2. The *S. cerevisiae* mating-type system.

(A) Haploid *S. cerevisiae* cells harbor either a mating-type α ($MAT\alpha$) or a ($MATa$) allele, and cells of the opposing mating-type can mate to form a diploid cell ($MAT\alpha/a$). The mating-type is defined by the mating-type locus (MAT).

(B) The MAT locus consists of different elements, which are designated as W, X, Y, Z1 and Z2. Despite the Y element (red representation), all other elements are equal (white representation) in $MAT\alpha$ and $MATa$. Only the Y region differs, and contains mating-type specific promoters and partial coding sequences that define the mating-type of the cell.

(C) The MAT locus and additional elements that belong to and are essential for the mating-type system locate on chromosome III. At the opposing ends of the chromosome, HML (left chromosome arm) and HMR (right chromosome arm) are located. HML and HMR represent silenced mating-type information, either for $MAT\alpha$ (HML) or $MATa$ (HMR). Mating-type switching is achieved by selective usage (gray dashed arrows) of HML or HMR as homologous donor sequences to repair the DSB at the $MAT\alpha$ or $MATa$ locus, respectively.

(D) Selective usage of the HML donor homology in $MATa$ cells is achieved by a large chromosomal loop, mediated by the RE element. Due to the chromosomal loop, $MATa$ and HML are in spatial proximity, enabling selective and efficient repair by the HML donor template.

(E) Chromosome loop formation in $MATa$ cells depends on Fkh1. Fkh1 binds to the RE element and is proposed to interact with phosphorylated threonine residues of unknown proteins directly at the $MATa$ locus. Fkh1- RE binding – and thus chromosome loop formation – is prevented in $MAT\alpha$ cells, due to a blocking of the Fkh1 binding sites at the RE by the $MAT\alpha$ specific protein Mata2.

Size and position of DNA elements are not drawn to scale but represent approximations. Size, structure and subunit compositions of proteins are arbitrary. $CEN3$: centromere 3; DSB: DNA double-strand break; Fkh1: forkhead transcription factor 1; HO: HO endonuclease; MAT : mating-type locus, P: phosphorylated protein residue; RE : recombination enhancer, Tel: Telomere.

Importantly, the decision which of the two intact homologous donor sequences is used for repair is not chosen randomly³³ (Figure 2C): If the $MAT\alpha$ allele is cut in a $MATa$ cell, the DSB is almost always (in more than 90% of the cases) repaired by using the HMR locus (which contains the silenced mating-type information for $MATa$)³⁴. In contrast, if the $MATa$ allele is cut in a $MATa$ cell, the DSB is almost

always (in more than 90% of the cases) repaired by using the *HML* locus (which contains the silenced mating-type information for *MATa*)³⁴. Consequently, the opposing mating-type information (in comparison to the original mating-type information at the *MAT* locus) is copied into the *MAT* locus, thus enabling switching from one mating-type to the other. This so-called donor preference is an important feature of the mating-type system and has been intensively investigated³⁵⁻³⁸.

A key finding to elucidate donor-preference was the discovery of the recombination enhancer (*RE*) element^{35,36}. The *RE* element comprises only about 1 kb and is located on the left arm of the same chromosome as the mating-type system, in a distance of only 17 kb to the *HML* locus³⁶ (Figure 2C). Intriguingly, the *RE* element mediates a large chromosomal loop between the *MATa* locus and the *RE* element itself^{37,38} (Figure 2D). Consequently, the *RE* element and the *HML* locus (which is 17 kb distant to the *RE* element) are in spatial proximity to the *MATa* locus in *MATa* cells. Chromosomal looping (and not local chromatin states) leads to the preferential usage of the *HML* donor homology to repair the DSB at the *MAT* locus, as artificial chromosome loop formation phenocopies *RE* element function³⁸. Interestingly, the *RE* element can promote chromosome loop formation not only *in cis* but also *in trans*, if artificially placed on another chromosome³⁷. The active *RE* element in *MATa* cells is bound by the forkhead transcription factor 1 (Fkh1)³⁹ {Coic:2006hn}, which has been shown to regulate donor preference³⁸. Particularly, a phosphothreonine binding motif of Fkh1 is required for donor preference³⁸, possibly indicating a direct interaction of Fkh1 with phosphorylated threonine residues of proteins directly at the *MATa* locus³⁸ (Figure 2E). Notably, the *RE* element is only active in *MATa* cells, as in *MATα* cells the *RE* element is bound by the *MATα* specific MATα2-Mcm1 repressor, which prevents binding of additional proteins such as Fkh1 to the *RE* element⁴⁰ (Figure 2E). Nevertheless, how the coupling and thus chromosome loop formation between the *RE* element and the *MAT* locus is achieved in detail, remains to be investigated.

The *RE* element is well conserved in the *Saccharomyces sensu stricto* species³⁹, however, conservation in other species has so far not been demonstrated. Thus, on the one hand, the existence of two homologous donor sequences on the same chromosome as the DSB, and the existence of the *RE*-mediated donor preference represent special features of DSB repair by homologous recombination. On the other hand, these special factors open the possibility to investigate the influence of donor preference and chromosomal architecture onto DSB repair.

2.3 The Recombinase Rad51

Core reactions in homologous recombination, namely homology recognition and strand exchange, are mediated by the recombinases Rad51 (in eukaryotes) and its homolog RecA (in prokaryotes)⁴¹. Both Rad51 and RecA form highly regular right-handed filaments on ssDNA (nucleoprotein filament), which results in stretching of the underlying DNA by a factor of 1.5, and unwinding by 15 degree in respect to canonical B-DNA²⁵. ssDNA binding and filament formation depends on the first of two DNA binding sites of Rad51/RecA. The second DNA binding site allows binding to dsDNA, which is required for invasion of the intact homologous donor sequence and thus strand exchange upon D-loop formation²⁵. Importantly, ATP binding is required for filament formation, but ATP hydrolysis appears crucial for disassembly²⁵. Notably, Rad51/RecA filaments are not static but highly dynamic structures, based on nucleation, stabilization and disassembly⁴².

In vivo, Rad51/RecA filament dynamics are supported and regulated by so-called “Rad51/RecA mediators”⁴². Nucleation on single-stranded DNA represents the first step of nucleoprotein filament formation and provides an important example for “Rad51/RecA mediator” function, as they facilitate nucleation by overcoming the nucleation barrier of single-strand DNA binding proteins (RPA in eukaryotes, SSB in *E.coli*). In yeast, the Rad51 mediator Rad52⁴³ supports the RPA-Rad51 replacement (Figure 3A), while the role of Rad52 in vertebrates is more modest and additional Rad51 mediator proteins like BRCA2⁴⁴ evolved to perform similar functions. In *E.coli*, RecF, RecO and RecR function as RecA mediators by supporting the replacement of the single-strand binding protein SSB to RecA²². Moreover, single-molecule *in vitro* studies on the *E.coli* system provided valuable insights into the mechanism of filament nucleation²²: nucleation on SSB-coated ssDNA requires a RecA dimer and can occur in parallel at multiple locations along the SSB-coated ssDNA²². Extension of the nucleation spot is achieved by addition of RecA monomers to both sides, thus filament growth is bidirectional, but 5'-3' growth is favored²².

In addition to Rad51 mediators, a group of Rad51 paralogs are thought to modulate Rad51 filament dynamics¹³. Known Rad51 paralogs comprise Rad55, Rad57, Shu1 and Psy3 in *S. cerevisiae*, and RAD51B, RAD51C, RAD51D, XRCC2 and XRCC3 in mammalian cells¹³. In contrast to Rad51, these proteins fail to form extensive nucleoprotein filaments and fail to catalyze DNA pairing reactions, despite sharing with Rad51 the conserved RecA core. Although RAD51C and RAD51D have

been implicated as cancer predisposition genes⁴⁵, the function of Rad51 paralogs remains largely unknown. Some detail regarding the function of Rad51 paralogs emerged from a recent study on Rad55 and Rad57⁴⁶. In this study Rad55 and Rad57 were shown to function together as a heterodimer in supporting Rad51 filament stabilization by counteracting the function of the anti-recombinase Srs2⁴⁶.

Taken together Rad51 represents a central protein of HR and forms dynamic nucleoprotein filaments, highly regulated by Rad51 mediators and Rad51 paralogs.

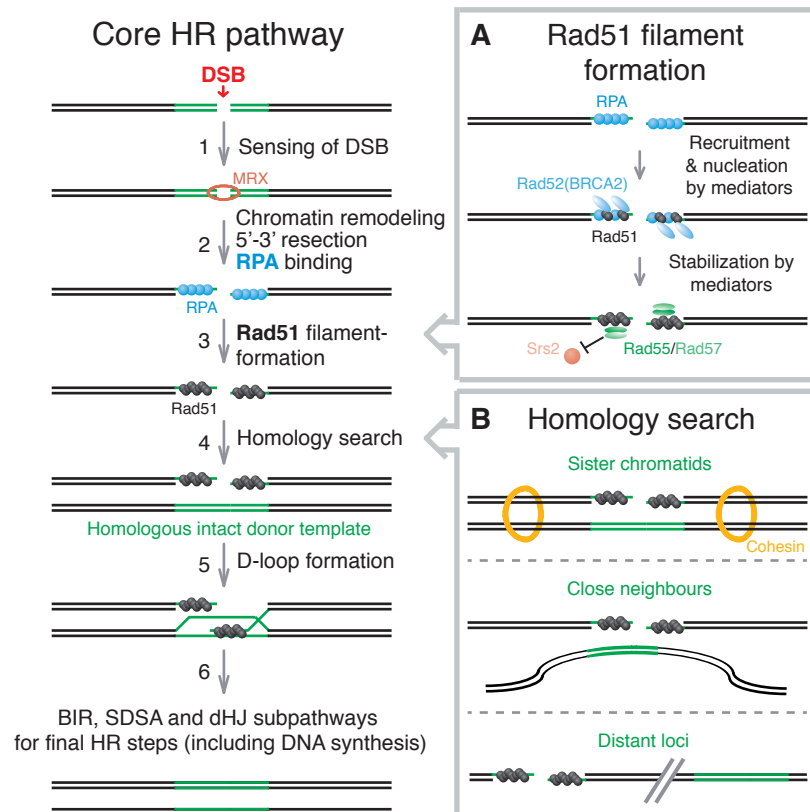


Figure 3. The recombinase Rad51 - a central protein in homologous recombination.

(A) Rad51 forms a filament on ssDNA at the DSB, and Rad51 mediators support filament formation. Rad51 filaments represent dynamic structures, based on nucleation, stabilization and disassembly. Rad51 nucleation on RPA-coated ssDNA is supported by Rad52 (yeast)/BRCA2(vertebrates), whereas Rad51 filament stabilization is supported by the heterodimer Rad55/Rad57 which counteracts the antirecombinase Srs2.

(B) Homology search, the process of finding a homologous donor sequence, is largely enigmatic. The intact homologous donor sequence can be located on the sister chromatid or on the same or another chromosome (for further details see section 2.5).

BIR: break-induced replication (subpathway of HR); dHJ: double-Holliday junction subpathway of HR; D-loop: displacement loop; DSB: DNA double-strand break; HR: homologous recombination; MRX: MRX complex, consisting of Rad50, Mre11 and Xrs2; SDSA: synthesis-dependent strand annealing (subpathway of HR).

2.4 Regulation of Homologous Recombination

In addition to the balanced regulation of Rad51 described above, HR activity is carefully regulated basically at all other steps of the pathway. This comprises numerous additional factors and posttranslational protein modifications, such as phosphorylation, ubiquitylation and SUMOylation.

Phosphorylation events upon DSB formation include phosphorylation dependent checkpoint responses^{47,48}, and phosphorylation of Rad51^{49,50} and histone 2A (H2A)⁵¹. Phosphorylation of H2A (from hereon called γ H2A) represents one of the earliest events upon DSB formation and is a highly conserved process. It occurs in *S. cerevisiae* directly on H2A at serine 129 and in mammalian cells on H2A.X (H2A histone variant, which is estimated to be present in 10% of all nucleosomes) at serine 139⁵¹. Phosphorylation is mediated by checkpoint kinases, and takes place over large regions flanking the DSB. This region can extend up to several hundred kilobases in yeast^{52,53} and up to megabases in mammals⁵⁴. Presently, demonstrated roles of γ H2A include its function as a recruitment scaffold⁵¹, such as for MDC1 in mammals (which itself serves also as a recruitment platform; see below) or for the chromatin remodelers INO80^{55,56} and SWR1⁵⁷. Besides INO80 and SWR1, additional chromatin remodelers have been implicated in DSB repair²⁰, including SWI/SNF⁵⁸, RSC^{59,60} and FUN30^{61,62,63}. Suggested functions for the different chromatin remodelers range from nucleosome exchange and nucleosome sliding to nucleosome eviction. These activities are thought to facilitate DSB repair-associated processes such as resection within chromatinized DNA. Nevertheless, detailed functions and explanations for redundancy of different chromatin remodelers are just beginning to emerge^{20,64}.

Next to posttranslational protein modification by phosphorylation, particularly protein conjugation by ubiquitin and its relative SUMO is an emerging topic in the DSB repair field over the recent years^{65,66,67,68,69}.

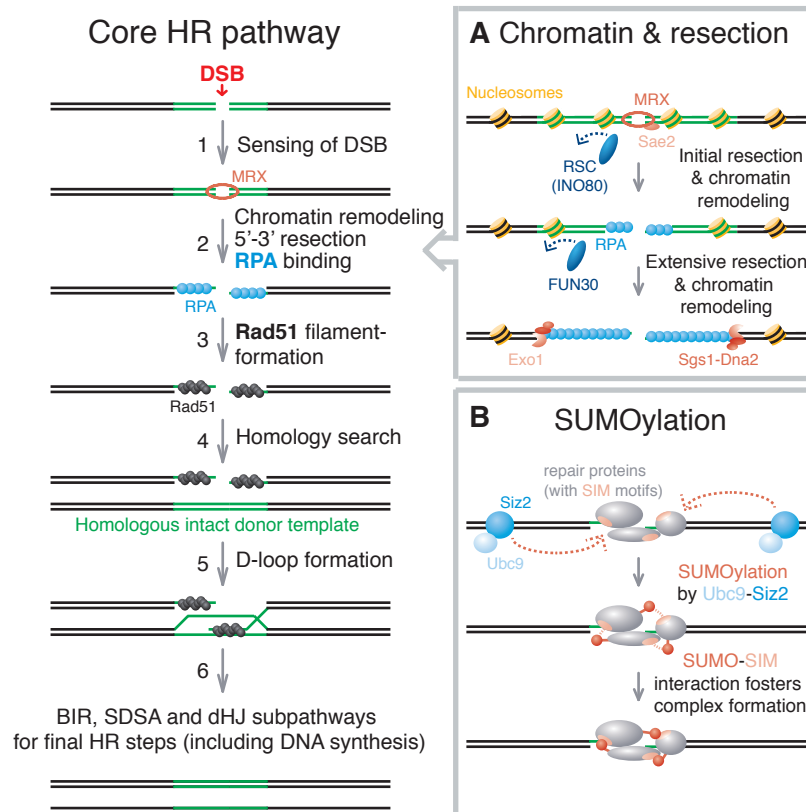


Figure 4. Regulation of homologous recombination.

(A) 5'-3'-Resection next to the DSB is a multistep process, requiring the MRX complex and Sae2 for initial resection, and Sgs1, Dna2 and Exo1 for extensive continuous resection. Moreover, resection and all other HR steps have to take place in the context of chromatinized DNA. Consequently, the chromatin remodeler RSC and INO80 have been implicated in the initial resection, whereas the chromatin remodeler FUN30 has been implicated in facilitating long-range resection.

(B) Upon DSB formation, a multitude of repair proteins are SUMOylated, catalyzed by the SUMO conjugating enzyme Ubc9 and mainly by the SUMO ligase Siz2. SUMOylation of repair factors and subsequent interaction with SIM (SUMO interacting motifs) motifs on other repair proteins likely fosters complex formation and thereby DSB repair.

BIR: break-induced replication (subpathway of HR); dHJ: double-Holliday junction subpathway of HR; D-loop: displacement loop; DSB: DNA double-strand break; HR: homologous recombination; MRX: MRX complex, consisting of Rad50, Mre11 and Xrs2; SDSA: synthesis-dependent strand annealing (subpathway of HR); SIM: SUMO-interacting motif.

Regarding ubiquitylation as a regulatory mechanism in DSB repair, major findings have been made in mammalian cells^{65,70}. It was found that phosphorylated H2AX (γ H2AX) recruits the scaffold protein MDC1, which itself provides a binding platform for the ubiquitin ligase RNF8. Subsequently, RNF8 ubiquitylates histones H2A and H2AX, and these ubiquitylated histones in turn recruit additional DNA repair proteins^{71,72,73}. In addition to RNF8, several other ubiquitin ligases locate to the DSB and function as well in recruiting further repair proteins^{74,75}, resulting in an intricate recruitment cascade. Thus, ubiquitylation in DSB repair is particularly known to serve as a signaling mark, leading to an entire ubiquitin-dependent DSB signaling response⁶⁶.

Regarding SUMOylation as a regulatory mechanism in DSB repair, it has recently been shown that – next to SUMOylation of single substrates^{76,77,78,79,80,81,82} – an entire group of DSB repair proteins become SUMOylated upon DSB induction⁸³ and other types of DNA damage^{83,84}. Intriguingly, only wholesale removal of SUMOylation acceptor sites of different substrates causes a delay in DSB repair⁸³, in line with the observed strong phenotypes of SUMO pathways mutants^{83,85,86,87}. This led to the model that individual SUMO modifications on different substrates act synergistically or redundantly, likely by enhancing protein-protein interactions and thus promoting protein complex formation to foster DSB repair⁸³ (Figure 1B).

2.5 Homology Search

Homologous recombination (HR) relies on the existence of a homologous donor sequence to repair the DSB. Importantly, to enable repair, the homologous donor sequence has to get into direct spatial proximity with its DSB-bearing counterpart²³, a process called homology search. Despite the essential need for homology search, most textbooks or reviews omit or only briefly refer¹³ to homology search, most likely because the knowledge about this fundamental step of the pathway is rudimentary²⁴. It has been even proposed that the process of homology search does not exist²⁴. The following paragraphs define the term homology search, describe the current knowledge and discuss hypothetical models for its potential mechanism.

Up to now, the majority of available data on homology search derived from investigations *in vitro*. These studies mostly used a short oligonucleotide and a plasmid that contains a homologous region to the oligonucleotide. Subsequently, D-loop formation (base-pairing) between the homologous sequences of the oligonucleotide and the plasmid is analyzed (which represents the end-product of homology search). Notably, recombinant Rad51 assembled as a filament on the oligonucleotide is sufficient for D-loop formation, also even in context of nucleosomes⁸⁸ (nevertheless, homology recognition in the context of heterochromatinized DNA requires the Rad51 mediator Rad54⁸⁹). However, it is important to note that these studies rely only on the stochastic movement of Rad51-coated oligonucleotides and plasmids in solution; thus the encounter of homologous sequences is based on probability. Moreover, the probability of an encounter between homologous sequences was largely increased in these studies by usage of a high number of homologous molecules⁸⁸. A recent single-molecule analysis expanded this experimental setup and analyzed how bacterial RecA detects homology on a single DNA template *in vitro*⁹⁰. In this study the authors demonstrated that the 3-dimensional conformation of DNA is important for homology recognition⁹⁰. Moreover, a contact between the Rad51-coated ssDNA and a non-homologous sequence could be visualized for the first time *in vitro*⁹⁰. These authors suggested that such nonhomologous contacts of the DSB with other DNA parts represent the basis for homology search, as homology search likely requires multiple probing for the homologous sequence. Nevertheless, single-molecule *in vitro* studies are also limited on the random encounter of the homologous sequences.

However, even if the oligonucleotide only randomly encounters its homologous sequence on the plasmid, it still has to recognize the homology. Consequently, these studies provide valuable insights into homology recognition. Hypothetically, homology recognition could be accelerated by short sliding of the nucleoprotein filament on the target dsDNA in order to find homologous sequences for Watson-Crick base pairing. Indeed, although it has been argued by some authors for more than a decade against such a sliding mechanism^{90,91}, sliding was indeed recently observed *in vitro*⁹². Sliding *in vitro* is estimated to proceed in a short-range of 80-300 base-pairs⁹², in line with previous studies suggesting that long-range sliding does not seem to occur⁹¹.

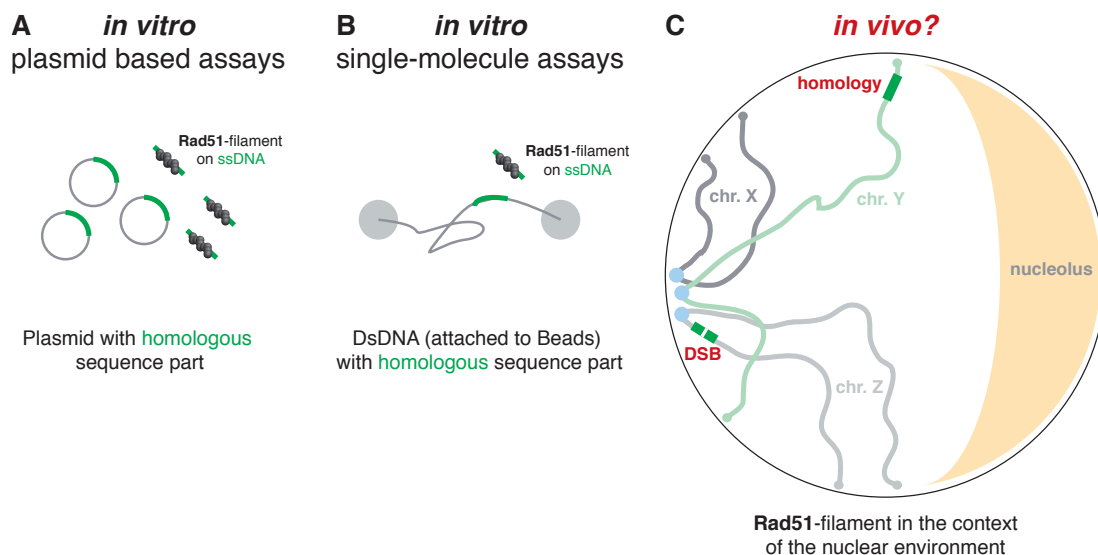


Figure 5. Analysis of homology recognition and homology search.

(A) Current data on homology search mainly derive from *in vitro* assays, which chiefly analyze the last step of homology search namely homology recognition or short-range homology search. A widely used assay to study D-loop formation (base pairing between the Rad51 nucleoprotein filament and its homologous donor sequence; the endproduct of homology search) is based on plasmids and oligonucleotides coated with Rad51-filaments.

(B) Single dsDNA molecules attached *in vitro* at both ends to beads (which can be moved by magnetic tweezers) were used to analyze the impact of stretching/unstretching onto D-loop formation.

(C) Highly schematic representation of a DSB (red) on one chromosome (light gray; for simplification, only 3 of 16 chromosomes are depicted according to *S. cerevisiae* nuclear organization (see section 5.3 for more details)). Note that a DSB *in vivo* consists of two flanking regions of ssDNA, which both harbor Rad51 filaments. Moreover, the ssDNA harboring the Rad51 filament is not a separate entity, but is attached to the entire DSB-harboring chromosome. How long-range homology search functions *in vivo* under these conditions remains completely enigmatic.

Note that the molecules schematically represented in (A), (B) and (C) are not depicted on the same scale. D-loop: displacement loop; DSB: DNA double-strand break; ssDNA: single-stranded DNA.

Although all published *in vitro* studies provide very valuable insights into homology recognition^{93,94} (short-range homology search), they are of limited value for understanding how the DSB gets into spatial proximity with its homologous donor

sequence *in vivo* (long-range homology search). Moreover, from the biophysical point of view, the behavior of a Rad51 nucleoprotein filament likely differs with the respect to movement and flexibility, depending on whether it coats a short oligonucleotide or a single-stranded part of a chromosome. Hence, the question how homology search functions *in vivo* in the context of entire chromosomes and the nuclear architecture has remained elusive.

Several models regarding the mechanism of homology search *in vivo* have been proposed. Starting from the most extreme view, it has been speculated that long-range homology search is not needed *in vivo*, as only local homology recognition (short-range homology search) might be required²⁴. However, such a model would require that homologous sequences locate in direct spatial proximity to each other, even before a DSB exists. Consequently, this model predicts a continuous pairing of all homologous sequences in the genome. Support for this model come from the finding that multiple fluorescent in situ hybridization (FISH) studies originally implicated pairing of homologous sequences. However, these data have been discussed to derive from artificial clustering mediated by the FISH methodology²³. In addition, it remains questionable how a cell might “know” which sequences are homologous to each other (without Watson-Crick base pairing). Moreover, constant pairing of homologous sequences would likely cause unwanted DNA transactions, like chromosomal translocations. Further in disagreement with a pre-pairing model, it could be demonstrated that homologous sequences do not have to pre-pair to enable efficient repair of DSB⁹⁵. Furthermore, repair can even take place between homologous sequences on different chromosomes in *S. cerevisiae*^{37,96,97,98,99,100,101,102,103}.

The findings that repair can take place between dispersed homologous sequences argued for the existence of long-range homology search. Thus an alternative model was proposed, namely that homology search functions efficiently genome-wide¹⁰⁴. Interestingly, this model became the consensual model for homology search in many publications, although data regarding an efficient genome-wide homology search is lacking²⁴. Efficient genome-wide homology search would require homology probing of every DNA sequence in the genome. How time-consuming a potential probing of the entire genome might be has been estimated for the genome of *S. cerevisiae*²³, indicating that the search time would exceed the actual measurable repair time by multiple orders of magnitude. However, such calculations rely on a predefined set of variables. One additional factor that was not

present in the original calculation is the recent discovery of an induced chromatin movement surrounding the DSB. Using fluorescent imaging of a DSB, different studies detected an induced movement of sequences around the DSB in comparison to the intact sequence^{105,106,107}. Such enhanced movements of DSBs intuitively suggest that the likelihood of encounters between homologous sequences would increase. However, evidence for a direct functional link between DSB movement and homology search is currently lacking^{105,106,107}. Moreover, even if the movement of a DSB would reflect homology search¹⁰⁸, it remains questionable whether the increased movement would sufficiently enhance the search time to an extent that allows for efficient genome-wide searches¹⁰⁹.

In conclusion, considerable progress has been made in analyzing the “behavior” of Rad51 *in vitro* and how it mediates homology recognition by short-range homology search. However, the currently proposed models for the mechanism of homology search *in vivo* are highly controversial, ranging from the model that long-range homology search does not exist to the model that long-range homology search occurs efficiently genome-wide.

3 Aims of This Study

Homologous recombination (HR) is one of the two major pathways to repair DNA double-strand breaks (DSB) and is thus pivotal for genome integrity. The HR pathway is largely error-free as it is based on the usage of an intact homologous donor sequence to repair the DSB.

Although HR has been studied for decades, homology search, the crucial step of exploring the genome for the intact homologous donor sequence, remained largely enigmatic. Current information about homology search is primarily based on *in vitro* experiments analyzing homology recognition. But how homology search might function *in vivo* in the context of entire chromosomes and the crowded nuclear environment remained puzzling, and hypothetical models range from an efficient long-range genome-wide scanning mechanism to the idea that long-range homology search does not exist at all *in vivo*.

To shed light into this central step of homologous recombination, this study aimed to visualize this process for the first time *in vivo*. The Jentsch lab demonstrated previously that a single persistent DNA double strand break results in an almost chromosome-wide binding-profile of the recombinase Rad51. The aim of this PhD thesis was to investigate this intriguing finding in more detail and to test whether this observed broad Rad51 distribution is linked to homology search. Specifically, we hypothesized that the observed broad Rad51 distribution correspond to transient encounters of the Rad51-coated DNA ends with chromosomal locations during homology probing.

4 Results

4.1 Homology Search Can Be Monitored *in vivo* by Rad51 ChIP

4.1.1 Broad Distribution of Rad51 ChIP Signals upon a Single DSB

In line with Rad51 nucleoprotein filament formation on single-stranded DNA (ssDNA) around the DSB, the recombinase Rad51 was found in multiple studies to bind directly next to the DSB *in vivo*^{110,111}. These studies performed Rad51 chromatin-immunoprecipitation (ChIP) experiments upon a single inducible DSB in the yeast mating-type system, using a *S. cerevisiae* strain in which the DSB cannot be repaired by homologous recombination^{**} due to the deletion of the *HML* and *HMR* donor templates (“donor-deficient” strain). Importantly, these studies investigated Rad51-binding only in direct proximity of the DSB (mostly up to 10 kb up- and downstream) and at homologous donor sequences^{110,111}.

In contrast, the Jentsch laboratory investigated for the first time Rad51-binding upon a single DSB genome-wide. For this analysis the same donor-deficient strain was used as in the studies described above, but additionally combined Rad51 ChIP experiments with whole genome tiling arrays (ChIP-chip)⁷⁶. Intriguingly, this experiment revealed Rad51 ChIP signals not only in direct proximity of the single DSB, but also very distant to the DSB (Figure 6). These DSB-distant Rad51 ChIP signals increased over time, covering almost the entire chromosome III 5 hours after DSB induction (on which the mating-type system and thus the single DSB are located). In particular, these DSB-distant Rad51 ChIP signals were mainly only detectable on the effected and not on other chromosomes (Figure 6).

The observed broad Rad51 distribution is in stark contrast to the previously reported Rad51 ChIP signals only in direct proximity of the DSB (where Rad51 filament formation takes place). We thus considered different models that might explain the broad Rad51 distribution. Hypothetically, these signals might have derived from Rad51-filament formation on the entire chromosomal axis, either on dsDNA or ssDNA (due to hypothetical long-range resection). Alternatively, Rad51 might assemble nonspecific on different chromosomal parts due to high nuclear protein level.

^{**} NHEJ can be neglected, as it occurs rarely *in S. cerevisiae*³³. Moreover, even if the HO cut site is repaired by NHEJ, it will be cleaved again by the HO endonuclease³³.

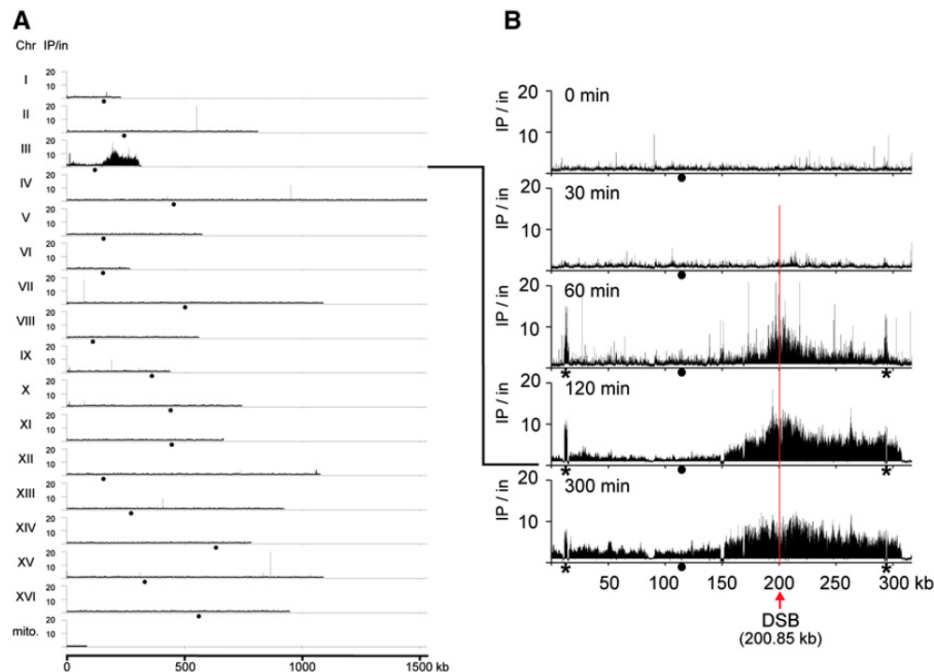


Figure 6. DSB-distant Rad51 signals upon a single DSB cover almost the entire DSB-harboring chromosome.

(A) A single DSB on chromosome III in the *MAT* locus results in a broad signal of the recombinase Rad51 (analyzed 5 hours upon DSB induction by Rad51 chromatin-immunoprecipitation combined with a genome-wide tiling-array (ChIP-chip)), but only on the effected chromosome (depicted are all 16 nuclear chromosomes and the mitochondrial (mito) genome).

(B) As in (A), but including a time-resolved analysis and highlighting chromosome III. DSB-distant Rad51 signals can be detected already 1 hour after HO expression induction (DSB induction), and largely locate to the right arm of chromosome III. Asterisks denote artificial peaks that arise due to being homologous to the *MAT* locus.

Data are depicted on a linear scale. Gaps in ChIP-chip data correspond to repetitive DNA. Chr.: chromosome; DSB: DNA-double-strand break; IN: input; IP: immunoprecipitation. (Figure taken from ⁷⁶)

However, both models appeared rather unlikely, as an almost chromosome-wide long-range resection and a nonspecific assembly of the recombinase Rad51 appear detrimental for genome stability. We thus entertained a different model in which we hypothesized that the broad distribution of Rad51 might originate from ongoing homology search (Figure 7).

In this “ongoing homology search” model we envisioned that the Rad51 signals directly at the DSB originate from the Rad51 nucleoprotein filament on ssDNA, whereas the DSB-distant Rad51 signals originate from transient encounters of the Rad51-coated DSB ends with other chromosomal regions during the process of homology search (Figure 7). Specifically, we hypothesized that the Rad51-directed ChIP experiments resulted also in signals derived from “frozen” interactions (by protein-DNA crosslinking) of the Rad51 nucleoprotein filament with chromosomal DNA during homology search. As homology search is unlikely to take place at the same locations at the same time in different cells, we assumed that the signal

intensity of the Rad51-directed ChIP (which derive from a large pool of cells) would directly reflect the average of homology search at the respective chromosomal location over all cells (Figure 7B).

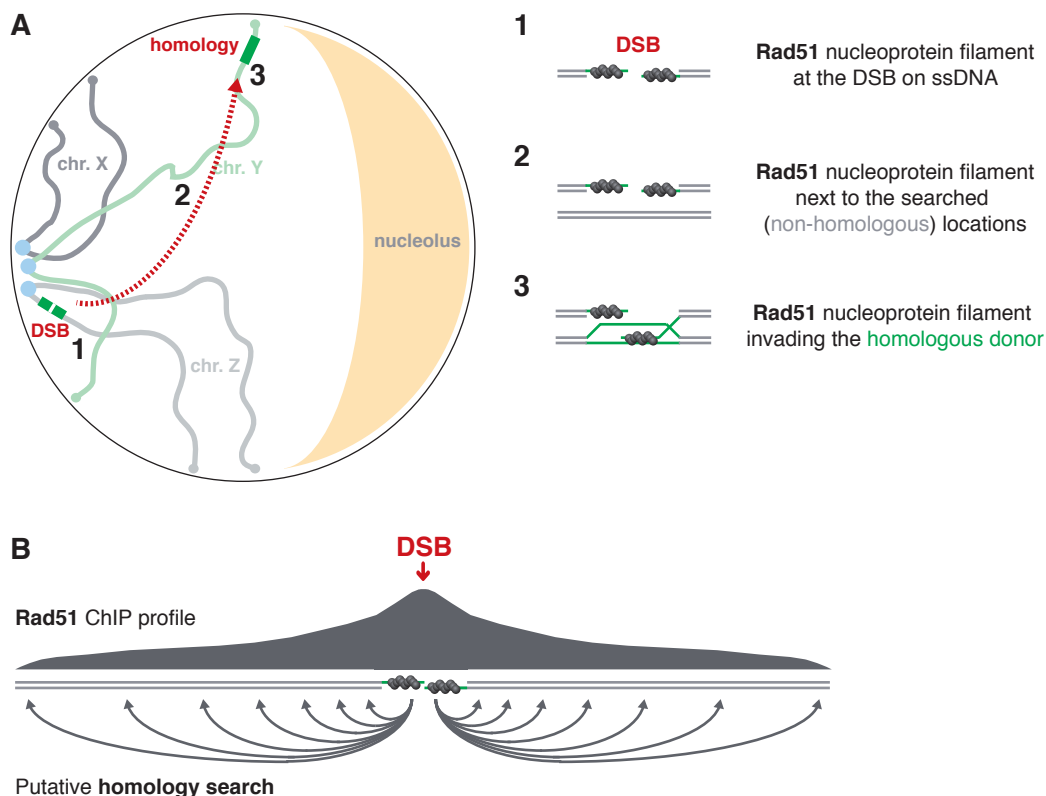


Figure 7. Model for a correlation between Rad51 ChIP signals and homology search.

(A) If a single DSB is present on one chromosome (for simplification, only 3 of 16 chromosomes are shown (chr. X, Y, and Z)), the DSB can be repaired via ectopic recombination by using a homologous donor template (green) either on the same or on another chromosome (depicted here). This requires direct spatial proximity between the DSB-harboring sequence and its homologous donor sequence. But how these homologous sequences come into direct spatial proximity (red dashed arrow) by the process of homology search remains enigmatic. We hypothesized that monitoring Rad51 signals in a genome-wide manner upon DSB induction might visualize homology search *in vivo*: It has previously been demonstrated that Rad51 binds directly next to the DSB (see scheme 1) and also to the homologous donor sequence once homology search was successful (see scheme 3). We speculated that Rad51 ChIP experiments additionally result in Rad51 ChIP signals at all searched non-homologous sequences (see scheme 2), as homology probing requires direct proximity of Rad51-bearing DSB and the searched sequences.

(B) Data resulting from ChIP experiments represent the average of a high number of cells. As homology search likely does not take place at the same place at the same time in different cells, a high Rad51 ChIP signal intensity at one specific DSB-distant location would indicate homology search at this location in many cells.

ChIP: chromatin-immunoprecipitation; chr: chromosome; DSB: DNA-double-strand break; ssDNA: single-stranded DNA.

4.1.2 DSB-distant Rad51 ChIP Signals are Specific

To address the origin of DSB-distant Rad51 ChIP signals, we first established Rad51-directed ChIPs combined with quantitative real-time PCR (RT-qPCR). ChIP-RT-qPCR has the advantage of being highly quantitative and less time-consuming in comparison to genome-wide profiling by ChIP-chip.

First, we induced a DSB in the same experimental mating-type system described above. Specifically, DSB-induction was performed by the addition of galactose – which induces the expression of the HO endonuclease - to a exponentially-grown donor-deficient *MAT α* strain. Thereafter, samples were crosslinked with formaldehyde at time points reflecting early (1 and 2 hrs) and later (5 hrs) events in DSB repair. Subsequent Rad51-directed ChIP and RT-qPCR analysis at different chromosomal locations revealed not only high Rad51 signals in direct proximity to the DSB (using primer pairs 0.2 and 6 kb downstream), but also Rad51 signals in far distance of the DSB (using primer pairs 54 and 75 kb downstream) (Figure 8A).

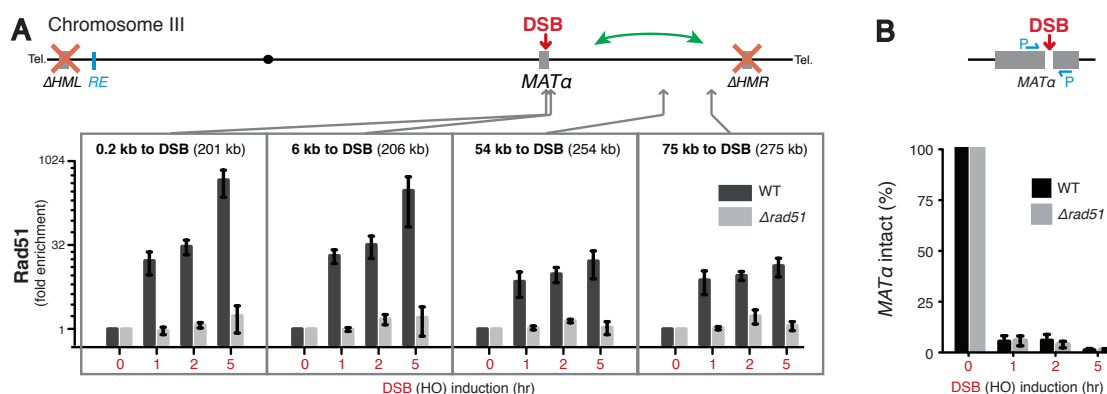


Figure 8. DSB-distant Rad51 signals can be detected by Rad51-directed ChIP analyzed by RT-qPCR.

(A) Top: Map of chromosome III of a donor-deficient *MAT α* strain depicting the *MAT α* locus (where a DSB can be induced by HO endonuclease), deleted *HML* and *HMR* sequences, recombination enhancer (*RE*), and centromere (black dot). Bottom: Rad51-directed ChIP at 0.2, 6, 54, and 75 kb away from the DSB. Rad51 enrichments are shown for the donor-deficient *MAT α* WT strain and the mutant derivative deficient in Rad51. Data are depicted on a log₂ scale and as the mean \pm SEM (standard error of the mean; n=3) of IP/Input ratio normalized to a control locus (chromosome X) and to the 0 hr time point.

(B) Samples of (A) were analyzed for DSB induction using a PCR primer set (blue) spanning the DSB. Loss of PCR products is an indicator for efficient DSB formation. DSB induction occurs similarly in WT and the mutant derivative deficient in Rad51. Data are depicted on a linear scale as mean \pm SEM (standard error of the mean; n=3) and are normalized to a control locus and against the signal before DSB induction (set to 100%).

DSB: DNA-double-strand break; HO: HO endonuclease; P: primer; *RE*: recombination enhancer element; RT-qPCR: quantitative real-time PCR; Tel: Telomere.

To control the specificity of the ChIP signals for Rad51, the same experiment was performed in parallel in a mutant derivative strain deficient in Rad51 ($\Delta rad51$). This experiment revealed only background ChIP signals, thus conforming the specificity of the Rad51 ChIP analysis (Figure 8A). Moreover, equally efficient induction of the DSB in WT and $\Delta rad51$ strains was controlled by a previously established quantitative method (using a primer pair for RT-qPCR analysis that spans the HO recognition sequence), in which loss of the PCR product gradually reflects DSB induction¹¹² (Figure 8B).

Notably, the DSB-distant Rad51 ChIP signals are considerably lower as the DSB-proximal Rad51 signals. This result is in line with the proposed model, in which the high DSB-proximal Rad51 signals would represent the Rad51 nucleoprotein filament at the DSB in all cells, whereas the lower DSB-distant Rad51 signals would represent transient snapshots of the ongoing homology search (which searches at different locations in different cells, thereby diluting the signal). The difference between the signal intensity proximal and distal to the DSB is most pronounced in the RT-qPCR analysis in comparison to the tiling-array analysis (ChIP-chip) (Figure 6 and Figure 8A), as very high signals become under-represented in ChIP-chip experiments.

In summary, we concluded that Rad51 chromatin-immunoprecipitation experiments are specific for Rad51, can be combined with RT-qPCR analysis and detect DSB-distant Rad51 ChIP signals.

4.1.3 DSB-distant Rad51 ChIP Signals Depend on Rad52 and Rad55/Rad57

Next we tested whether the DSB-distant Rad51 ChIP signals depend on known Rad51 mediators. Therefore, we analyzed DSB-distant Rad51 ChIP signals by RT-qPCR in mutant derivative strains deficient for the Rad51-loading factor Rad52, and the Rad51-stabilization factors Rad55 and Rad57. In all these mutants, Rad51 was unable or strongly hampered to form a filament at the DSB (Figure 9A and ^{110,111}). In addition, also the DSB-distant Rad51 signals were lost in the mutant strains (Figure 9A) despite similar DSB-induction efficiencies compared to the WT strain (Figure 9B).

Moreover, by analyzing Rad51 protein levels on a Western-blot upon SDS-gel separation with a Rad51 antibody (same as used in the ChIP experiments described above), we discovered that the Rad51 protein levels increase over time upon induction of a single DSB (data not shown). Importantly, this increase in Rad51 levels upon DSB induction was not affected in the mutant derivative strains deficient for Rad52, Rad55 and Rad57 (data not shown). This finding excludes the possibility that the DSB-distant Rad51 signals derive artificially from high Rad51 protein levels in the nucleus. Moreover, the dependency on known Rad51 mediators suggests that the DSB-distant Rad51 signals derive from specifically assembled Rad51.

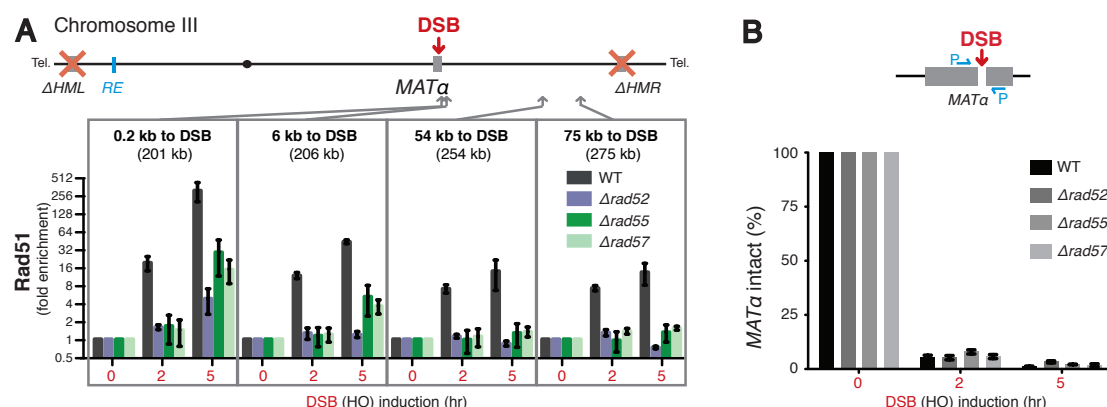


Figure 9. The DSB-distant Rad51 signals depend on the Rad51 mediators Rad52 and Rad55/Rad57.

(A) Rad51-directed ChIP at 0.2, 6, 54, and 75 kb away from the DSB. Rad51 enrichments are shown for the donor-deficient *MATα* WT strain and mutant derivatives deficient in Rad52, Rad55 and Rad57. Data are depicted on a log2 scale and as the mean \pm SEM (standard error of the mean; $n=3$) of IP/Input ratio normalized to a control locus (chromosome X) and to the 0 hr time point.

(B) Samples of (A) were analyzed for DSB induction using the same method as in Figure 8B. DSB induction is as efficient in WT as in mutant derivatives deficient in Rad52, Rad55 or Rad57. Data are depicted on a linear scale as mean \pm SEM (standard error of the mean; $n=3$) and are normalized to a control locus and against the signal before DSB induction (set to 100%).

DSB: DNA-double-strand break; HO: HO endonuclease; P: primer; *RE*: recombination enhancer element; Tel: Telomere.

4.1.4 DSB-distant Rad51 ChIP Signals are a General Phenomenon upon Single DSBs in *Saccharomyces Cerevisiae*

To further investigate the model that the DSB-distant Rad51 ChIP signals might be linked to homology search, we tested whether DSB-distant Rad51 ChIP signals are general, and not a specialty of the evolved mating-type system in *S. cerevisiae*. Therefore, we first cloned single HO cleavage sites at central locations of chromosome I or chromosome IV (in strains harboring a deletion of the endogenous HO cleavage site in the *MAT* locus on chromosome III), the smallest and the second largest chromosome of *S. cerevisiae*, respectively. DSB formation was induced by expression of HO endonuclease under control of a galactose-inducible promoter, and chromosomal Rad51 ChIP profiles were followed by ChIP-chip.

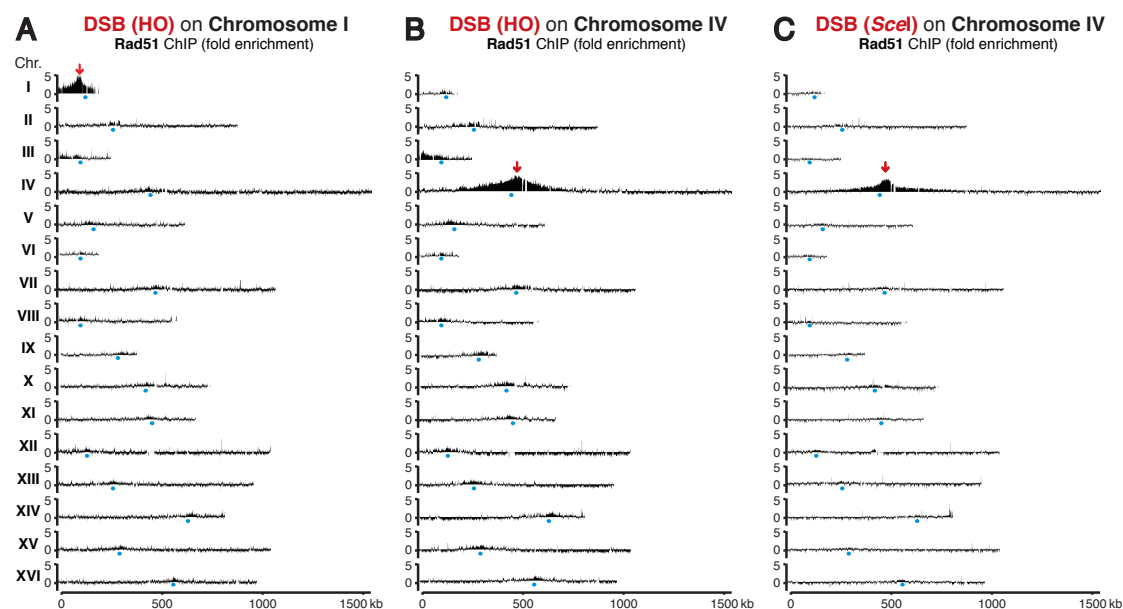


Figure 10. The DSB-distant Rad51 ChIP signals are a mating-type independent phenomenon upon a single DSB.

(A) Rad51-directed ChIP-chip using a strain bearing a single HO-cleavage site (red arrow) on a central location of chromosome I (120 kb). Profiles for all chromosomes are shown 5 hrs after HO expression. In addition to the symmetric Rad51 distribution surrounding the DSB on chromosome IV, small Rad51 enrichments are detectable around centromeres (blue dots) of all chromosomes, and on the left arm of chromosome III, peaking at the *RE* element. The origin of these signals are discussed in detail in sections 4.2.1 and 4.2.2. Single spikes in the ChIP-chip data correspond to single oligonucleotides, and are hybridization artifacts.

(B) As in (A), but using a strain bearing a single HO-cleavage site (red arrow) on a central location of chromosome IV.

(C) As in (A), but using a strain bearing a single *Scel*-cleavage site (red arrow) on a central location of chromosome IV (491 kb).

ChIP-chip data represent the mean of two experiments, including a dye swap experiment (for details see Materials and Methods, section 6.3.4). Data are depicted on a log2 scale. Blue dots represent position of centromeres. Gaps in ChIP-chip data correspond to repetitive DNA. Chr: chromosome; DSB: DNA-double-strand break; HO: HO endonuclease; *Scel*: *Scel* endonuclease.

Indeed, similar to the findings described above, Rad51 ChIP signals were not only detectable in direct proximity to the DSB, but also very distant to the DSB, encompassing the entire chromosome I (230 kb) and up to approximately 500 kb on chromosome IV (Figure 10A and B). Moreover, analogous to the situation in the mating-type system, the majority of the Rad51 ChIP signals located on the broken chromosome ^{††} (Figure 10A and B).

To further exclude the possibility that the observed behavior of Rad51 is a special phenomenon of the evolved *MAT* system, we created a strain that harbors a recognition sequence for the *SceI* endonuclease instead of the *HO* endonuclease cleavage site (which is naturally present in the *MAT* system) on chromosome IV. Expression of the *SceI* endonuclease under control of a galactose-inducible promoter was achieved from a plasmid. Again, Rad51 ChIP-chip experiments revealed a similar broad distribution of Rad51 ChIP signals 5 hours after DSB induction, mainly covering large parts of the affected chromosome (Figure 10C).

In conclusion, the broad distribution of Rad51 ChIP signals upon DSB formation is not a specialty of the mating-type system. However, in contrast to the asymmetrical behavior of the Rad51 ChIP signals in the *MAT* system, the Rad51 ChIP signals broaden apparently symmetrical on chromosomes I and IV (Figure 10A-C). The cause of this difference will be discussed in section 4.1.6 and 4.2.1.

^{††} Notably, additional minor Rad51 ChIP signals on the left arm of chromosome III and around the centromeres of all other chromosomes can be detected and are discussed in detail in sections 4.2.1 and 4.2.2.

4.1.5 DSB-distant Rad51 ChIP Signals Exceed the Area of Resection

Prompted by these findings, we next tested whether the DSB-distant Rad51 ChIP signals indeed exceed the maximal distance of resection. This would be in line with the model that the DSB-distant Rad51 ChIP signals derive from snapshots of ongoing homology search and not from a Rad51 nucleoprotein filament on ssDNA caused by long-range resection.

To directly compare the extent of Rad51 ChIP signals with the extent of resection, we decided to monitor the binding profile of the ssDNA-binding factor RPA and the Rad51-loading mediator Rad52. RPA binds exclusively to ssDNA¹¹³; hence monitoring its binding pattern upon DSB formation does indirectly measure the extent of resection¹¹⁴. First, we performed ChIP with an antibody against endogenous RPA (described to recognize all three subunits of RPA, namely Rfa1, Rfa2 and Rfa3) in a donor-deficient *MATα* strain (as for Rad51). This experiment revealed a 10-fold enrichment of RPA directly next to the DSB (0,2 kb) 5 hours after DSB induction, but no signal at more distant locations at which the DSB-distant Rad51 ChIP signals can be detected (54 and 75 kb) (Figure 11A). This finding suggests that the extend of resection (ssDNA) is limited in comparison to the broad distribution of Rad51 ChIP signals. Nevertheless, the 10-fold enrichment of RPA observed at the DSB is rather low in comparison to the high Rad51 enrichment at the DSB.

We thus aimed to exclude the possibility that the absence of RPA ChIP signals at DSB-distant locations is due to detection limitations. Therefore, we expressed a C-terminally epitope-tagged version of the Rfa1 subunit of RPA (9-myc tag) from its endogenous genomic location and promoter. To control for the functionality of the Rfa1-9myc protein, we tested the efficiency of DSB-induction (Figure 11B) and performed growth assays under normal and DSB inducing conditions (by addition of the DSB-inducing agent zeocin) (Figure 11C). This revealed – if at all – only a highly marginal phenotype upon zeocin treatment caused by the 9-myc tag (Figure 11C). We therefore performed ChIP with an anti-myc antibody and analyzed the fold enrichment by RT-qPCR proximal and distal to the DSB. Interestingly, the fold enrichment proximal to the DSB is considerably enhanced, but is still almost absent at locations distal to DSB (Figure 11A), confirming the results described above using an antibody against endogenous RPA.

Of note, the untagged control strain resulted in a small artificial background signal directly at the DSB, an experimental artifact known to be caused by the 9-myc tag (data not shown and personal communication Claudio Lademann).

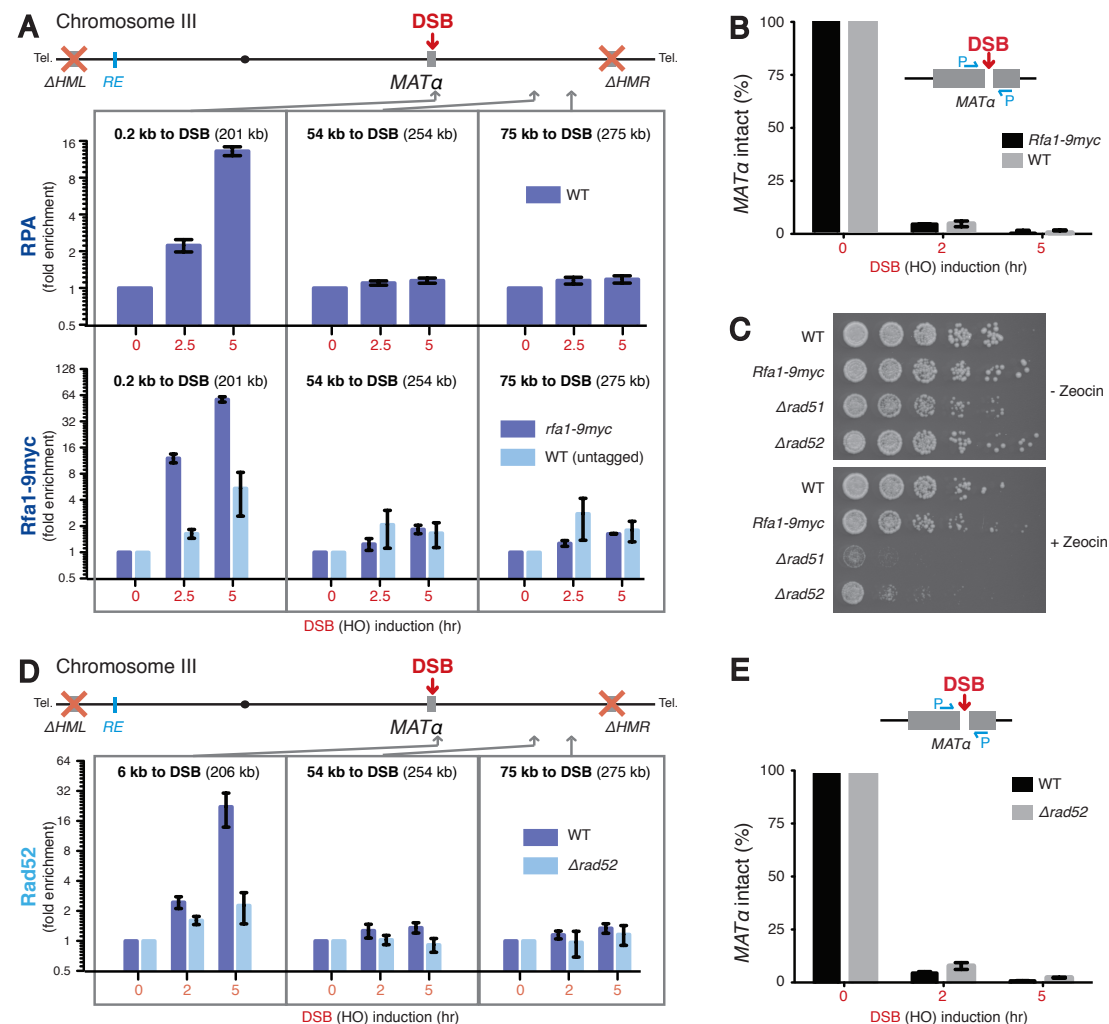


Figure 11. RPA- and Rad52-directed ChIP experiments upon induction of a single DSB.

(A) Upper panel: RPA-directed ChIP experiment, revealing signals (0, 2, 5 hrs after DSB induction) 0.2 kb next to the DSB, but not at distant sites (54 and 75 kb to the DSB). Lower panel: Similar to the upper panel, but detecting the RPA subunit by a Myc-directed ChIP in *Rfa1-9myc* expressing strain.

(B) Samples of (A; lower panel) were analyzed for DSB induction as in Figure 8B. *Rfa1-9myc* cells induce the DSB as WT.

(C) Equal amounts of cells of the indicated *MAT α* donor deficient strains were spotted in serial 5-fold dilutions (from left to right) onto media plates (YPD), either with or without the DSB-inducing agent zeocin. Mutant derivatives strains deficient for Rad51 and Rad52 were spotted as controls. Images were taken after 48 hours of growth at 30 °C.

(D) Rad52-directed ChIP experiment revealing signals (0, 2, 5 hrs after DSB induction) 6 kb next to the DSB, but not at distant sites (54 and 75 kb to the DSB). The absence of signals in the Δ rad52 mutant strain demonstrates the specificity of the Rad52-directed ChIP.

(E) Samples of (D) were analyzed for DSB induction as in Figure 8B. The experiment indicates similar DSB induction in WT and Δ rad52 cells.

Despite (B) and (E), all data are depicted on a log2 scale. Data are depicted as the mean \pm SEM (standard error of the mean; n=3) of IP/Input ratio normalized to a control locus (chromosome X) and to the 0 hr time point. Chr: Chromosome; DSB: DNA-double-strand break; HO: HO endonuclease; P: primer; *RE*: recombination enhancer element; Tel: Telomere.

As for RPA, we also performed ChIP with an antibody against endogenous Rad52. As Rad52 replaces RPA with Rad51, we expected similar ChIP signals for Rad52 as for RPA. Indeed, Rad52 can be detected proximal to the DSB, but not at specific locations distal to the DSB at which Rad51 can be detected (Figure 11D and E).

To compare the extent of resection with the DSB-distant ChIP Rad51 signals in detail in a chromosome-wide and time-resolved manner, we next performed ChIP-chip against Rfa1-9myc and Rad52. As expected from the RT-qPCR experiments, the resulting ChIP profiles revealed major differences in comparison to the Rad51 ChIP profiles (Figure 12A). Whereas Rad51 ChIP signals distribute already 1 hour after DSB induction asymmetrically over a large part of chromosome III (especially the right arm), RPA and Rad52 decorate only a highly confined region around the DSB (Figure 12A).

The region of RPA and Rad52 ChIP signals increases symmetrically over time, with a maximal extent of approximately 20-30 kb to both sides of the DSB after 5 hours (Figure 12A). This is generally consistent with previous measurements of resection rates¹¹⁵, however our values are about 2-3 fold larger. This difference might be explained by the fact that previous measurements relied on signal-loss (loss of dsDNA), whereas we analyzed signal-gain (gain of RPA signals). Nevertheless, the values determined by the two different assays indicate that the DSB-distant Rad51 ChIP signals exceed by far the maximal area of resection. To confirm this finding independently of the MAT system, we performed time-resolved ChIP-chip experiments against Rfa1-9myc in a strain containing a single HO cleavage site on chromosome IV. Like for DSB formation in *MAT*, the broad Rad51 distribution significantly exceeded the maximal binding pattern of RPA^{‡‡} (Figure 12B).

Notably, the simultaneous detection of RPA and Rad51 ChIP signals might appear contradictory to a model of mutual exclusive replacement of RPA to Rad51, but can be explained by recent findings that Rad51 loading might occur in patches²²) or by continuous RPA/Rad51 exchanges. Both would result in patches of RPA and Rad51 on the ssDNA - likely in every cell at a different position - and would thereby result in the observed RPA ChIP signals despite also detecting Rad51 ChIP signals in parallel. In line, immunohistochemistry experiments upon DSB induction revealed parallel staining of RPA and Rad51 in more than 80% of DSB foci (data not shown).

^{‡‡} Notably, whereas the main binding of RPA is confined to 20-30 kb to both sides of the DSB, additional lower but reproducible RPA binding signals can be detected in the chromosome IV system as well as in the *MAT* system (Figure 12A and B). The potential origin and function of these signals are discussed in detail in section 4.3.1.

In summary, the Rad51 ChIP signals distribute over a much broader chromosomal area than the maximal region of RPA and Rad52 ChIP signals and thus the maximal extent of resection. Consequently, the DSB-distant Rad51 signals cannot derive from a Rad51 nucleoprotein filament on ssDNA that extends from the DSB to the chromosome ends. Instead, the data further support the model that the DSB-distant Rad51 ChIP-signals correspond to “snapshots” of ongoing homology search.

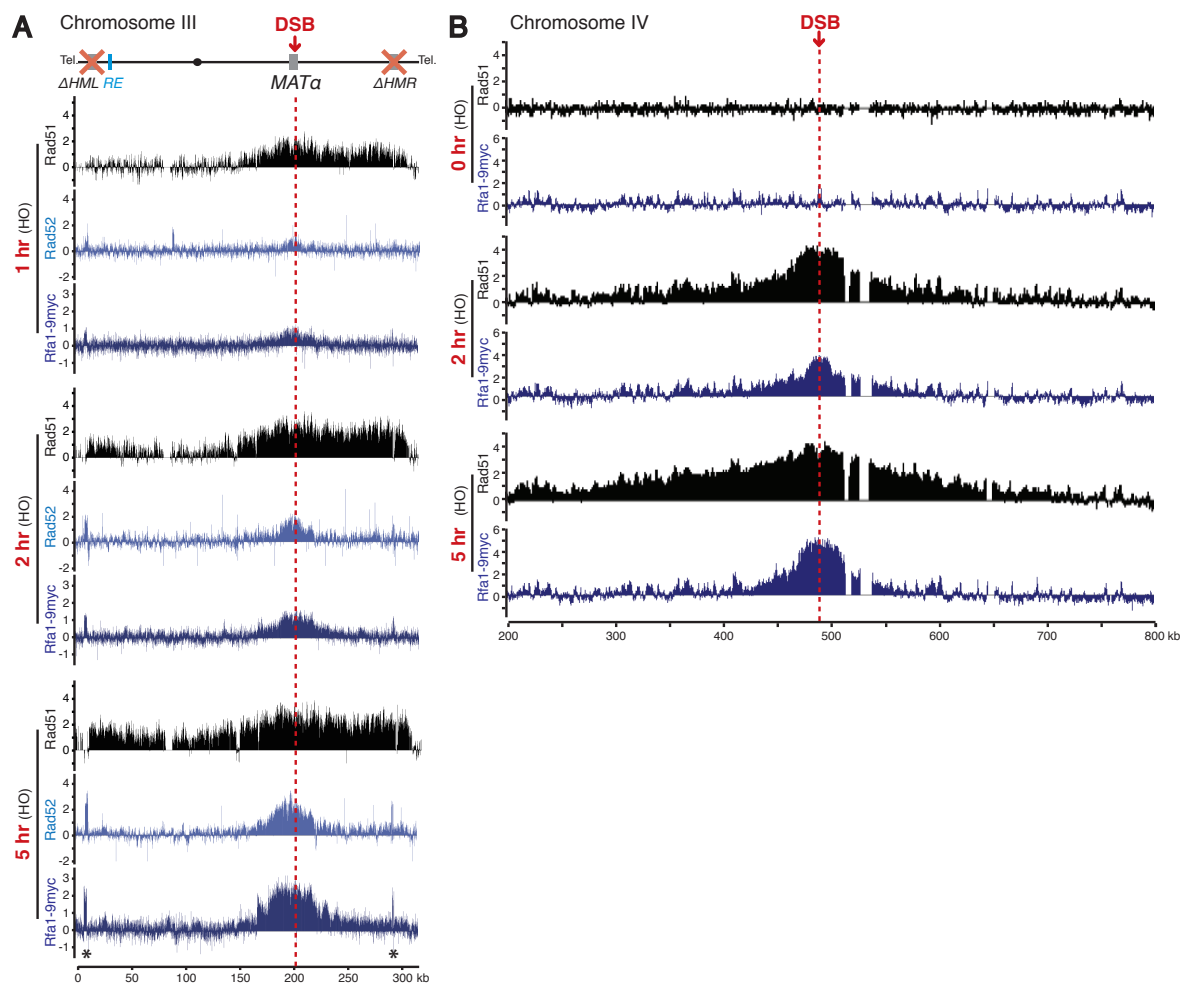


Figure 12. DSB-distant Rad51 ChIP signals exceed the area of resection.

(A) Top: Map of chromosome III of donor-deficient *MATa*. Bottom: Time-resolved ChIP-chip profiles of Rad51, Rad52, and RPA (Rfa1-9myc) for chromosome III obtained 1, 2 and 5 hrs after HO induction. Asterisks denote experimental Rad52 and RPA peaks, which resulted from the use of tiling arrays that (unlike the strains used for ChIP) harbored *HML* and *HMR* sequences. Note that different tiling arrays (with a different median genome probe density) were used for Rad51, RPA and Rad52 ChIP-chip experiments (see Materials and Methods, section 6.3.4), which has been controlled to not affect the overall results (data not shown).

(B) Time-resolved ChIP-chip of Rad51 (same data as in Figure 10) and RPA (Rfa1-9myc) obtained in the strain of Figure 10A (single HO-cleavage site on chromosome IV). Profiles for a region of chromosome IV (200 – 800 kb) are shown before (0 hr) and 2 and 5 hrs after HO induction. Red arrows and red dashed lines indicate DSB positions. ChIP-chip data represent the mean of two experiments and are depicted on a log2 scale. Gaps in ChIP-chip data correspond to repetitive DNA. DSB: DNA-double-strand break; HO: HO endonuclease; *RE*: recombination enhancer element; Tel: Telomere.

4.1.6 DSB-distant Rad51 ChIP Signals are Indicative of Recombination

Competence

A key prediction of the ongoing homology search model is a correlation between Rad51 ChIP signal intensity and recombination competence: If the DSB-distant Rad51 ChIP signals indeed monitor homology search, a high Rad51 signal at one location would indicate that homology search takes place at this location in many cells. Thus, if a homologous donor sequence would be present at a location with a high Rad51 ChIP signal intensity, the homologous donor sequence should efficiently be used for repair. Conversely, if a homologous donor sequence would be present at a location where a lower Rad51 ChIP signal can be detected, it should be less efficiently used for repair.

To test this prediction we took advantage of the mating-type donor preference. Cells harboring the *MAT α* allele at *MAT* efficiently use the donor sequence of the *HMR* locus (which is located on the right side of the DSB), whereas cells harboring the *MATa* allele at *MAT* efficiently use the donor of the *HML* locus (which is located on the left side of the DSB)³³. Importantly, this donor preference does not result from differences in local chromatin states³³. We thus assumed that homology search might preferentially take place on the right side of the DSB in *MAT α* cells, and on the left side of the DSB in *MATa* cells. Intriguingly, as described above, the DSB-distant Rad51 ChIP signals indeed preferentially locate to the right side of the DSB in *MAT α* cells (Figure 13A), thus reflecting donor preference in *MAT α* cells. To test whether this phenotypic behavior is changed according to donor-preference in *MATa* cells, we performed Chip-chip against Rad51 upon DSB induction in *MATa* cells. Strikingly, in these cells Rad51 ChIP signals distribute preferentially on a broad region on the left arm of chromosome III already 1 hour after induction of the DSB (Figure 13B), in line with donor preference in *MATa* cells. This is in stark contrast to *MAT α* cells in which only weak Rad51 ChIP signals are present in this region even after 2 hours (Figure 13A), whereas high Rad51 ChIP signals appear to the right side of these cells. Hence, the DSB-distant Rad51 ChIP signals correlate with mating-type donor preference.

Interestingly, we observed a broad DSB-distant Rad51 ChIP peak on the left arm of chromosome III in *MATa* cells (Figure 13B). This peak exactly locates to the recombination enhancer (*RE*) element and is absent in *MAT α* cells (Figure 13A). As described above, the *RE* element has been shown to be sufficient for the

establishment of donor preference in *MATa* cells^{35,36}. Upon *RE* deletion, *MATa* cells behave as *MATα* cells and use the *HMR* locus on the right side for repair (instead of the *HML* locus on the left side). We thus deleted the *RE* element in *MATa* cells (*RE* was deleted by deleting 800 bp of the *RE*, which has been shown to be the main element for *RE* function³⁶; this deletion does not interfere with neighboring gene function, but the residual *RE* sequences retain marginal donor preference activity³⁶) and investigated potential changes in the Rad51 profile. Intriguingly, deletion of the *RE* was sufficient to completely change the *MATa* Rad51 profile to the *MATα* Rad51 profile (Figure 13C), again reflecting the known donor preference of this strain.

Notably, DSB-distant Rad51 ChIP signals can be detected on the right side of the DSB in all of the different mating-type strains (Figure 13A-C). Also this is in agreement with a model in which the DSB-distant Rad51 ChIP signals reflect homology search, as it has been previously shown that also *MATa* cells (which “normally” use the *HML* locus on the far left side for repair) can repair the DSB by using the *HMR* locus on the right side if *HML* is absent³⁴. Conversely, *MATα* cells can use the normally inefficient *HML* donor if *HMR* is absent³⁴, which is also in line with Rad51 signals emerging in *MATα* cells at the left arm of chromosome III at late time points (Figure 13B). Thus, the repair decision is most likely a matter of kinetics: the donor sequence that is earlier in closer proximity of the DSB is used for repair. To quantitatively address this aspect, we performed Rad51 ChIP in *MATα*, *MATa* and *MATa ΔRE* strains analyzed by RT-qPCR (Figure 13D). Indeed, in *MATa* cells the Rad51 signal after 1 hour is higher around the “correct” *HML* donor homology on the left side in comparison to the Rad51 signal to the *HMR* donor homology on the right side.

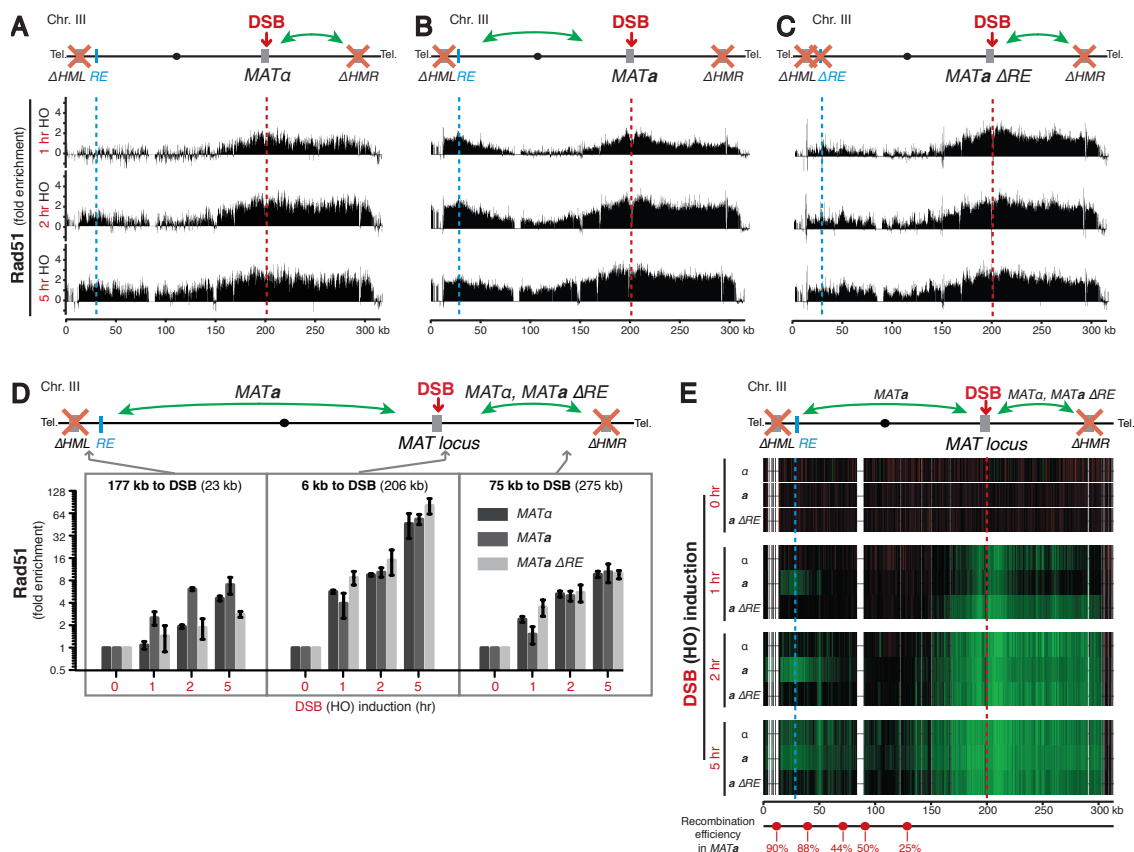


Figure 13. The DSB-distant Rad51 ChIP signals correlate with donor preference in the mating-type system.

(A-C) Top: Maps of chromosome III of donor-deficient *MAT α* , *MAT α* , *MAT α Δ RE* (deleted for the recombination enhancer (*RE*) element) strains and known donor preferences (green arrows; ~90% donor preference in each strain according to ³⁶) of similar repair-proficient strains. Bottom: Rad51-directed ChIP-chip profiles of these strains obtained 1, 2, and 5 hrs after HO induction. Rad51-directed ChIP-chip data of (A) are identical to those of Figure 12G and used for comparison. Positions of the DSB (red dashed lines) and *RE* (blue dashed lines) are indicated. Gaps in the profiles correspond to repetitive DNA.

(D) Rad51-directed ChIP experiments quantitatively analyzed by RT-qPCR controlling the difference in the Rad51 profile between *MAT α* , *MAT α* , and *MAT α Δ RE* cells. Note that 1 hr after DSB induction the ChIP-signals for Rad51 in *MAT α* cells are relatively low (delayed) 75 kb distant to the right of the DSB, but conversely relatively high 187 kb distant to left of the DSB.

(E) Representation of the results from (A-C) without normalization to the 0 hr dataset, and in comparison to recombination efficiency data. Green indicates Rad51 enrichment, red depletion. The lower map shows positions (red dots) where donor-sequences had been inserted and recombination efficiency (in percentage; data from ³⁶) with *MAT* determined.

All data are depicted on a log2 scale. ChIP data are depicted as the mean \pm SEM (standard error of the mean; n=3) of IP/Input ratio normalized to a control locus (chromosome X) and to the 0 hr time point. ChIP-chip data represent the mean of two experiments. Gaps in ChIP-chip data correspond to repetitive DNA. Chr: Chromosome; DSB: DNA-double-strand break; HO: HO endonuclease; *RE*: recombination enhancer element; Tel: Telomere.

To further substantiate the correlation between the DSB-distant Rad51 ChIP signals and repair competence, we compared the obtained Rad51 ChIP profile in *MAT α* cells with previously published data in *MAT α* cells, in which the homologous donor sequence (*HMR*) was integrated at different locations on chromosome III and subsequently analyzed for repair efficiency³⁶. Intriguingly, recombination was

reported to be high (90, 88%) when *HMR* was inserted at positions (12 kb [natural position of *HML*], 41 kb) where the Rad51 ChIP signal intensity is also high, whereas recombination was reported to be low (44%, 50%, 25%) when *HMR* was inserted at positions (at 67, 91, 133 kb) where the Rad51 ChIP signal intensity in our profile are also low (Figure 13E). Thus, this comparison substantiates a correlation between the Rad51 signal intensity and recombination competence.

To further corroborate the correlation between the DSB-distant Rad51 ChIP signals and recombination competence, we constructed *MAT*-independent donor-proficient strains^{§§}. In brief, an HO-cleavage site was integrated at the very same chromosomal location (491 kb) on chromosome IV as in the experiments before, but included flanking sequences of the GFP open-reading frame. In addition, the same sequence with an uncleavable HO site was integrated at three alternative locations on the same chromosome (134, 304, and 329 kb from the DSB, respectively), thereby providing donor sequences for repair. To be able to exclusively monitor DSB repair by the donor homology, a 23 bp “unique” sequence was integrated into the donor homology. If DSB repair takes place via gene conversion using the donor homology, this short unique sequence is copied next to the DSB, which can be monitored by PCR using specific primers. According to our model and the data describe above, a homology should be more efficiently used if it is integrated at locations of high Rad51 ChIP signals compared to locations of lower Rad51 ChIP signals. Indeed, we found that a donor homology was more efficiently for repair if it located at 134 kb distance to the DSB (in a region of high Rad51 ChIP signals) compared to locations in 304 and 329 kb distances (in regions of low Rad51 ChIP signals).

Taken together, the DSB-distant Rad51 ChIP signals correlate well with recombination competence. Particularly, this observation also excludes the hypothetical model that the observed Rad51 ChIP profile may have derived from Rad51 molecules assembled unspecifically along dsDNA away from the DSB at *MAT*.

^{§§} As these experiments were mainly performed by Claudio Lademann (PhD student in the lab), the corresponding data is not illustrated in this thesis, but shortly mentioned due to their significance for the ongoing homology search model.

4.1.7 DSB-distant Rad51 ChIP Signals are Traceable during Active Repair

We showed that DSB-distant Rad51 ChIP signals precisely correlate with the recombination competence (donor preference) in the *MAT* and a *MAT*-independent system. As these data derived from donor-deficient strains, they also suggested that homology search does not require the presence of a homology. To test this, we measured repair kinetics and monitored Rad51 in a donor- and thus repair-proficient *MATa* strain that harbored the *HML* locus at its endogenous location as a homologous donor sequence. Repair kinetics were measured by RT-qPCR using a primer pair which only gives rise to a product if repair takes place (Figure 15A, top part). Despite the great distance (if the chromosome is depicted linearly) between the DSB and the *HML* donor homology located at the left end of chromosome III, repair is highly efficient, starting approximately 1 hour after DSB induction (Figure 14A). In line with previously published data¹¹¹, the repair product increases over time, with most cells repairing the DSB between 2 to 5 hours after induction (Figure 14A). To monitor the DSB-distant Rad51 ChIP signals in this repair proficient strain, we first performed RT-qPCR with primers proximal to the DSB (6 kb downstream), close to the *HML* donor homology (177 kb upstream of the DSB) and at the *RE* element (171 kb upstream of the DSB) (Figure 14B). Indeed, a signal for Rad51 not only proximal but also distal to the DSB can be detected (Figure 14B).

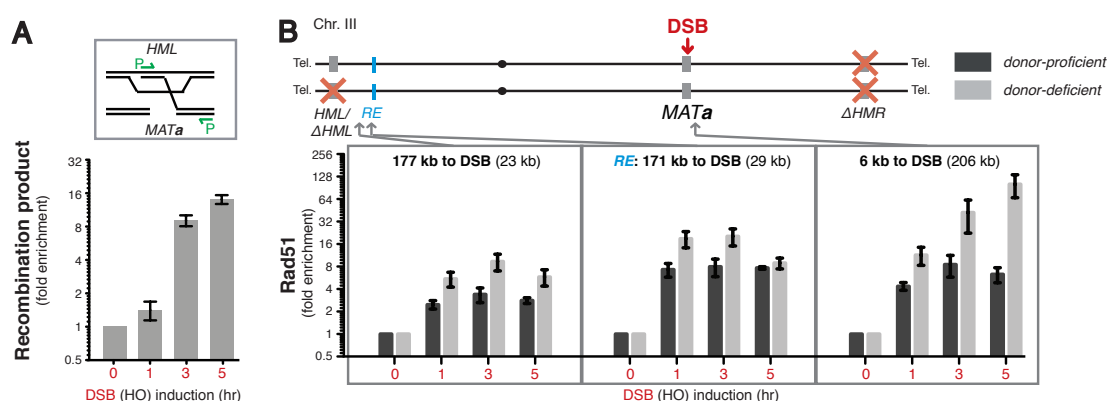


Figure 14. The DSB-distant Rad51 ChIP signals can be detected during ongoing repair.

(A) DSB repair of the *MATa* donor-proficient strain monitored by RTq-PCR. PCR scheme with primers used (green) is shown on top. Detectable repair occurred already 1 hr after DSB induction when Rad51 levels reach *HML* and constantly increased for up to 5 hrs.

(B) Rad51-directed ChIP shows that signals after DSB induction are generally lower in a donor-proficient strain (*HML* containing) compared to a donor (repair)-deficient strain ($\Delta HML \Delta HMR$).

All data are depicted on a log2 scale. ChIP data are depicted as the mean \pm SEM (standard error of the mean; n=3) of IP/Input ratio normalized to a control locus (chromosome X) and to the 0 hr time point. Chr: Chromosome; DSB: DNA-double-strand break; HO: HO endonuclease; P: primer; RE: recombination enhancer element; Tel: Telomere.

Notably, the overall Rad51 signal strength was considerably lower compared to signals derived from the donor-deficient derivative strain (as expected since repair takes place during the experiment) (Figure 14B), but the overall silhouette of the Rad51 profiles appeared similar (Figure 14B and Figure 15A).

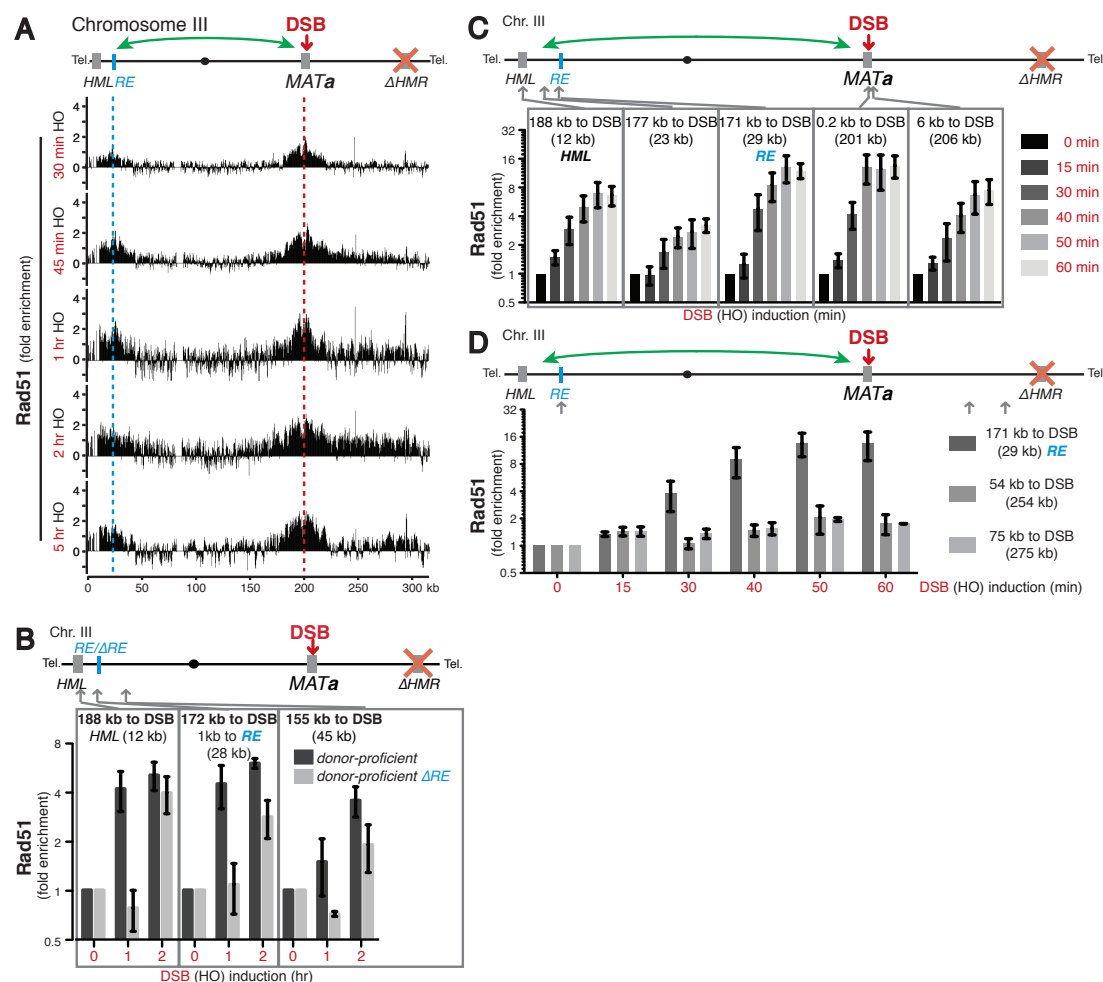


Figure 15. The DSB-distant Rad51 ChIP signals can be detected during ongoing repair.

(A) Rad51-directed ChIP-chip profiles with a donor-proficient strain bearing intact *HML*. Profiles depict early (30 min, 45 min, 1 hr) and late (2 and 5 hrs) time points after transient HO induction (turned off by glucose addition 1 hr after induction), showing early enrichment of Rad51 around the *RE* (blue), and enrichment at the right flank of *HML* (*HML* itself is not present on this array because of homology to *MAT*).

(B) Early Rad51 ChIP signals on the left arm of chromosome III depend on the presence of *RE*. *HML*-specific primers¹¹¹ do not hybridize to *MAT*. Donor-proficient strains are identical to (C), however, the *RE*-deficient strain (gray bars) bears a *RE*-deletion as in Figure 13C.

(C) Rad51-directed ChIP data in the donor-proficient strain at early time-points after DSB induction, showing that Rad51 localizes to the *RE* almost as early as to the DSB.

(D) Similar to (E), but demonstrating that Rad51 localizes earlier at the *RE* in comparison to locations on the right arm of chromosome III.

All data are depicted on a log2 scale. ChIP data are depicted as the mean \pm SEM (standard error of the mean; $n=3$) of IP/Input ratio normalized to a control locus (chromosome X) and to the 0 hr time point. ChIP-chip data represent the mean of two experiments. Gaps in ChIP-chip data correspond to repetitive DNA. Chr: Chromosome; DSB: DNA-double-strand break; HO: HO endonuclease; *RE*: recombination enhancer element; Tel: Telomere.

To map the DSB-distant Rad51 ChIP signals during repair in detail, we performed time-resolved ChIP-chip experiments, especially focusing on very early time-points (as repair starts to take place already approximately 1 hour after HO induction). Interestingly, the Rad51 directed ChIP-chip revealed a distinct peak at the *RE* as early as 30 min after induction of HO endonuclease^{***} (Figure 15A). At this time point DSB-proximal Rad51 signals are highly confined to 5-10 kb around the DSB, and can only be additionally observed proximal to the *RE* (Figure 15A).

Notably, the Rad51 profile around the *RE* subsequently expanded over time (Figure 15A) and accumulated next to the *HML* donor homology. Hence, we concluded that the DSB-distant Rad51 ChIP signals and thus the putative ongoing homology search appear to be directly guided by the recombination enhancer element. In line with this model, RT-qPCR experiments revealed that the Rad51 signals on the left chromosome arm depended on the *RE* (Figure 15B). Moreover, Rad51 ChIP signals were detected at the *RE* as early as at the DSB, and occurred with similar signal intensities at the *RE* and the DSB (Figure 15C). Additionally, Rad51 signals appear considerably earlier on the left than on the right chromosomal arm (Figure 15D).

From these data we thus conclude that DSB-distant Rad51 ChIP signals can be monitored not only in the absence but also in the presence of a homologous donor sequence.

^{***} Note that the time from galactose addition until full galactose-induced HO expression is reported to last itself already around 30min.

4.1.8 DSB-distant Rad51 ChIP Signals Depend on a DNA-Binding Site of Rad51

Rad51 (RecA) harbors two DNA-binding sites. One site binds to ssDNA to allow nucleoprotein filament formation, whereas the second DNA-binding site allows homology probing in dsDNA upon strand invasion^{116,117}. As homology search involves constant homology probing, we speculated that homology search might depend on the second DNA-binding site of Rad51.

To test this idea, we made use of a recently described separation-of-function mutant variant of Rad51 (Rad51-II3A), in which three charged amino acids (R188, K361 and K371) of the second DNA-binding site were replaced by alanine residues¹¹⁷. Rad51-II3A is known to form filaments on ssDNA like the WT protein, but lacks the ability to bind DNA with its second DNA-binding site¹¹⁷. We integrated the gene for the *rad51-II3A* variant (expressed as the only source of Rad51 from its endogenous locus) in the yeast genome and performed Rad51 ChIP upon DSB induction in the mating-type system in comparison to a Rad51 WT control strain. Interestingly, RT-qPCR analysis revealed only a modestly lower signal of Rad51-II3A at a DSB-proximal location (0.2 kb downstream), whereas no Rad51 ChIP signals were detectable at DSB-distant locations (54 and 75 kb downstream) (Figure 16A).

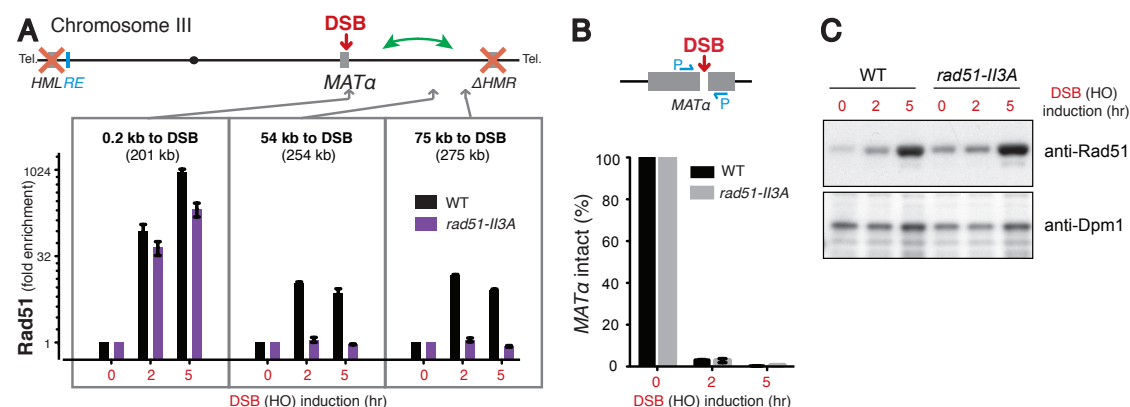


Figure 16. DSB-distant Rad51 ChIP signals depend on the second DNA-binding site of Rad51.

(A) Rad51-directed ChIP in donor-deficient *MATa* WT and *rad51-II3A* (R188A, K361A, K371A) mutant strains, indicating that DSB distant Rad51 ChIP signals are lost with the respective mutant. ChIP data are depicted on a log2 scale as the mean \pm SEM (standard error of the mean; $n=3$) of IP/Input ratio normalized to a control locus (chromosome X) and to the 0 hr time point.

(B) Samples of (A) were analyzed for efficient DSB induction, using the same method as in Figure 8B. DSB induction is as efficient in WT as in *rad51-II3A* cells. Data are depicted on a linear scale as the mean \pm SEM (standard error of the mean; $n=3$) and are normalized to a control locus (chromosome X) and against the signal before DSB induction (set to 100%).

(C) Samples of (A) were analyzed for Rad51 protein levels, revealing similar protein levels.

Chr: Chromosome; DSB: DNA-double-strand break; HO: HO endonuclease; RE: recombination enhancer element; Tel: Telomere.

Notably, DSB induction (Figure 16B) and Rad51 protein levels were similar in Rad51 WT and *rad51-II3A* cells (Figure 16C). We thus concluded that the DSB-distant Rad51 signals depend on the second DNA-binding site of Rad51, in line with the ongoing homology search model. Moreover, this finding also excludes the hypothetical possibility that the DSB-distant Rad51 ChIP signals are only a result of spatial proximity between the DSB and chromatin without homology probing.

4.2 Nuclear Organization Influences Homology Search

Collectively, we demonstrated in the previous sections that the DSB-distant Rad51 ChIP signals depend on Rad51 mediators, locate outside of the maximal area of resection, correlate with recombination competence, depend on the second DNA binding site of Rad51, and are a general phenomenon upon formation of a single DSB in *S. cerevisiae*. All these findings are not only in perfect accordance with the proposed ongoing homology search model, but also disprove alternative models for the origin of the DSB-distant Rad51 ChIP signals. Namely, that the DSB-distant Rad51 ChIP signals derive (1) not from Rad51 filaments on long tracks of ssDNA, (2) not from high Rad51 protein levels in the nucleus, (3) not from Rad51 filament formation on dsDNA, (4) and not from spatial proximity between DSB and chromatin without homology probing. Consequently, we here conclude that the DSB-distant Rad51 signals indeed monitor ongoing homology search *in vivo*. This enables to study for the first time how homology search functions mechanistically in the crowded environment of the nucleus. Thus, we next aimed to investigate how homology search is influenced by chromosomal and nuclear organization.

4.2.1 The *RE* element can Guide Homology Search *in trans*

The data presented in the previous sections demonstrate that homology search preferentially functions on the broken chromosome. Moreover, our findings showed that the *RE* element establishes donor preference in the yeast mating-type system by guiding homology search *in cis* to the “correct” donor sequence (*HML*) in *MATa* cells (Figure 13). Previously, it has been demonstrated that the *RE* does not only increase recombination efficiency *in cis*, but also *in trans* when transplanted to another chromosome than chromosome III³⁷. Hence, we speculated that the *RE* can also guide homology search *in trans* to another chromosome, likely due to tethering of the *MAT*-bearing chromosome with the *RE*-bearing chromosome.

To test this idea, we transplanted (in a *MATa* strain deleted for the endogenous *RE* on chromosome III) approximately 800 bp of the *RE* (the main part responsible for donor-preference³⁶) to chromosome V.

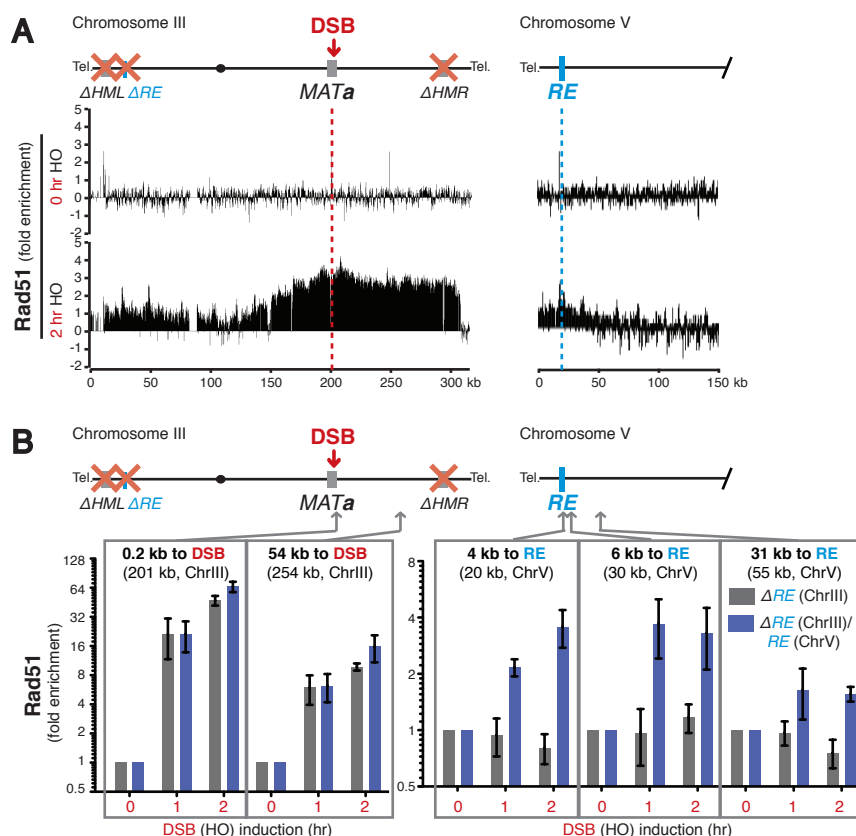


Figure 17. The *RE* element can guide homology search in *trans* from *MAT* to chromosome V.

(A) Rad51-directed ChIP-chip profile depicting chromosome III (left) and an area of chromosome V (right) in a donor-deficient *MATa ΔRE* strain, in which the *RE* element has been transplanted to chromosome V. Rad51 signals are enriched around the transplanted *RE*.

(B) Rad51-directed ChIP in the strain of (A) and a control strain without *RE* transplantation to chromosome V. Homology search is guided from the DSB on chromosome III to the *RE*-bearing chromosome V after DSB induction.

All data are depicted on a log2 scale. ChIP data are depicted as the mean \pm SEM (standard error of the mean; $n=3$) of IP/Input ratio normalized to a control locus (chromosome X) and to the 0 hr time point. ChIP-chip data represent the mean of two experiments. Gaps in ChIP-chip data correspond to repetitive DNA. DSB: DNA-double-strand break; *RE*: recombination enhancer element; Tel: Telomere.

DSB induction at the *MAT* locus on chromosome III and subsequent genome-wide Rad51-directed ChIP analysis revealed a similar Rad51 profile on chromosome III compared to the data obtained in a strain lacking the transplanted *RE* element (Figure 13C and Figure 17A, left panel), but revealed additional Rad51 signals at and around the *RE* on chromosome V (Figure 17A, right panel). Notably, the Rad51 signals at and around the transplanted *RE* are rather small in signal intensity (Figure 17A, right panel).

Such a small signal intensity is in line with previously reported recombination data³⁷, showing that recombination via this *RE* position can take place *in trans*, though less efficiently in comparison to the endogenous location and activity *in cis*. To corroborate the Rad51-directed ChIP-chip data, we performed quantitative RT-

qPCR with primer pairs for chromosome V (in 4, 6 and 31 kb distance to the location of the transplanted *RE*), comparing the strain bearing the transplanted *RE* or a control strain without the transplanted *RE* (Figure 17B). This experiment demonstrates that the Rad51 ChIP signals on chromosome V indeed directly result from the transplanted *RE* (Figure 17B). Thus, the *RE* can guide homology search not only to otherwise distant elements *in cis*, but also *in trans* to other chromosomes.

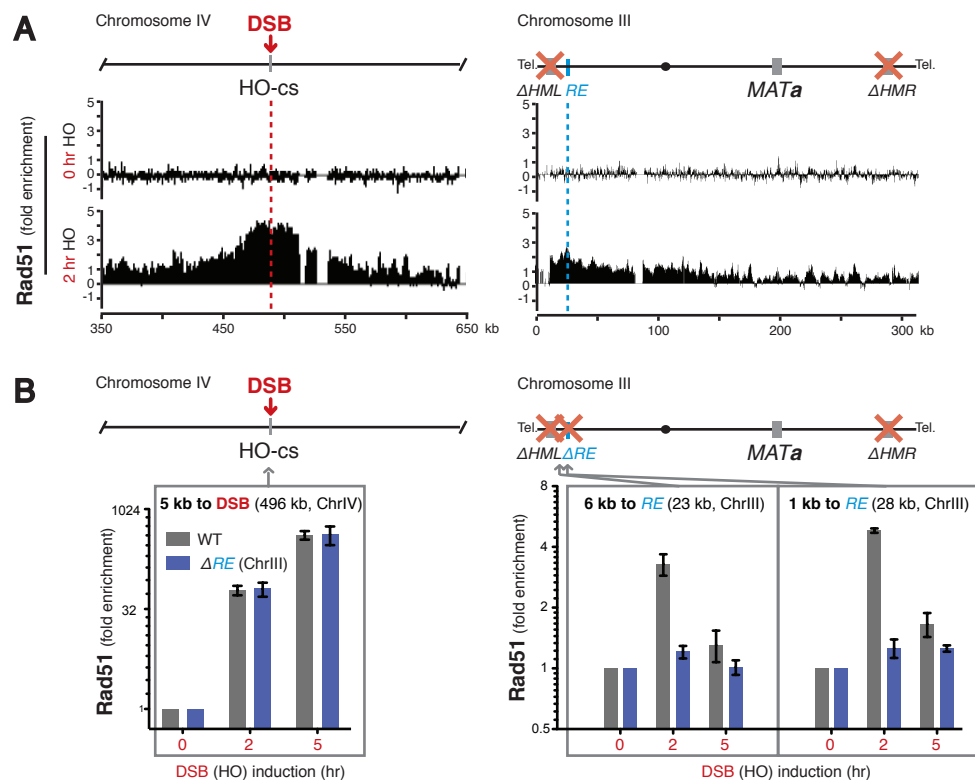


Figure 18. The *RE* element can guide homology search *in trans* from an HO-cleavage site to another chromosome.

(A) Rad51-directed ChIP-chip profile depicting an area of chromosome IV (left) bearing the inducible DSB and depicting the entire chromosome III (right). Rad51 signals are not only present on the broken chromosome, but also on the left arm of chromosome III, peaking at the *RE* element. Data derived from the same experiments as depicted in Figure 10B.

(B) Rad51-directed ChIP in a strain bearing a single HO-cleavage site at 491 kb on chromosome IV and a derivative strain bearing a deletion of the *RE* element on chromosome III. Homology search is only guided from the DSB to chromosome III after DSB induction if the *RE* is present.

All data are depicted on a log2 scale. ChIP data are depicted as the mean \pm SEM (standard error of the mean; $n=3$) of IP/Input ratio normalized to a control locus (chromosome X) and to the 0 hr time point. ChIP-chip data represent the mean of two experiments. Gaps in ChIP-chip data correspond to repetitive DNA. DSB: DNA-double-strand break; *RE*: recombination enhancer element; Tel: Telomere.

Establishment of donor preference by the *RE* element has been investigated using parts of the entire *RE* element, allowing the discovery of specific sequences mediating donor-preference³⁶. However, it is currently unclear which region of the *MAT* locus is required for *RE*-mediated donor preference. Intriguingly, we observed that only the HO recognition sequence is sufficient to guide homology search to the

RE. Specifically, when we induced a DSB on chromosome IV by the HO endonuclease (using a *MATa* strain in which the endogenous HO cleavage site on chromosome III was deleted, but the endogenous *RE* on chromosome III was still present (Figure 10A)), we observed Rad51 ChIP signals at and around the endogenous *RE* on chromosome III (Figure 18A).

Likewise, HO-mediated DSB induction in a strain bearing an HO-recognition site on chromosome I resulted in Rad51 ChIP signals at and around the endogenous *RE* on chromosome III (Figure 10A). Notably, in both strains, only a 36 base pairs recognition sequence (bearing no flanking sequences of the *MAT* locus) for the HO endonuclease was integrated on either chromosome I or chromosome IV. To substantiate this finding we also deleted the endogenous *RE* in the corresponding strain and analyzed Rad51 signals by RT-qPCR. This revealed a complete loss of Rad51 ChIP signals in the area in which the *RE* is normally located (Figure 18B).

4.2.2 Centromeres can Guide Homology Search *in trans*

Close inspection of the genome-wide Rad51 ChIP-chip data upon DSB induction on chromosome I or chromosome IV revealed Rad51 ChIP signals also at centromeres of all chromosomes. Importantly, these signals are not only detectable directly at centromeres, but also on surrounding regions.

As these signals are relatively small and do not obviously peak at a specific location, we evaluated these ChIP signals in columns, combining in each column all Rad51 ChIP signals present in a chromosomal region of 20 kb (Figure 19). This analysis indeed revealed reproducible Rad51 ChIP signals 40 to 80 kb around the centromeres of all chromosomes specifically upon DSB induction on chromosome I or chromosome IV (Figure 19), independently whether the DSB is induced by the HO or the *SceI* endonuclease (data not shown).

Notably, in the strains in which we found centromeric Rad51 ChIP signals, the DSB was positioned relatively close to the centromere of the respective broken chromosome (approximately 30 and 40 kb for chromosome I and IV, respectively). In *S. cerevisiae*, clustering of centromeres, also in interphase, represents a well-known hallmark of nuclear organization^{118,119,120,121}. Thus, we speculated that centromere-proximal DSB induction on one chromosome could result in detectable homology search around the centromeres *in trans* on all other chromosomes due to spatial proximity. To test this model, we generated a strain analogous to the strain bearing a *SceI* cleavage site close to the centromere of chromosome IV, but placed the *SceI* cleavage site 270 kb away from the centromere. Subsequent Rad51 ChIP analysis revealed a highly similar profile of Rad51 on the effected chromosome in both strains (Figure 20A), however, no centromeric Rad51 ChIP signals were detectable (Figure 20B). Furthermore, centromeric Rad51 ChIP signals were also not detectable upon DSB formation in *MAT* on chromosome III, probably because the centromere of chromosome III is far away from *MAT* (Figure 20B). Moreover, experiments described in the following sections include Rad51-directed genome-wide ChIP experiments with strains bearing inducible DSBs either close to the centromere of chromosome V or XII, which revealed again detectable Rad51 ChIP signals at centromere-proximal regions of all unaffected chromosomes (Figure 21, Figure 22, and data not shown).

We thus conclude that centromere-proximal DSBs do not only result in an efficient homology search on the affected chromosome, but also results in detectable homology search (Rad51 ChIP) signals in centromere-proximal regions of all other chromosomes, likely due to centromere-clustering. Notably, this centromere-linked behavior of homology search might explain why centromere-proximal sequences have been described to recombine more efficiently¹⁰⁰.

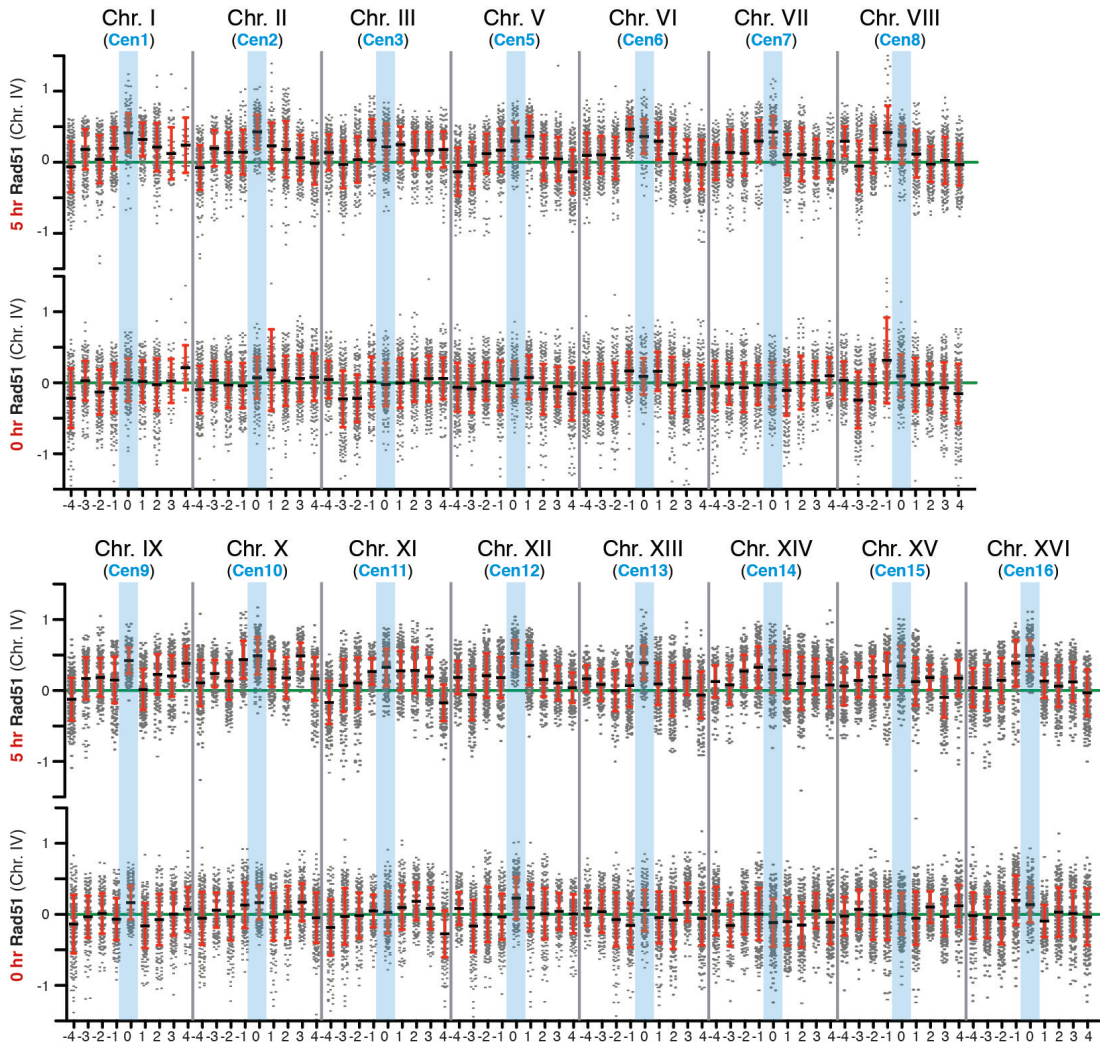


Figure 19. Rad51 ChIP signals can be detected at and around all centromeres upon formation of a centromere-proximal DSB.

Rad51-directed ChIP-chip signals before (0 hr) and after (5 hrs) DSB induction on chromosome IV (*Scel* cleavage site at position 491 kb). ChIP Signals surrounding the centromeres of all yeast chromosomes are depicted in columns (with the exception of 49 outlier signals [ChIP artifacts], from approximately 55,000 total signals) within 20 kb windows (numbered from -4 to 4) centered around the corresponding centromere.

Data are depicted on a log₂ scale, the mean of the entire genome is set to 0 (indicated as a horizontal green line), and the standard deviation is plotted in red. Data derived from the same datasets as depicted in Figure 10. Chr: chromosome; Cen: centromere.

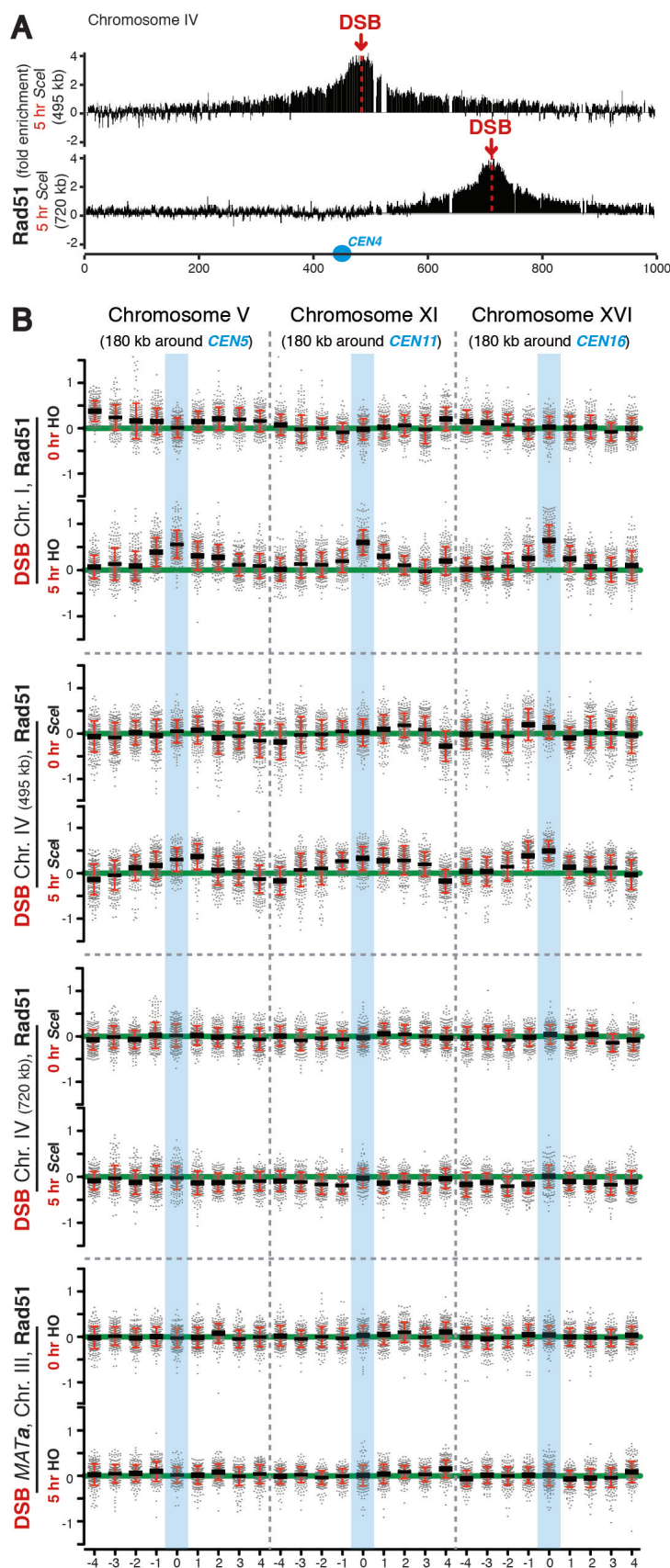


Figure 20. Rad51 ChIP signals around centromeres require a centromere-proximal DSB.

(A) Rad51-directed ChIP-chip profile of chromosome IV in strains bearing a single *Scel* cleavage site either at a centromere-proximal (upper panel) or centromere-distal (lower panel) position. Apart from their shifted position on the chromosome, the profiles appear with similar silhouettes. The position of the centromere is indicated by a blue dot. ChIP-chip data represent the mean of two experiments

(B) Rad51 ChIP signals before and 5 hrs after DSB induction surrounding centromeres of yeast chromosomes V, XI and XVI (shown as examples). Grouped in columns are all ChIP-chip signals (with the exception of 5 outlier signals [ChIP artifacts], from approximately 25,000 total signals) within 20 kb windows centered around the corresponding centromere. Significant Rad51 signals are detectable around all centromeres when the DSB is induced by either HO or *Scel* on chromosome I or chromosome IV, respectively (upper two panels). The signals are lost when the *Scel*-cleavage site on chromosome IV is placed to a centromere-distant position (compare second upper and middle panel). No Rad51 signals around centromeres can be detected via HO break induction at the *MAT* locus (second lowest panel). The mean of the entire genome is set to 0 (highlighted as a horizontal green line), and the standard deviation is plotted in red. Data correspond to Figure 10A and C, Figure 13B and Figure 20A.

All data are depicted on a log2 scale. Chr: chromosome; Cen: centromere; DSB: DNA double-strand break; HO: HO endonuclease; *Scel*: *Scel* endonuclease.

To confirm these earlier findings, we used the repair assay described in section 4.1.6 and inserted donor homologies at different distances to the centromere of chromosome VII. Subsequently, we induced a centromere-proximal DSB on chromosome IV and measured repair with the donor homologies on chromosome VII. This experiment revealed that repair is indeed more efficient if a homology is located in proximity to the centromere (data not shown^{‡‡}). Taken together, homology search (and thus recombination efficiency) appears to be influenced by centromere-clustering, an integral part of nuclear organization in *S. cerevisiae*.

^{‡‡} Experiments were mainly performed by Claudio Lademann (PhD student in the lab)

4.2.3 Homology Search upon Single DSBs in Proximity of Different Nuclear Landmarks

Prompted by the previous findings we next asked whether homology search is generally influenced by nuclear organization. Next to centromere-clustering, telomere positioning represents an important phenomenon of nuclear organization in *S. cerevisiae*¹²¹. Telomeres are positioned at the nuclear periphery^{122,123}, mediated by telomere-binding proteins, such as Sir4 involved in the establishment of silent telomeric chromatin¹²⁴. Moreover, preferential spatial proximity between several telomeres has been reported¹²², which depends on similar chromosome arm length rather than on specific factors^{123,125}.

To elucidate how homology search is influenced by telomere positioning, we generated a strain harboring a *Scel* endonuclease cleavage site in the subtelomeric region (to avoid cloning into the repetitive telomeric DNA) of the left chromosomal arm of chromosome V (at the location 23 kb), and performed Rad51-directed ChIP-chip experiments before and after DSB induction (Figure 21A). This experiment revealed the expected distribution of Rad51 preferentially on the effected chromosome V: downstream of the DSB (away from the telomere), Rad51 ChIP signals were detectable to a distance of approximately 150 kb. However, minor Rad51 signals might be present spanning almost the entire chromosome until the right chromosomal end (Figure 21A, left panel). Upstream of the DSB (further into the telomeric and subtelomeric region), the Rad51 signals do not appear to be obviously effected by the subtelomeric location (of note, telomeric oligonucleotides are not present on the tiling array due to their repetitive nature) (Figure 21A, left panel).

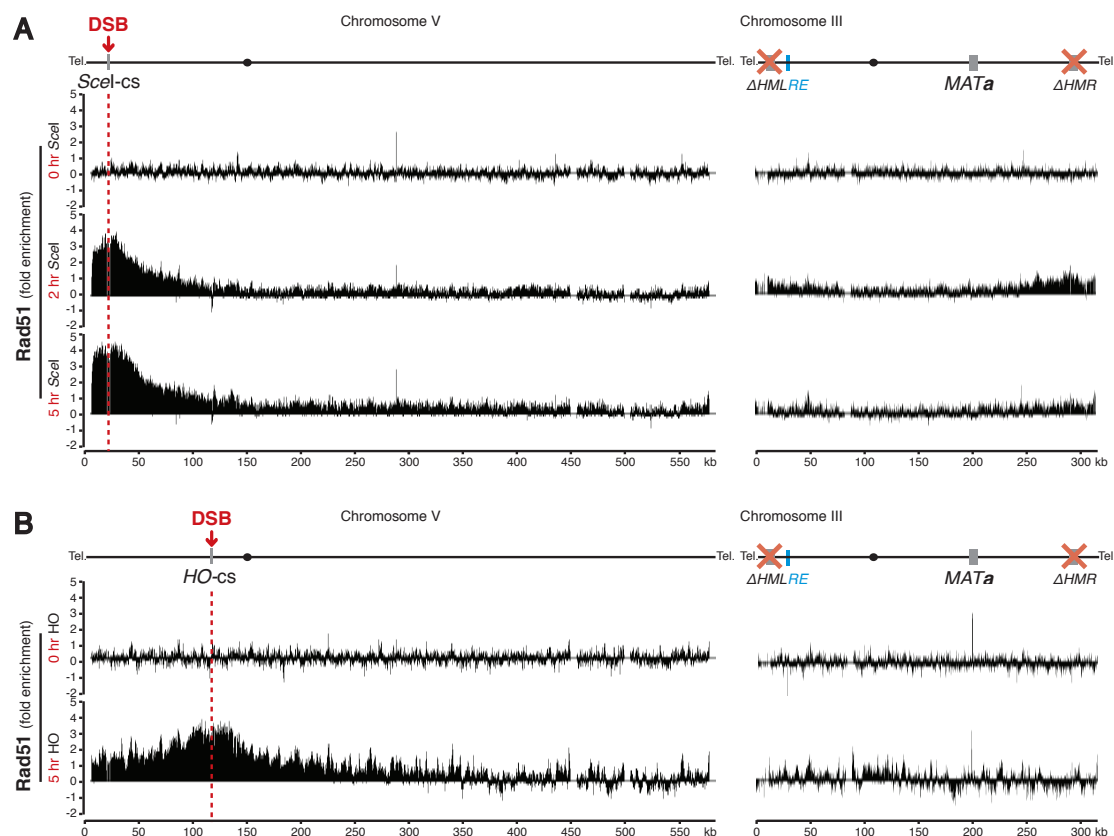


Figure 21. Homology search upon DSB induction at a telomere-proximal location.

(A) Rad51-directed ChIP-chip profiles of chromosomes V (left) and III (right) before (0 hr) and after DSB (*Scel*) induction (2 and 5 hrs) in a strain bearing a single *Scel* cleavage site on chromosome V at a telomere-proximal location. Note the appearance of Rad51 signals on the right and mildly on the left chromosomal arm of chromosome III upon DSB induction, especially after two hours.

(B) Rad51-directed ChIP-chip profile of chromosomes V (left) and III (right) before (0 hr) and after DSB (HO) induction (5 hrs) in a strain bearing a single HO cleavage site on chromosome V at a location which is approximately 100 kb downstream of the DSB in (A). Note that the DSB is centromere-proximal and thus Rad51 signals can be detected on all other centromeres (data not shown).

Telomeric oligonucleotides are not present on the tiling array due to their repetitive nature. ChIP-chip data are depicted on a log2 scale. Data in (A) represent the mean of two experiments, whereas data in (B) derive from one single experiment. Gaps in ChIP-chip data correspond to repetitive DNA. DSB: DNA double-strand break; HO: HO endonuclease; HO-cs: HO endonuclease DNA cleavage site; *Scel*: *Scel* endonuclease; *Scel*-cs: *Scel* endonuclease DNA cleavage site; Tel.: telomere.

Importantly, we also found Rad51 ChIP signals on the right and very mildly on the left chromosomal end of chromosome III (Figure 21A, right panel). Moreover, small signals were also detected on telomeres of other chromosomes (especially at telomeres on chromosomes with similar short chromosomal arms; data not shown). Notably, no Rad51 ChIP signals at telomeres of the unaffected chromosomes can be observed when we analyzed a strain bearing an endonuclease cleavage site in 120 kb distance to the left telomere of chromosome V (Figure 21B), however, it should be noted that the strain derives from a different strain background and is based on a different endonuclease (HO). Taken together, a telomere-proximal DSB on chromosome V does not only result in Rad51 ChIP signals on same chromosome, but also in Rad51 signals at the chromosomal ends of chromosome III and potentially

very mildly at the ends of other chromosomes. However, further experiments have to be carried out to support these initial findings.

To further elucidate the behavior of homology search in the context of nuclear organization, we investigated homology search upon a DSB that is proximal to the tandem array of genes encoding ribosomal subunits (rDNA repeats). In *S. cerevisiae*, the rDNA repeats locate to one single genomic locus on chromosome XII and comprise 100 to 200 repeats of 9.1 kb each, resulting in an overall size of 1 to 2 megabases (depending on the number of repeats present in the individual strain/cell) and a volume of approximately one third of the nucleus¹²¹. Interestingly, high-throughput 3C data showed that the left chromosomal arm (upstream of the rDNA repeats) lacks interaction with the right chromosomal arm (downstream of the rDNA repeats), thus the rDNA repeats separate both chromosomal arms¹¹⁹. Hence, we generated two strains bearing either a *Scel* cleavage site distal or proximal (in a distance of approximately 55 kb upstream to avoid resection proceeding into the rDNA repeats) to the rDNA repeats, and followed homology search upon DSB induction by Rad51-directed ChIP-chip experiments before and after DSB induction (Figure 22). As for strains harboring DSBs on other chromosomes, the Rad51 profile monitored upon induction of a DSB proximal to the rDNA repeats preferentially locates to the affected chromosome XII (Figure 22A). In addition, the overall Rad51 profile appears similar in comparison to the Rad51 profile of a DSB located distal to the rDNA repeats (Figure 22B). However, downstream of the rDNA-proximal DSB, Rad51 can be traced with high signals until but not beyond the rDNA repeats (Figure 22A). Importantly, the scale of the chromosomal axis depicted in Figure 22 derives from SGD (Saccharomyces genome database), which annotates the overall length of the rDNA region as approximately 40 kb, whereas the actual length ranges from 1-2 megabases. On the one hand, in light of this considerable size of the rDNA repeats, it might not appear astonishing that Rad51 cannot be detected on the other side of the rDNA repeats upon DSB induction. On the other hand, this is also in line with the separation of both chromosomal arms by the rDNA repeats, as high degree of spatial proximity of both arms would likely result in traceable Rad51 signals. Whether homology search can proceed into the rDNA repeats themselves remains to be tested by RT-qPCR using unique primers, as oligonucleotides representing the rDNA repeats are not present on the genome-wide tiling arrays.

In summary, these data indicate that in addition to centromeres and the *RE* element also nuclear organization by telomeres and rDNA-repeats influence

homology search (Rad51 ChIP signals). Experiments that might further strengthen the conclusion that homology search is influenced by nuclear organization, and implications from this conclusion for the overall mechanism of homology search are described in detail in the discussion (section 5.3).

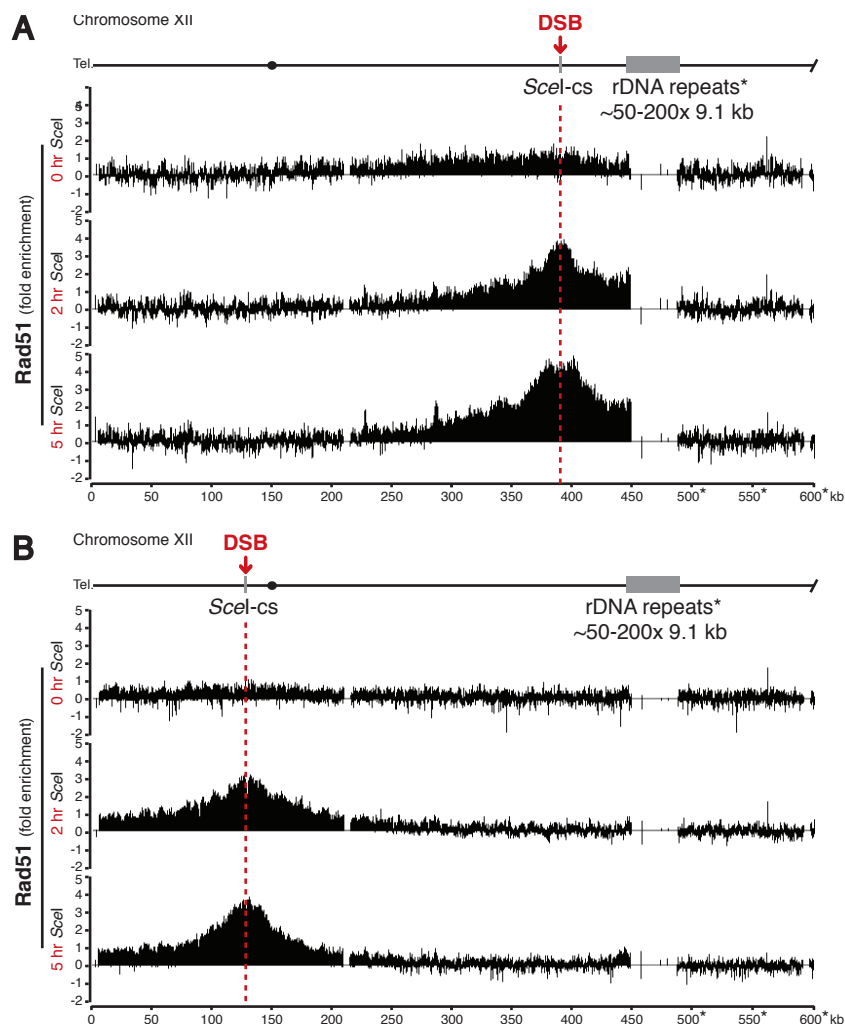


Figure 22. Homology search upon DSB formation at an rDNA repeat-proximal location.

(A) Rad51-directed ChIP-chip profile of a part of chromosome XII before (0 hr) and after DSB (*Scel*) induction (2 and 5 hrs) in a strain bearing a single *Scel* cleavage site on chromosome XII at a rDNA repeat-proximal location. Note that in this dataset Rad51 signals around the *Scel* cleavage site are detectable even before break induction (0 hr), which might result from a higher *Scel* background expression due to a high number of transformed *Scel* endonuclease encoding plasmids in this experiment.

(B) As in (A), but using a strain bearing a single *Scel* cleavage site on chromosome XII at a rDNA repeat-distal location. Note that the DSB is centromere-proximal and thus Rad51 signals can be detected on all other centromeres (data not shown). ChIP-chip data in (A) and (B) represent single experiments.

Gaps in ChIP-chip data correspond to repetitive DNA (such as the rDNA repeats). The rDNA region consists of 100-200 repeats with each 9.1 kb length. Asterisks: Importantly, the scale of the chromosomal axis derives from the SGD (Saccharomyces genome database), which annotates the overall length of the rDNA region as approximately 40 kb, whereas the actual length ranges from 1-2 megabases (depending on the number of repeats in the individual cell/strain). ChIP-chip data are depicted on a log2 scale. Data in (A) and (B) derive from single experiments. Gaps in ChIP-chip data correspond to repetitive DNA. DSB: DNA double-strand break; *Scel*: *Scel* endonuclease; *Scel*-cs: *Scel* endonuclease DNA cleavage site; Tel.: telomere.

4.3 Components and Requirements of Homology Search

The possibility to study for the first time homology search *in vivo*, also allows for an investigation of the components and requirements of homology search.

4.3.1 Role of the Single-Strand Binding Protein RPA during Homology Search

The main ChIP signals of RPA and Rad52 are restricted to the area of resection (as described in detail in section 4.1.5). Nevertheless, close inspection of the RPA- and Rad52 ChIP profiles upon DSB induction on chromosome IV or in the *MAT α* locus on chromosome III reveal low, but highly reproducible signals for both factors at DSB-distant locations. Upon DSB induction on chromosome IV, RPA signals mildly distribute further away from the DSB, in a symmetrical manner similar to Rad51 (Figure 12H). These RPA signals could hypothetically derive from sustained symmetrical long-range resection around the DSB in a minor pool of cells. However, upon DSB induction in the *MAT α* locus, these minor RPA and Rad52 ChIP signals distribute not symmetrically around the DSB (Figure 23A). They rather locate to the entire right arm of the chromosome (Figure 23B), where the strongest homology search-reflecting Rad51 ChIP signals are locating as well. It should be noted that these RPA and Rad52 ChIP signals are rather low and almost not detectable by RT-qPCR experiments (Figure 12A and B). However, ChIP-chip analysis indicates that these signals are significant, as these signals can be observed on huge chromosomal regions (which includes a high number of different oligonucleotides) around the DSB.

To directly test whether these signals are of biological relevance, we tested whether the distribution of the minor RPA pools is different depending on the mating-type. We thus performed ChIP experiments for Rfa1-9myc in *MAT α* cells. Intriguingly, Rfa1-9myc ChIP signals distribute again to the right side of DSB, but significantly more pronounced on the very left chromosomal arm (Figure 23C) and peaking around the *RE* (Figure 23D), in line with donor preference in *MAT α* cells.

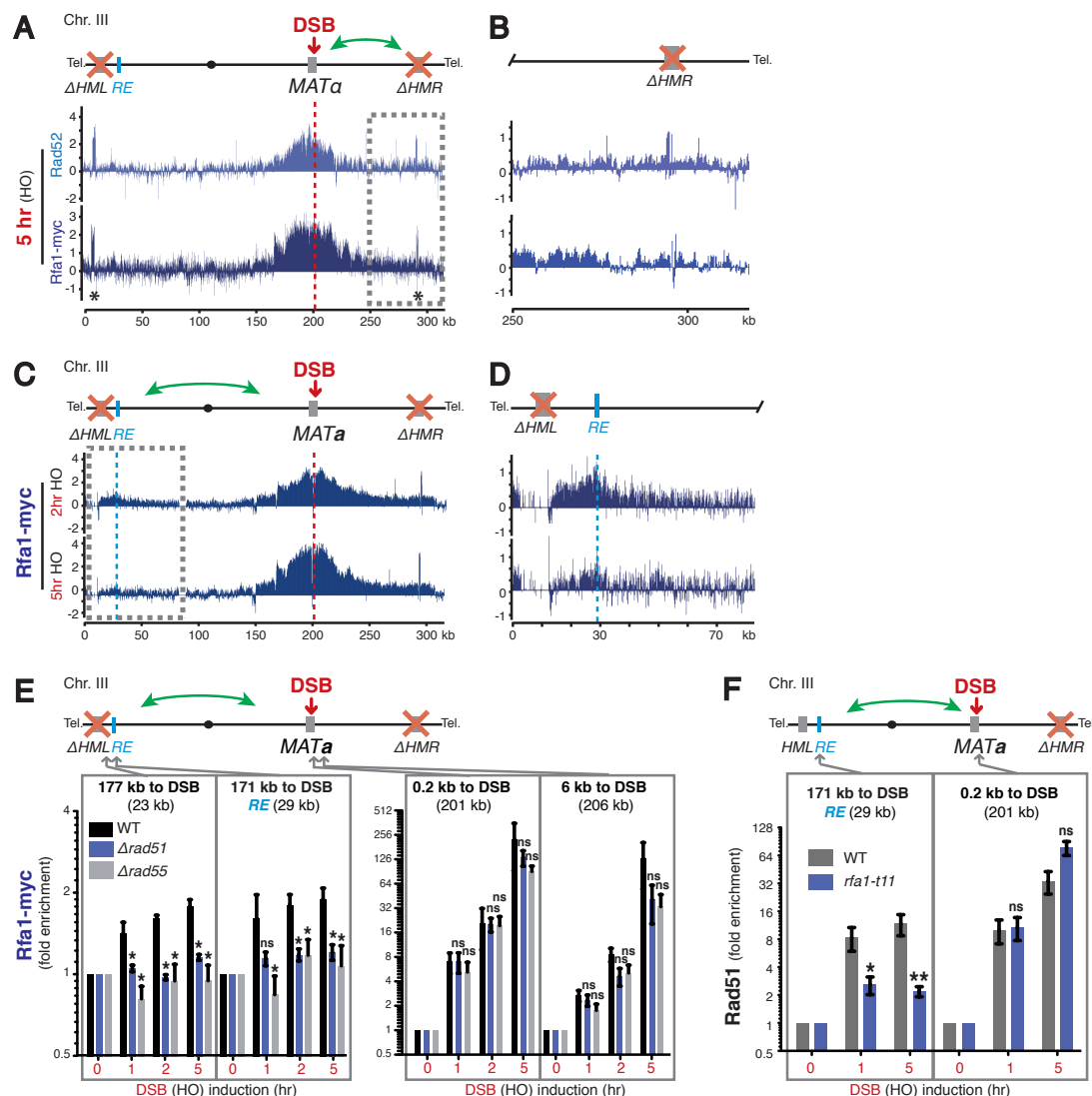


Figure 23. The single-strand binding protein RPA has a potential role during homology search.

(A) Rfa1-9myc and Rad52-directed ChIPs result in a minor RPA and Rad52 pool (highlighted in the boxed area) on the right side of the DSB, in a *MATa* donor-deficient strain. These data represent a part of data depicted in Figure 12G.

(B) Enlarged representation of the boxed area in (A)

(C) Rfa1-9myc-directed ChIP as in (A), but in a *MATa* donor-deficient strain. In addition to the minor RPA pool on the right side of the DSB, a minor RPA pool peaking at the *RE* can now be detected on the left chromosomal arm (highlighted in the boxed area).

(D) Enlarged representation of the boxed area in (C).

(E) Rfa1-9myc-directed ChIP using donor-deficient *MATa* cells as in (C), investigating the appearance of RPA by RT-qPCR in areas surrounding the *RE*. These DSB-distant but not the DSB-proximal RPA signals depend on Rad51 and Rad55.

(F) Rad51-directed ChIP in donor-proficient *MATa* WT and *rfa1-t11* (K45E) mutant strains, indicating reduction of Rad51 signals around the *RE* in the mutant.

All data are depicted on a log2 scale. ChIP data are depicted as the mean \pm SEM (standard error of the mean; n=4) of IP/Input ratio normalized to a control locus (chromosome X) and to the 0 hr time point. Asterisks indicate p < 0.1; double asterisks indicate p < 0.015; ns: not significant (Kruskal–Wallis one-way analysis of variance). ChIP-chip data represent the mean of two experiments. Gaps in ChIP-chip data correspond to repetitive DNA. DSB: DNA-double-strand break; Tel.: Telomere.

This finding indicates that the DSB-distant RPA ChIP signals might be caused by homology search. First, it is not evident from the literature and from this study that the extent of resection is different depending on the mating-type. Second, long-range

resection along the entire chromosomal axis as the cause for the DSB-distant RPA ChIP signals (e.g. at the *RE*) can be excluded, as these signals are traceable at the DSB and the *RE*, however not in-between these locations. Hence, the minor RPA pool might be caused by homology search.

To directly test this hypothesis and to exclude that the signals derive artificially by crosslinking chromatin in spatial proximity, we performed Rfa1-9myc ChIP experiments in *MATa* cells deficient (deleted for Rad51 or Rad55) in homology search. To monitor the RPA ChIP signals quantitatively by RT-qPCR, we investigated locations with highest RPA ChIP signals, specifically the *RE* (171 kb to DSB) and a location between the *RE* and *HML* (177 kb to DSB). Intriguingly, no RPA ChIP signals can be observed at these locations in $\Delta rad51$ or $\Delta rad55$ cells (deficient in homology search), compared to significant ChIP signals in WT cells (Figure 23E). Importantly, resection appears to proceed normally in these mutant derivatives, as RPA ChIP signals at locations close to the DSB (0.2 and 6 kb) is similar between WT, $\Delta rad51$ and $\Delta rad55$ cells (Figure 23E). Consequently, the DSB-distant RPA ChIP signals depend on Rad51 and Rad55, and are thus likely caused by homology search.

To substantiate this finding we took advantage of a previously described replication-proficient but recombination-deficient RPA mutant variant (*rfa1-t11*)¹²⁶. Rad51 still forms filaments in *rfa1-t11* cells, but is defective in Rad51-mediated strand invasion¹²⁶. Therefore, we performed Rad51-directed ChIP in *MATa rfa1-t11* and WT cells, and analyzed Rad51 ChIP signals directly next to the DSB (0.2 kb) and at a location of ongoing homology search (at the *RE*; 171 kb to DSB). Interestingly, whereas Rad51 filament formation indeed appears not to be affected (Figure 23F), Rad51 ChIP signals at the *RE* are drastically reduced (Figure 23F). Thus, homology search appears to be affected in the *rfa1-t11* mutant variant.

In summary, these data argue for a role of the single-strand binding protein RPA during homology search. The weak RPA ChIP signals at positions of ongoing homology search might be explained by patches of RPA locating next to patches of Rad51 nucleoprotein filaments, thus creating at all transient encounters of homology search also a ChIP signal for RPA. Such a model would also explain why the DSB-distant RPA ChIP signals are lost in cells expressing mutants defective in homology search. However, the finding that Rad51 ChIP signals are reduced in cells expressing an RPA mutant variant, argues for a more active role of RPA during homology search.

4.3.2 Efficient Homology Search Requires Rad54

Rad54 is a well-known mediator of homologous recombination implicated to function at a variety of different steps of the repair pathway¹²⁷. It belongs to the Snf2/Swi2 family of SF2 helicases, which contains a motor domain for translocation on dsDNA without separation of the DNA double-strand¹²⁸. Described functions of Rad54 during homologous recombination range from early to late steps in the pathway¹²⁹, by stabilizing the presynaptic Rad51 filament¹¹⁰, facilitating D-loop formation¹³⁰, promoting branch migration¹³¹, and removing Rad51 from DNA when repair has been completed¹³².

Especially due to its described function in mediating D-loop formation, we hypothesized that Rad54 might be directly involved in homology search. We generated a mutant strain deficient in Rad54 ($\Delta rad54$) and performed preliminary Rad51-directed ChIP experiments before and after DSB induction at the *MAT* locus. Interestingly, the DSB-distant (homology search-reflecting) Rad51 ChIP signals were indeed lowered in the $\Delta rad54$ mutant in comparison to WT, whereas the DSB-proximal Rad51 ChIP signals were only mildly affected (Figure 24). However, homology search does not appear to be completely blocked, as residual homology search-reflecting Rad51 ChIP signals were traceable (Figure 24).

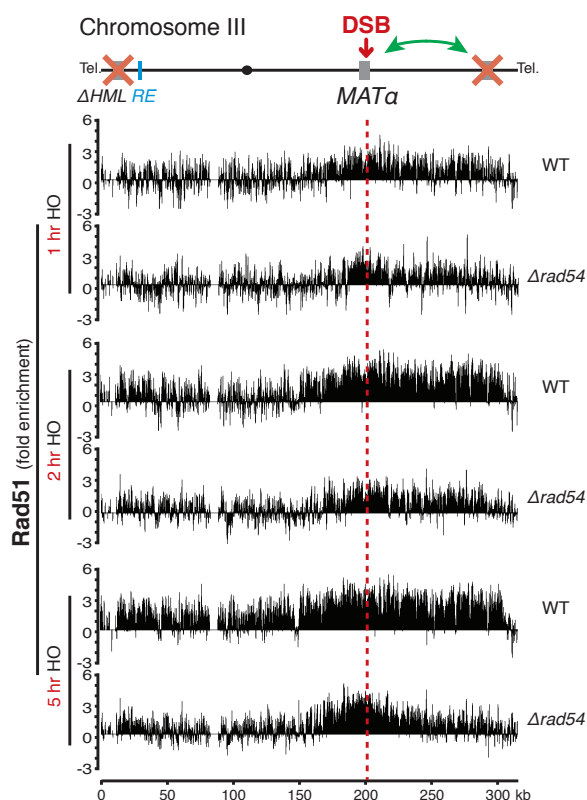


Figure 24. The Snf2/Swi2 family motor protein Rad54 is required for efficient homology search.

Rad51-directed ChIP-chip profiles of the entire chromosome III, 1, 2 and 5 hours upon DSB (HO) induction in donor-proficient *MATα* WT and $\Delta rad54$ mutant strains. Note that the Rad51 ChIP signals are most prominently reduced at DSB-distant locations in the $\Delta rad54$ mutant strain. However, also DSB-proximal signals appear slightly reduced.

Single spikes correspond to artificial signals (in this specific experiment a high grade of background noise is present). ChIP-chip data derive from a single experiment and are depicted on a log2 scale. Gaps in ChIP-chip data correspond to repetitive DNA. DSB: DNA double-strand break; HO: HO endonuclease; *RE*: recombination enhancer element; Tel: telomere.

Rad54 functions preferentially in mitotic DSB repair together with the recombinase Rad51, whereas its homologue Rdh54 has been demonstrated to interact preferentially with the meiosis-specific Rad51 homologue Dmc1¹³³. However, Rdh54 has been described to partially compensate for a loss of Rad54 in mitotic DSB repair¹³⁴. Thus, we hypothesized that the residual homology search signal might depend on Rdh54, and investigated Rad51 signals in a mutant strain deficient for Rdh54, and a mutant strain deficient for both, Rad54 and Rdh54^{§§}. Interestingly, in the $\Delta rdh54$ mutant strain, Rad51 signals at the break site were similar to WT, whereas distant Rad51 homology search signals were reduced, but to a lesser extent than $\Delta rad54$ mutant strains. In line, when both, Rad54 and Rdh54 were deleted, homology search appears to be almost completely blocked. We thus found homology search depends on Rad54 and its homologue Rdh54. Moreover, these results demonstrate that homology search is not an intrinsic feature of the Rad51 recombinase on its own, but requires additional factors.

^{§§} As these experiments were mainly performed by Claudio Lademann (PhD student in the lab), the corresponding data is not illustrated in this thesis, but shortly mentioned due to their significance in supporting the Rad54 data.

4.3.3 Phosphorylation of Histone 2A Follows Homology Search

Mec1/Tel1-mediated phosphorylation of histone 2A (γ H2A) represents one of the earliest responses upon DSB formation⁴⁷ (see section 2.4 for details). Importantly, this posttranslational modification can be observed over large regions around a DSB¹³⁵, in mammals even at the scale of megabases⁵⁴. However, potential functions of the γ H2A modification over such large distances on chromatin remain rather speculative⁴⁷.

Interestingly, published genome-wide ChIP studies upon DSB induction in *S. cerevisiae* cells of the *MAT α* mating-type revealed γ H2A ChIP signals on almost the entire chromosome III, especially on the right arm⁵². The significance of this observation had not been discussed in the respective paper, however, it suggested to us that the pattern of γ H2A might be linked to homology search. To test this idea, we first established γ H2A-directed ChIP (Figure 25). Using a γ H2A-directed antibody, ChIP signals were detected proximal (6 kb) and distal (54 and 75 kb) to the DSB in the *MAT* locus (Figure 25A). In contrast, no γ H2A ChIP signals were detected directly next to the DSB (0.2 kb) (Figure 25A), in line with previous reports¹³⁵ that histone eviction occurs locally around the DSB upon resection.

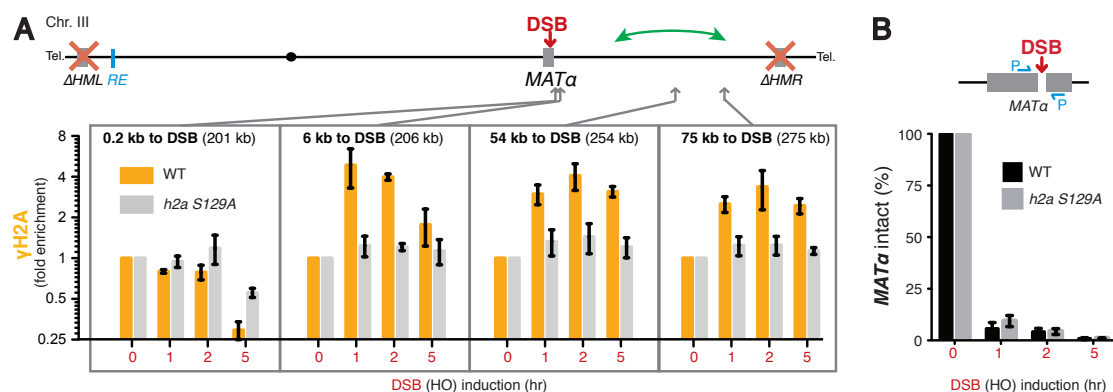


Figure 25. Specificity of γ H2A-directed ChIP experiments.

(A) Upon DSB induction, the γ H2A-directed ChIP control experiment reveals signals at 6, 54 and 75 kb next to the DSB. However, no γ H2A ChIP signals are detectable directly at the break (0.2 kb), and they gradually disappear over time 6 kb away from the DSB, most likely due to formation of ssDNA (resection). The absence of ChIP signals in the phospho-site *h2a S129A* mutant demonstrates the specificity of the γ H2A-directed ChIP. ChIP data are depicted as the mean \pm SEM (standard error of the mean; $n=3$) of IP/Input ratio normalized to a control locus (chromosome X) and to the 0 hr time point.

(B) Samples of (A) were analyzed for efficient DSB induction, using the described method in Figure 8B. DSB induction is as efficient in WT as in *h2a S129A* mutant variant cells. Data are depicted on a linear scale as mean \pm SEM (standard error of the mean; $n=3$) and are normalized to a control locus and against the signal before DSB induction (set to 100%).

DSB: DNA-double-strand break; HO: HO endonuclease; RE: recombination enhancer element; Tel.: telomere; γ H2A: phosphorylated form of histone 2A at Serine 129 (*S. cerevisiae*).

Accordingly, γ H2A ChIP signals at a distance of 6 kb to the DSB constantly decline after 1 hour of DSB formation (Figure 25A), in agreement with the finding that resection affects this location at this time (Figure 12). Notably, γ H2A ChIP signals are specific, as no signals were detected in a strain expressing the respective phosphorylation-defective H2A mutant (serine 129 to alanine) (Figure 25A), despite similar DSB induction in this mutant variant strain with a WT strain (Figure 25B).

We next tested whether γ H2A ChIP signal distribution is different depending on the mating-type (as the homology search-reflecting Rad51 ChIP signal distribution). Therefore, we performed γ H2A-directed genome-wide ChIP experiments in *MAT α* and *MAT a* cells. As reported⁵², γ H2A signals preferentially locate to the right side of the DSB in *MAT α* cells (Figure 26A). Moreover, overlay of the γ H2A and Rad51 profiles demonstrates an intriguing similarity (Figure 26A), apart from the area of ssDNA around the DSB.

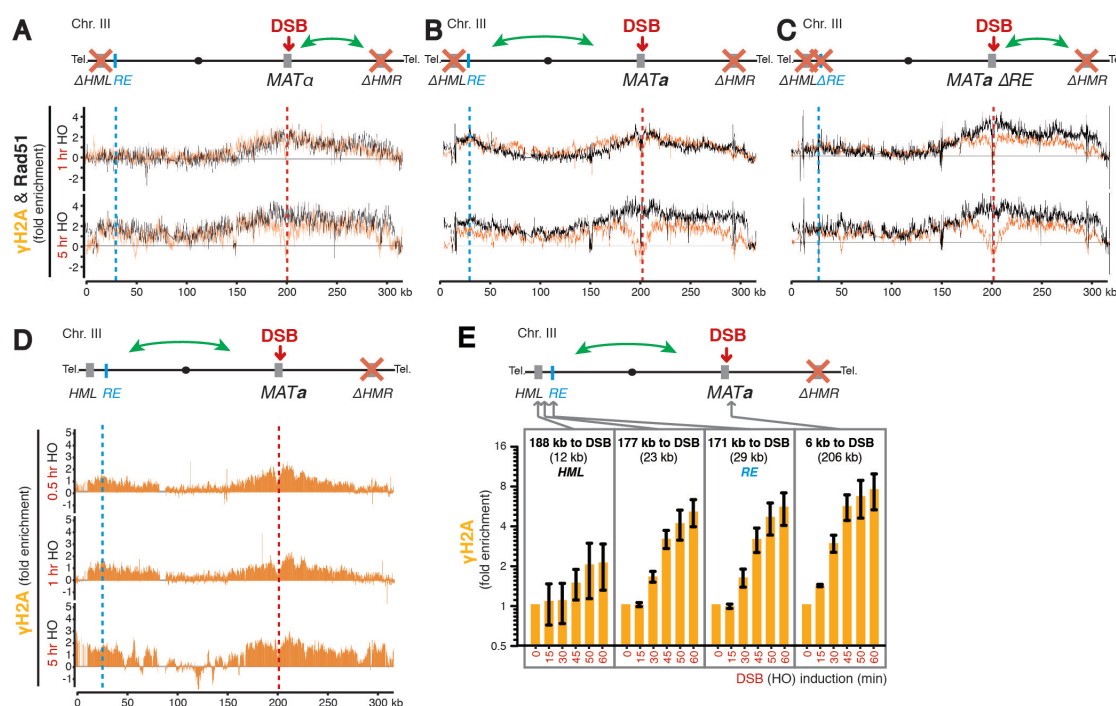


Figure 26. γ H2A ChIP signals follow homology search in the mating-type system.

(A-C) Comparison of γ H2A and Rad51 distribution during homology search in the different mating-type strains of Figure 13A-C. Overlay of ChIP-chip profiles obtained with antibodies specific for γ H2A (orange) and Rad51 (black; represents the same data as in Figure 13A-C). The main difference between the two profiles is observed in the area of ssDNA around the DSB.

(D) Early appearance of γ H2A (determined by ChIP) not only at *MAT*, but also at the *RE* and toward *HML* (see map), in the DSB-repairing, donor-proficient strain.

(E) As in (D), but investigating early time-points (15, 30, 40, 50, 60 min) upon DSB induction quantitatively by RT-qPCR.

All data are depicted on a log2 scale. ChIP data are depicted as the mean \pm SEM (standard error of the mean; $n=3$) of IP/Input ratio normalized to a control locus (chromosome X) and to the 0 hr time point. ChIP-chip data represent the mean of two experiments. Gaps in ChIP-chip data correspond to repetitive DNA. Chr: Chromosome; DSB: DNA-double-strand break; *RE*: recombination enhancer element; Tel: telomere; γ H2A: phosphorylated form of histone 2A at Serine 129 (*S. cerevisiae*).

Importantly, the same phenotypic behavior was observed in *MATa* cells (Figure 26B): corresponding to the donor preference for repair and the homology-search reflecting Rad51 ChIP signals, γ H2A ChIP signals distribute preferentially on the left arm of chromosome III, peaking at the *RE*. Moreover, deletion of the *RE* is sufficient to revert the γ H2A ChIP signal distribution of *MATa* cells into the profile of *MAT α* cells (Figure 26C). Thus, the observed γ H2A ChIP profile reflects the pattern of homology search in the mating-type system as observed before for Rad51 ChIP signals.

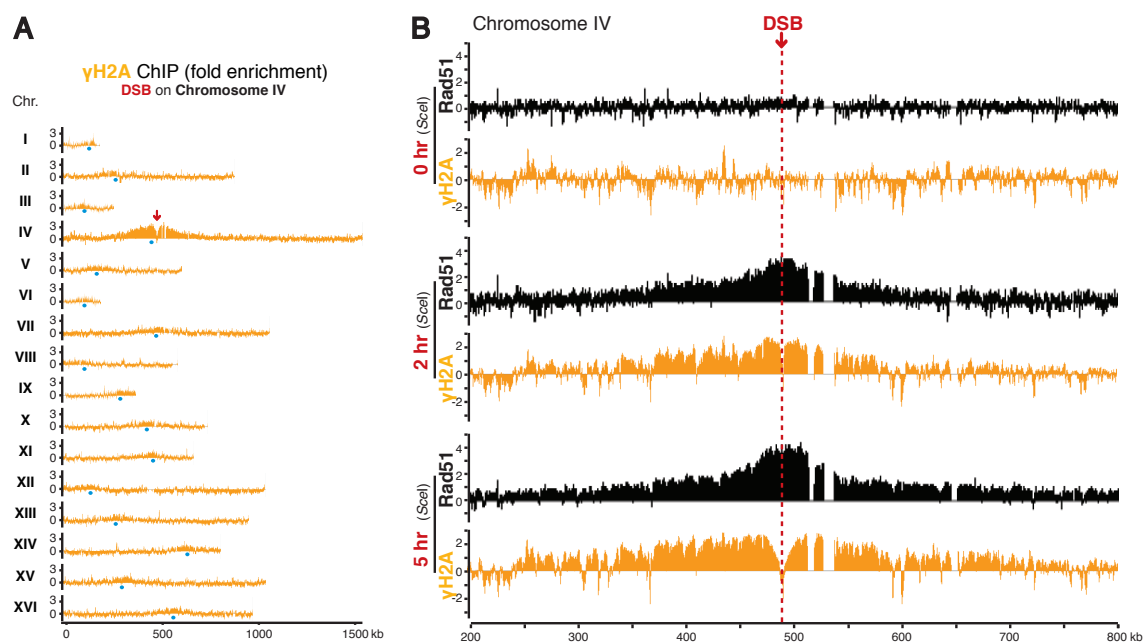


Figure 27. γ H2A ChIP signals also follow homology search on *MAT*-independent chromosomes.

(A) γ H2A-directed ChIP-chip using a strain bearing a single *SceI*-cleavage site (red arrow) on chromosome IV. Profiles for all chromosomes are shown 5 hrs after HO expression. γ H2A accumulates mainly on the broken chromosome, similar to Rad51. Single spikes in the ChIP-chip data correspond to single oligonucleotides, and are hybridization artifacts. Centromeres are indicated as blue dots.

(B) Comparison of γ H2A and Rad51 distribution in a strain bearing a single *SceI* cleavage site (red arrow) on chromosome IV. ChIP-chip profiles obtained with antibodies specific for γ H2A (orange) and Rad51 (black, 5 hrs time point represents same data as in Figure 10C). The main difference between the two profiles is observed in the area of ssDNA around the DSB.

ChIP-chip data are depicted on a log2 scale and represent the mean of two experiments. Gaps in ChIP-chip data correspond to repetitive DNA. *CEN*: Centromere; *Chr*: Chromosome; *DSB*: DNA-double-strand break; *SceI*: *SceI* endonuclease; *SceI*-cs: *SceI* endonuclease DNA cleavage site; *Tel*: telomere; γ H2A: phosphorylated form of histone 2A at serine 129 (*S. cerevisiae*).

Moreover, the observed γ H2A ChIP signal distribution argues against a model in which the distribution of γ H2A is solely explained by a linear spreading mechanism: in *MATa* cells, γ H2A ChIP signals can be observed at regions surrounding the DSB and the *RE*, but not at sequences in between. To substantiate this finding, we performed γ H2A-directed ChIP experiments at early time-points upon DSB induction, and analyzed the γ H2A ChIP signals around the DSB and the *RE*. Indeed, a signal

for γ H2A can be detected at the *RE* as early as at the DSB (Figure 26D and E). In line with this finding, a recent study also reported γ H2A ChIP signals at the *RE* upon DSB induction, however, without discussing its link to homology search³⁸.

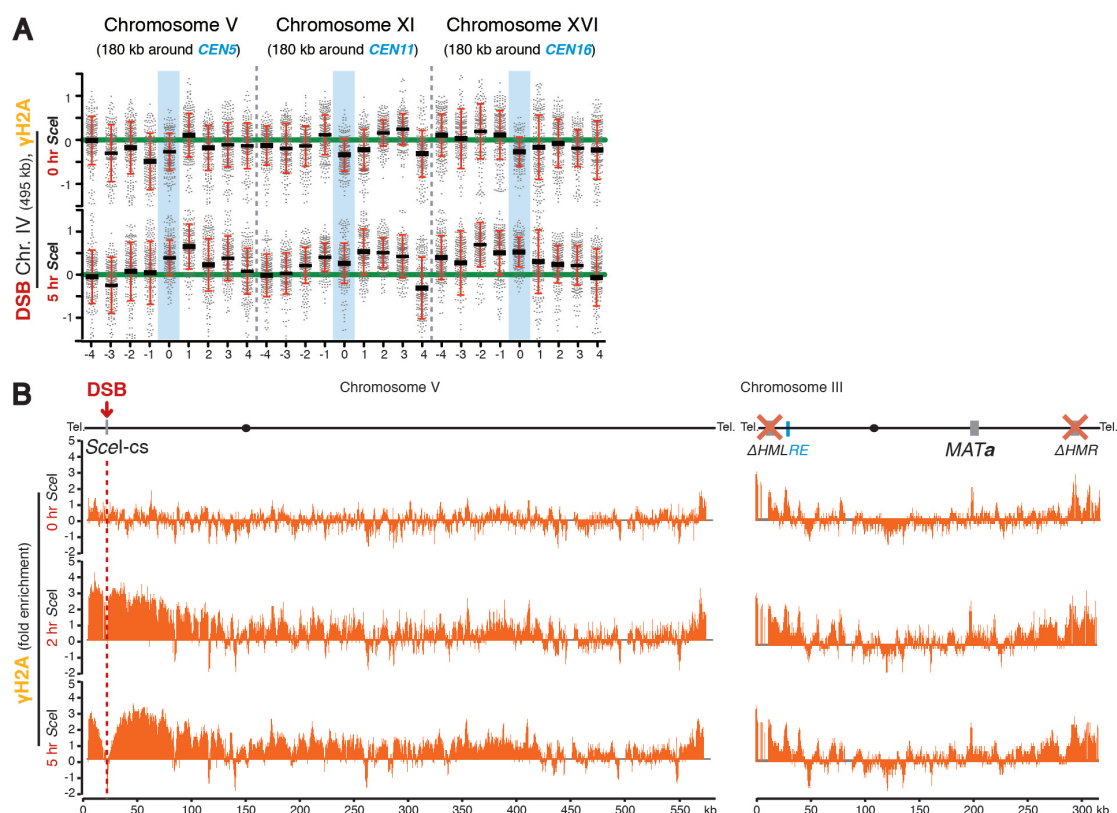


Figure 28. The γ H2A ChIP profile follows homology search according to nuclear organization.

(A) γ H2A ChIP-chip signals before and 5 hrs after DSB induction surrounding centromeres of yeast chromosomes V, XI and XVI. Grouped in columns are all ChIP-chip signals within 20 kb windows centered around the corresponding centromere. Similar to Rad51, γ H2A is enriched around the centromeres. The mean of the entire genome is set to 0 (highlighted as a horizontal green line), and the standard deviation is plotted in red.

(B) γ H2A-directed ChIP-chip profiles of chromosomes V (left) and III (right) before (0 hr) and after DSB (*Scel*) induction (2 and 5 hrs) in a strain bearing a single *Scel* cleavage site on chromosome V at a telomere-proximal location. γ H2A signals are mildly detectable at telomeres even without DSB induction as previously described^{53,136}. However, note that γ H2A signals mildly increase upon DSB induction (on the left telomere of chromosome V) on the right and mildly on the left chromosomal arm of chromosome III.

ChIP-chip data are depicted on a log2 scale and represent the mean of two experiments. Gaps in ChIP-chip data correspond to repetitive DNA. *CEN*: Centromere; Chr: Chromosome; DSB: DNA-double-strand break; *Scel*: *Scel* endonuclease; *Scel*-cs: *Scel* endonuclease DNA cleavage site; Tel: telomere; γ H2A: phosphorylated form of histone 2A at serine 129 (*S. cerevisiae*).

To further test the hypothesis that the γ H2A distribution derives from ongoing homology search, we monitored the genome-wide γ H2A profile upon DSB induction on chromosome IV. Indeed, the observed γ H2A ChIP signal distribution on the effected chromosome again highly resembles the Rad51 ChIP signals (Figure 27A and B). Moreover, γ H2A ChIP signals can also be observed around the centromeres of all chromosomes (Figure 28A). In addition, γ H2A and Rad51 ChIP signal

distributions are also highly similar in a third DSB induction system (HO-recognition site close to the left telomere of chromosome V; see Figure 28B). In conclusion, the observed ChIP signal distributions of γ H2A and Rad51 are highly similar.

Next, we tested whether the γ H2A ChIP signal distribution depends on ongoing homology search. Indeed, DSB-distant γ H2A ChIP signals were reduced in a strain deleted for Rad51 (Figure 29). In line, DSB-distant γ H2A ChIP signals were also decreased in strains deleted for Rad52, Rad55 and Rad57 (Figure 29). Thus, the distribution of γ H2A appears to depend on ongoing homology search. Moreover, this finding also argues that γ H2A ChIP signals constitute another marker for homology search.

We next asked whether the process of homology search itself depends on the concurrent phosphorylation of H2A. If homology search would depend on the concurrent phosphorylation of H2A, a phosphorylation-defective H2A mutant (*h2a S129A*) should be impaired in homology search. Hence, we performed Rad51 ChIP experiments as readout for homology search in WT cells and an *h2a S129A* mutant variant strain. Interestingly, no differences in the Rad51 signal can be detected in a *MAT α* strain 1 to 5 hours after DSB induction (Figure 29). This suggests that the formation of γ H2A is not required for efficient homology search at the genomic locations tested. Nevertheless, γ H2A formation concurrent to homology search might be required in chromatin environments not present at the local positions tested so far, calling for a genome-wide analysis of homology search using the respective non-phosphorylatable H2A mutant.

In summary, we discovered that the γ H2A ChIP profiles differ in the two yeast-mating types, that the γ H2A and Rad51 ChIP profiles highly correlate and that the γ H2A profile depends on Rad51, Rad52 and Rad55/57. This provides substantial evidence that the γ H2A distribution follows ongoing homology search. Moreover, our findings show for the first time that a single DSB on one chromosome does not only result in γ H2A formation *in cis* on the broken chromosome, but also *in trans* on other chromosomes. This indicates that the widely used DSB marker γ H2A does not exclusively label areas of DSBs.

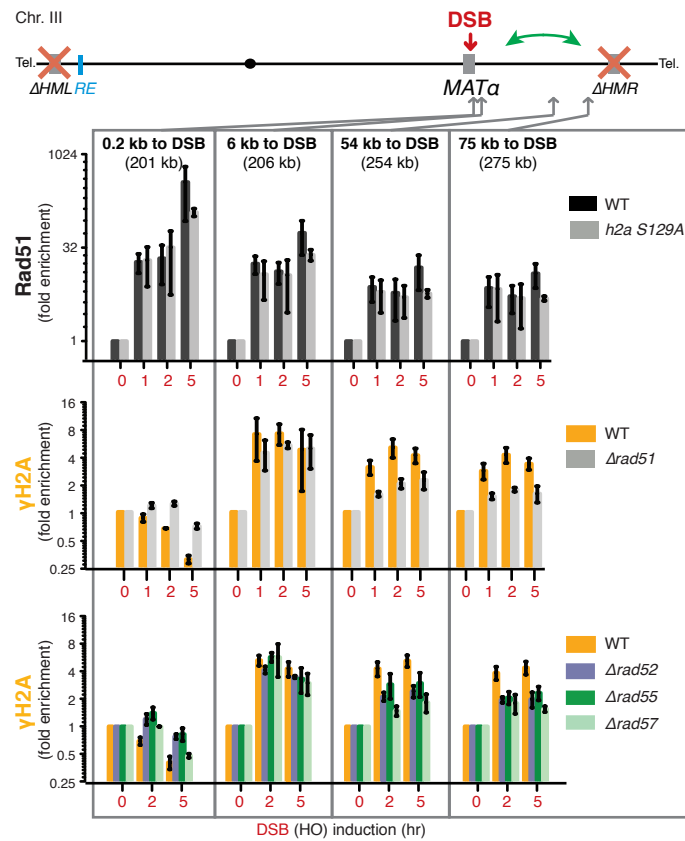


Figure 29. γH2A ChIP signals follow homology search.

Rad51 and γH2A distribution after DSB induction in donor-deficient WT and mutant *MATa* cells. Rad51 distribution (homology search) does not depend on γH2A (H2A phosphorylation-site mutant; *h2a S129A*) (upper panel), however, DSB-distant γH2A signals depend on Rad51 (middle panel), Rad52, Rad55, and Rad57 (lower panel).

All ChIP data are depicted on a log2 scale as the mean \pm SEM (standard error of the mean; $n=3$) of IP/Input ratio normalized to a control locus on chromosome X and to the 0 hr time point. Chr: Chromosome; DSB: DNA-double-strand break; HO: HO endonuclease; *RE*: recombination enhancer element; Tel: telomere; γH2A: phosphorylated form of histone 2A at serine 129 (*S. cerevisiae*).

5 Discussion

5.1 Monitoring Homology Search *in vivo*

Homologous Recombination (HR) represents one of the two main pathways to repair DNA double-strand breaks (DSBs), and numerous mechanisms and components of the pathway are well known^{9,13,14}. However, the fundamental step of homology search, by which the broken sequence and its undamaged homologous counterpart come into direct spatial proximity to allow subsequent repair, remained largely enigmatic^{23,24}. Substantial progress has been recently made on how the recombinase Rad51 (or its prokaryotic homolog RecA) facilitate the recognition of the homologous donor template *in vitro*^{90,92,94}. However, it is important to distinguish between local homology recognition (short-range homology search) and long-range homology search in the nuclear environment²³: Rad51/RecA recombinases facilitate homology recognition, however only when the homologous sequences already co-localize²⁴. Hence, how the broken sequence and its homologous undamaged counterpart get into spatial proximity by long-range homology search remained mysterious, especially in the context of the crowded nuclear environment.

In this study, homology search and its preferred chromosomal probing locations were monitored for the first time *in vivo*. In previous studies, Rad51 was mainly reported to locate directly next to the DSB^{110,111}, in line with Rad51 filament formation on resected DNA next to the DSB. However, the Jentsch lab found an unexpected broad distribution of ChIP signals for the recombinase Rad51 over almost an entire chromosome upon formation of a single DSB⁷⁶. In this study, we demonstrate by several lines of evidence (and by excluding hypothetical alternative models) that the broad distribution of Rad51 (DSB-distant Rad51 ChIP signals) reflects ongoing homology search in the nuclear environment.

Several lines of additional evidence make a strong case for the DSB-distant Rad51 ChIP signals being indicators of ongoing homology search. First, the appearance of the DSB-distant Rad51 ChIP signals coincides with DSB repair (Figure 14 and Figure 15). Second, the observed DSB-distant Rad51 ChIP signals represent not only a specific phenomenon of the yeast mating-type system, but represent also a general phenomenon upon formation of DSBs in *S. cerevisiae* (Figure 10, Figure 20, Figure 21 and Figure 22). Lastly, the DSB-distant Rad51 ChIP

signals perfectly correlate with repair competence: donor homologies placed at locations of high DSB-distant Rad51 ChIP signals are more efficiently used for repair than donor homologies placed at locations with lower DSB-distant Rad51 signals (data not shown^{***} and Figure 13).

Moreover, we excluded hypothetical alternative models as the cause of DSB-distant Rad51 ChIP signals. Specifically, we first excluded that the DSB-distant Rad51 signals derive from Rad51 filaments on long tracks of ssDNA by comparing Rad51 ChIP signals with the extent of resection (Figure 11 and Figure 12). Second, we excluded that the DSB-distant Rad51 ChIP signals derive from Rad51 filament formation on dsDNA by matching the Rad51 ChIP signal distribution with known donor preferences in the yeast mating-type system (Figure 13). Lastly, we excluded - by the use of a separation-of-function mutant variant of Rad51¹¹⁷ (*rad51-II3A*; Figure 16) - that the DSB-distant Rad51 ChIP signals derive from spatial proximity between the DSB and other sequences without homology probing.

Taken together, the collected data strongly suggests that the DSB-distant Rad51 ChIP signals are indicative of transient encounters of the Rad51-coated DSB ends with other DNA sequences during ongoing homology search. Thus, this finding demonstrates that homology search can be monitored *in vivo*. Furthermore, the ability to monitor homology search *in vivo* sheds light into numerous fundamental questions, such as: is every sequence in the genome detected to the same efficiency, or does the nuclear organization influences homology search? What are the components and requirements for homology search?

The following sections will propose answers to these questions by integrating findings from this and earlier studies. Moreover, a comprehensive model for homology search will be proposed ("facilitated 3D/1D homology search model"), which will constitute a framework for the further investigation of homology search and its mechanism in the nuclear environment.

^{***} Experiments were mainly performed by Claudio Lademann (PhD student in the lab); see section 4.1.6 for details.

5.2 Conflicting Models for Homology Search

Studies on homology search so far proposed opposing models for the area of homology search in the genome, ranging from an efficient genome-wide homology search model to a model in which homology search does not exist. This section first introduces these previously proposed concepts, and the subsequent sections discuss these concepts in light of the data collected in this study.

Data on homology search hitherto largely derived from studies investigating homology recognition *in vitro* or investigating ectopic recombination *in vivo* in *S. cerevisiae*. *In vitro*, Rad51/RecA-mediated homology recognition (short-range homology search) has been described to proceed rapidly and efficiently^{93,137,138}, even in the context of nucleosomes^{88,89}. However, these studies are based on random encounter of the homologous sequences and on short Rad51-coated oligonucleotides (see introduction 2.5 for more details). Thus, despite providing information on the mechanism of short-range homology search and local homology recognition, these studies are limited in elucidating how the DSB-bearing chromosome gets into spatial proximity with its intact homologous donor sequence in the crowded nuclear environment (long-range homology search).

Insights into the mechanism of long-range homology search *in vivo* mainly derived from studies in yeast, demonstrating that HR can rather efficiently take place between ectopic (non-allelic) homologous sequences dispersed in the genome (ectopic recombination). In the yeast mating-type system, which harbors the DSB and the homologous donor sequences on the same chromosome, repair (using the *HML* donor homology in 187 kb distance to *MAT*) occurs mostly between 2 and 7 hours upon DSB induction¹¹¹. Moreover, also repair between homologous sequences on different chromosomes can occur in a similar time frame, which was exemplified by placing two copies of the *URA3* gene either on chromosome II or chromosome V, and measuring repair upon DSB induction in one of the *URA3* gene copies^{96,97}. From these and other studies on the efficiency of ectopic recombination in *S. cerevisiae*^{37,98,99,100,101,102,103}, and due to the efficient Rad51/RecA-mediated homology recognition *in vitro*^{93,137,138}, it has been concluded that homology search exists^{139,140} and that homology search proceeds efficiently in a genome-wide manner^{98,104} (Figure 30A).

However, two reviews/opinion articles from Barzel & Kupiec²³ and Weiner et al.²⁴ from 2008 and 2009 provided substantial arguments conflicting the hypothesis of

an efficient genome-wide homology search: both articles calculated that an efficient genome-wide search would require a time that would exceed the observed time of DSB repair by far^{23,24}. Barzel & Kupiec²³ estimated that every individual probing event of a genome-wide search in *S. cerevisiae* could only last 2.5×10^{-4} seconds if one considers a two hours time frame for repair²³. However, a comparison is provided²³, noting that the addition of a single nucleotide by a DNA polymerase during replication already takes 40 times longer, thus making the calculated time frame for a homology probing event virtually impossible. In addition, Weiner et al.²⁴ referred to the considerably lower diffusion of chromosomes in comparison to proteins^{141,142,143}, and estimated – in comparison to the time a single repressor molecule needs to locate to its cognate site in a bacterial chromosome¹⁴⁴ – that a genome-wide chromosomal homology search would require weeks²⁴. Moreover, given the complexity of mammalian genomes¹⁴⁵ and their constraints in chromatin mobility¹⁴⁶, an efficient genome-wide homology search appears even more unlikely in these cells^{23,24}.

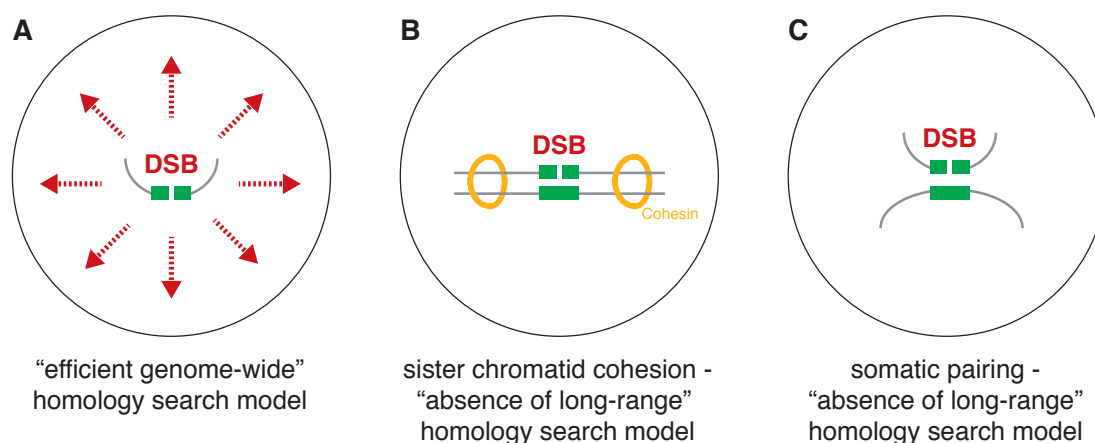


Figure 30. “Efficient genome-wide” versus “absence of long-range” homology search models.

(A) Due to a high efficiency of homology recognition *in vitro*, and due to a high efficiency of ectopic recombination in *S. cerevisiae*, it has been proposed that homology search (red dashed arrows) scans efficiently the entire genome.

(B) As HR largely takes place in the G2 cell cycle phase, repair can use the homologous information on the sister chromatid, which resides in spatial proximity due to cohesin-mediated cohesion (yellow rings). Consequently, long-range homology search might not be required.

(C) The somatic pairing model proposes that all homologous sequences in the nucleus are in close spatial proximity, thus also abolishing the need for long-range homology search.

See the main text for more detailed information on the individual models for long-range homology search. DSB: DNA double-strand break; HR: homologous recombination.

Despite agreeing that an efficient genome-wide homology search appears timely virtually impossible (based on the defined parameters), both articles come to a different conclusion. Weiner et al.²⁴ argued that HR largely takes place in the G2 phase of the cell cycle²⁵, which enables DSB repair by using the homologous

information on the sister chromatid. As sister chromatids reside in spatial proximity due to cohesin-mediated cohesion¹⁴⁷, one might question whether the step of homology search is required to enable DSB repair by HR (Figure 30B). Hence, Weiner et al. propose that there is no requirement for a long-range homology search²⁴. Similarly, Barzel & Kupiec²³ argue against the requirement for a long-range homology search mechanism, however, their model takes the efficiency of ectopic recombination in *S. cerevisiae* into account: to explain the apparent contradiction between the efficient ectopic recombination of homologous sequences on different chromosomes and a timely virtually impossible efficient genome-wide homology search, a DSB-preceding co-localization of homologous sequences is proposed (somatic pairing model)²³. Specifically, a model is provided in which all homologous sequences are proposed to be juxtaposed to their counterparts²³ (Figure 30C).

5.3 Homology Search is Influenced by the Nuclear Organization

The data presented in this study shed light into the opposing models for homology search (genome-wide versus absence of long-range homology search), and argue for an alternative model for long-range homology search that depends largely on the nuclear organization.

Specifically, the observed homology search-associated Rad51 profiles clearly suggest that homology search exists, arguing against the “no homology search” and the “somatic pairing” models. Moreover, microscopy-derived data demonstrate that homologous sequences do not have to co-localize before DSB formation^{95,105,148,149}. Hence, as homology search exists, does it probe the entire genome to the same efficiency? The observed homology search-associated DSB-distant Rad51 ChIP signals provide an answer to this question, as the distribution of homology search is not equal over the entire genome. This clearly demonstrates that homology search does not probe every sequence in the genome by the same frequency. Moreover, based on this data, an influence of the nuclear organization onto homology search became apparent. In particular, the data suggest a model in which the efficiency of homology search is influenced by spatial proximity: First, homology search is mainly observable on the broken chromosome, which is in line with a higher probability of intrachromosomal versus interchromosomal interactions in *S. cerevisiae*¹¹⁹ revealed by chromosome conformation capture (3C) technology^{150,151}. Second, homology search appears mostly symmetrically to both sides of the DSB (with the notable

exception of chromosome III (Figure 13)) (Figure 12, Figure 20, Figure 22), with the signal intensity gradually decreasing away from the DSB (Figure 12, Figure 20, Figure 22), which is in line with a higher probability to encounter sequences that are close to each other on a linear chromosomal scale¹¹⁹. Third, the pattern of homology search in the mating-type system also follows spatial proximity: *HMR* (the donor homology on the right side of *MAT*) can be efficiently used for repair, in line with a rather compact structure of the respective chromosomal arm (chromosome III)¹¹⁹ that brings *HMR* in spatial proximity to *MAT*. Moreover, the donor homology *HML* (preferred in *MATa* cells) locates on the far left end of chromosome III, but the recombination enhancer (*RE*) element establishes spatial proximity of *HML* with *MAT*^{87,38}. In line, the *RE* element guides homology search to otherwise distant chromosomal locations *in cis* or *in trans* (Figure 13, Figure 15, Figure 17).

Together, these data argue for a model in which homology search probing occurs with a higher frequency on chromosomal locations that reside in spatial proximity to the DSB. If true, one would hypothesize that the nuclear 3D organization in general would substantially influence the pattern of homology search. Whereas in mammalian cells the nucleus is compartmentalized by chromosome territories^{145,152,153,154,155}, the small *S. cerevisiae* nucleus appears relatively dynamic. Nevertheless, also in *S. cerevisiae* chromosomal territories are statistically implicated¹⁵⁶, and several well-known nuclear landmarks exist in interphase cells^{120,121} (Figure 31). First, approximately a third of the nuclear volume is filled by the nucleolus, which is situated with a crescent-shape adjacent to the nuclear periphery¹⁵⁶. Second, on the opposing nuclear site, the centromeres of the individual chromosomes localize in one cluster. Centromere-clustering¹¹⁸ is mediated by cell cycle independent embedding of the spindle pole body (SPB) into the nuclear membrane, and cell cycle independent attachment of the centromeres to the SPB via microtubules¹⁵⁷. Third, telomeres comprise another important nuclear landmark, as they localize to the nuclear periphery¹²¹. Interestingly, these few landmarks - together with defining chromosomes as confined polymers undergoing passive Brownian motion - appear sufficient to mathematically predict the overall large-scale nuclear organization of *S. cerevisiae*^{158,159} (Figure 31).

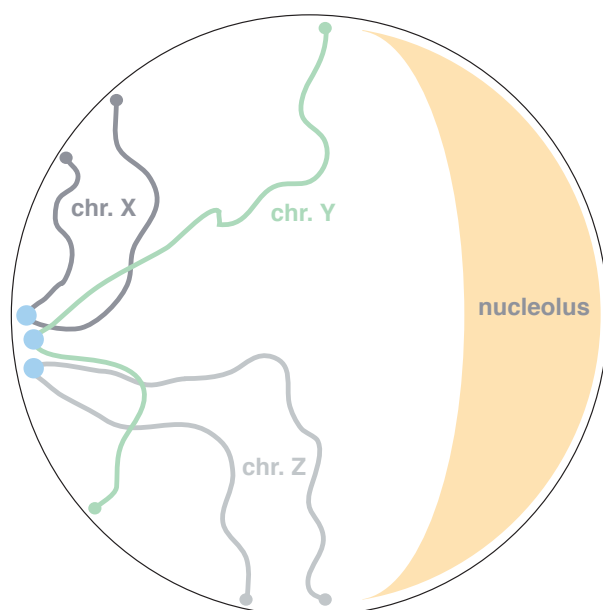


Figure 31. Nuclear organization in *S. cerevisiae*.

Schematic model highlighting the large-scale nuclear organization in *S. cerevisiae*. For simplification, only 3 of 16 chromosomes are shown (chr. X, Y and Z). The nucleus is mainly organized by centromere (blue dots) clustering, telomere (dots at the chromosomal ends) localization to the nuclear periphery, and positioning of the nucleolus (light orange crescent-shape). Note that centromere-clustering locates to opposing nuclear site, and that proximity between individual telomeres is thought to largely derive from similar chromosomal arm length (e.g. compare chromosomes Y and Z). Importantly, whereas this model depicts a static view, chromosomes are highly mobile. See the main text for a detailed description. Chr: Chromosome. Figure similar to ¹²¹.

In this study, characteristics of homology search in the context of these most prominent nuclear landmarks were investigated for the first time. Intriguingly, centromere-proximal DSBs (investigated for chromosome I, IV, V and XII; Figure 19, Figure 20, Figure 21 and Figure 22) resulted in traceable Rad51 ChIP signals (reflecting homology search) around the centromeres of all chromosomes, whereas such a behavior was not observable upon centromere-distal DSBs (chromosome III, IV, V, and XII; Figure 20, Figure 21 and Figure 22). Consequently, it appears highly likely that homology search upon a centromere-proximal DSB does not only probe efficiently on the broken chromosome, but also around the centromeres of all other chromosomes due to spatial proximity. Important further experiments to substantiate these results include investigation of homology search upon (1) destruction of centromere clustering by addition of the microtubule-depolymerizing drug nocodazol¹¹⁸, and (2) DSB formation on a transformed centromeric plasmid (which likely will be integrated into the centromere cluster).

Moreover, this study reports first data onto the characteristics of homology search upon telomere-proximal DSB. Telomeres locate to the nuclear periphery¹²¹, and interactions between individual telomeres have been reported by microscopy and 3C technology^{119,122,123,125}. Specifically, spatial proximity between the telomeres of the same chromosome *in cis*, and proximity between telomeres of short chromosomes *in trans* have been reported^{122,123,125}. However, in comparison to the spatial proximity between individual centromeres, the spatial proximity between individual telomeres is rather mildly pronounced^{119,160}, likely because telomere proximity largely depends on chromosome arm length rather than on specific

factors^{123,125}. In this study, homology search upon DSB-induction proximal to the left telomere of chromosome V was studied, which revealed homology search not only on the broken chromosome, but particularly additionally on the right telomeric arm of chromosome III (Figure 21). Moreover, these experiments revealed also very mild homology search-associated Rad51 ChIP signals at the telomeres of other chromosomes with a similar chromosomal arm length (data not shown). Particularly intriguing would be the idea that these signals reflect the proximity between individual telomeres. On the one hand, the observed Rad51 ChIP signals at telomeres of chromosomal arms with a similar length (as the chromosomal arm bearing the DSB) might reflect the preferential association of telomeres of similar chromosomal arm length^{123,125}. On the other hand, the explicit Rad51 signals on the right telomere of chromosome III (upon DSB induction proximal to the left telomere of chromosome V) might reflect a preferential interaction between these two telomeres. Notably, this preferential interaction has so far not been described in the literature. This could either be explained by differences between individual yeast strains or a unique interaction upon DSB induction. Consequently, it remains to be tested by additional experiments whether a telomere proximal DSB results in traceable homology search associated signals on other telomeres. This may include (1) monitoring homology search upon DSB induction on different telomeres with characterized telomere interactions *in cis* or *trans*, (2) monitoring homology search upon unhinging of a telomere from the nuclear periphery by deletion of *sir4* and *ku70*¹²², and (3) testing by microscopy or 3C based methods whether the left telomere of chromosome V indeed preferentially interacts with the right telomere of chromosome III.

To substantiate the impact of nuclear organization on homology search and thus the outcome of recombination even further, additional nuclear landmarks could be investigated. This may include implicated clusters transcriptionally linked genes, *ARS* (autonomously replicating sequence) and tRNA genes^{119,160,161}. Such experiments would not only substantiate the impact of the nuclear organization onto homology search, but also provide the possibility of detecting new features of nuclear organization. In that regard, it should be noted that improving the signal to noise ratio of Rad51 ChIP signals would likely be a necessity for these experiments (as already the pronounced clustering of centromeres results only in weak traceable Rad51 ChIP signals).

In conclusion, the data presented in this study provide strong evidence that homology search is influenced by the nuclear organization, and that homology

search preferentially probes chromosomal locations, which reside in spatial proximity. This argues that the kinetics of recombination will differ depending on the spatial proximity of the homologous donor sequence to the DSB, in line with previous reports stating that homology search is the rate-limiting step during HR¹⁶².

5.4 Revisiting earlier Data in View of Homology Search being Influenced by Nuclear Organization

How can the previously reported high efficiency of ectopic recombination in *S. cerevisiae* – which led to the proposal of an efficient genome-wide homology search – be explained in the light of these results? To answer this question, it is important to highlight that the data presented here in this study do not exclude that homology search also probes positions at which no Rad51 ChIP signals can be detected. On the contrary, it appears likely that a detection threshold for Rad51 ChIP signals exists: if homology search encounters a certain genomic locus very infrequently, it is not expected to result in detectable Rad51 ChIP signals, as homology search would locate only in an extremely low minority of cells at the same time to the same place. Hence, the presented Rad51 ChIP data do not exclude that homology search probes the entire genome (at least in *S. cerevisiae*; see section discussion 5.5). However, chromosomal regions that reside at distant 3D locations in the nucleus are searched much less frequently than chromosomal regions at close 3D locations to the DSB.

Importantly, despite being largely neglected in the literature, the previous reports on the astonishing efficiency of ectopic recombination in *S. cerevisiae* also observed differences in recombination efficiency depending on the chromosomal location: first, a genome-wide analysis of recombination between retrotransposons observed higher intrachromosomal compared to interchromosomal recombination rates¹⁶³. Second, Burgess and Kleckner¹⁰⁰ noted that different layers of recombination rates between pairs of loxP sites exist, with higher recombination rates when the loxP sites locate to the same chromosome, and when the loxP sites locate close to the centromeres of different chromosomes. Third, it should be noted that the recombination efficiency in the *S. cerevisiae* *MAT* system has been often used as an example for the proposed high efficiency of a genome-wide homology search. However, homology search in the *MAT* system represents a special feature, as the *MAT* system likely evolved to satisfy the needs for an optimal switch (which avoids probing of the entire genome). Lastly, the other main experiment highlighted in the

literature as an argument for a high efficiency of a genome-wide homology search, might also be influenced by the nuclear organization: in this experiment, a DSB and a homologous donor were either positioned to chromosome II or chromosome V, and efficient interchromosomal recombination between the positions was observed^{96,97}. However, the specific position (used for integration of the DSB or the homologous donor) on chromosome V is close (on a linear chromosomal axis) to the respective centromere (35 kb), and the specific position (used for integration of the DSB or the homologous donor) on chromosome II is in the center of the right chromosomal arm in a distance of 230 kb to the respective centromere. Thus, it seems likely that these locations are close enough in 3D to enable the observed recombination efficiency (Figure 31).

In conclusion, experimental systems bearing special features appear to have contributed to the efficient genome-wide homology search model.

5.5 Facilitated 3D/1D Homology Search Model

As described above, the results of this study strongly suggest that homology search probes chromosomal locations with a higher frequency if they reside in spatial proximity. However, an important question remains: can also sequences that locate far distant to the DSB be found in a reasonable time frame (Figure 32)? Hence, does homology search function (infrequently) genome-wide despite preferentially probing in spatial proximity?

The rough calculations onto the speed of homology search provided by Barzel & Kupiec²³ and Weiner et al.²⁴ argued that a genome-wide homology search would be timely impossible. However, the findings of this study and other meanwhile published data suggest that the parameters used for these calculations probably need adjustments. In particular, the estimated time needed for homology search and the assumed mobility of chromosomes have to be corrected, and the contribution of a 1D sliding mechanism during short-range homology search has to be integrated. Moreover, a process called parallel intersegmental homology probing might also contribute to the efficiency of homology search.

Regarding the estimated time needed for homology search, Barzel & Kupiec²³ estimated that homology search finds its target sequence in approximately two hours. However, as described in the previous section, this estimation derives from experiments in which the chromosomal locations allow a rather fast homology finding due to spatial proximity. In addition, the observed Rad51 ChIP profiles clearly indicate that homology search can continue for more than 5 hours, in line with data that repair takes place even 8 hours after DSB induction⁹⁷. Consequently, the time in which homology search has to find its target is likely considerably longer than previously defined.

Moreover, previous calculations on the speed of homology search were based on the idea of individual homology probing events²³. However, a recent *in vitro* study reported the observation of a short-range range 1D sliding mechanism during homology search, in which the Rad51 nucleoprotein filament slides for 80 – 300 bp on the encountered dsDNA⁹². Such a 1D sliding mechanism (Figure 32) likely substantially facilitates homology search by different ways. On the one hand, homology recognition itself would be highly accelerated by a short sliding as it enables the finding of Watson-Crick base pairing between both homologous sequences⁹². Hence, the invading Rad51 nucleoprotein filament would not have to

melt the encountered dsDNA for every probing event on the entire length, but only the next basepairs in the direction of sliding. On the other hand, homology search *in vivo* has to proceed in the context of chromatinized DNA. As homology probing on DNA wrapped around a nucleosome appears rather unlikely, homology probing presumably involves chromatin remodeling by nucleosome sliding and/or histone eviction. Consequently, probing of an entire DNA section by 1D sliding and parallel chromatin remodeling appears more efficient than multiple individual probing events that repeatedly involve chromatin remodeling and subsequent chromatin restoration. Thus, 1D sliding likely reduces the required energy and the time frame for an individual probing event, thereby substantially facilitating homology search.

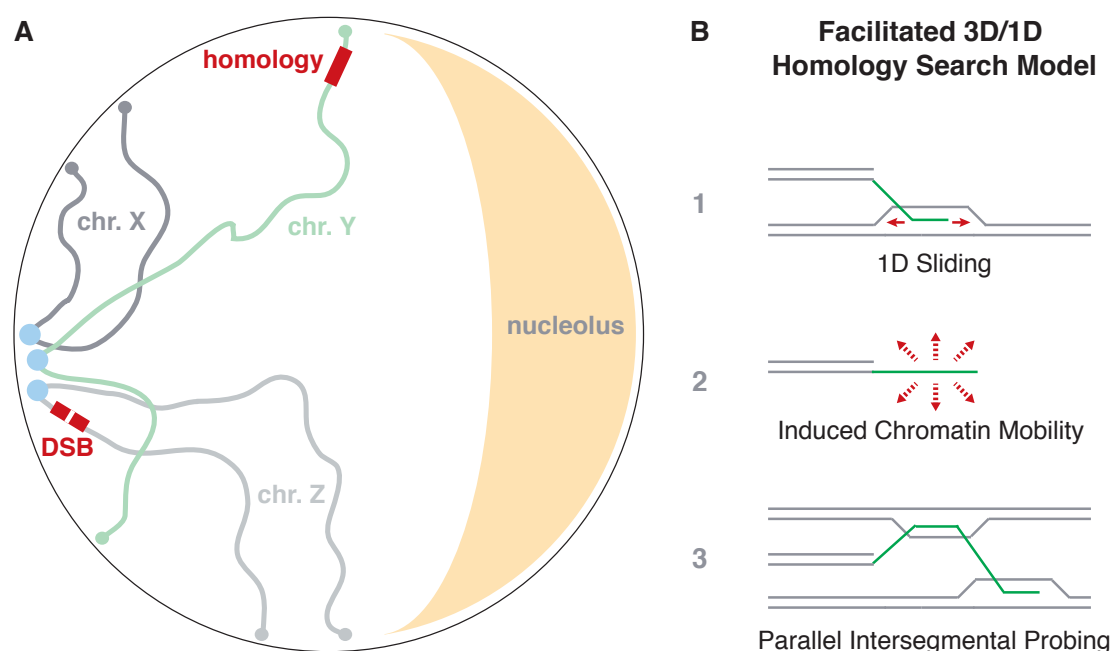


Figure 32. Facilitated 3D/1D homology search model.

(A) As described in Figure 31, nuclear organization in *S. cerevisiae* is mainly established by centromere (blue dots) clustering, telomere positioning (dots at the ends of the individual chromosomes), and the location of the nucleolus (light orange crescent-shape). Based on this nuclear organization, it remained mysterious how homologous recombination can occur between a broken sequence (DSB) and a far distant homologous counter-sequence (as depicted e.g. a DSB close to the centromere of chromosome and a homologous sequence close to a telomere of another chromosome).

(B) Facilitated homology search model: to enable an – at least infrequent – encounter of far distant homologous sequences (as depicted in (A)), homology search might include mechanisms to facilitate the speed of homology search. This includes (1) short-range 1D sliding of the nucleoprotein filament on the encountered sequence, (2) induced chromatin mobility, and (3) parallel intersegmental homology probing. For simplicity, each model only includes one end of the broken chromosome. See main text for details on the proposed models.

Chr: Chromosome; DSB: DNA double-strand break.

Facilitated homology search by 1D sliding raises the intriguing idea that 1D sliding *in vivo* might be fostered by protein activities. 1D sliding *in vivo* is likely based on a transient D-loop like structure (Figure 24). Such a transient D-loop like structure

might be supported by binding of the single-strand binding protein RPA to the displaced strand, thereby explaining the potential function of RPA during homology search (Figure 23). Moreover, an ideal candidate for a factor fostering 1D sliding *in vivo* is the translocase Rad54¹³⁰. Rad54 bears an ATP-dependent motor domain for translocation on dsDNA¹²⁸. As demonstrated for its homolog Rdh54, processive translocation *in vitro* covers at average surprisingly a distance of approximately 10,000 base pairs¹⁶⁴. Intriguingly, we observed that Rad51 ChIP signals (reflecting homology search) are drastically reduced in a strain deficient for Rad54 (Figure 24), and completely lost in a strain deficient for Rad54 and Rdh54 (data not shown). This raises the hypothetical but intriguing possibility that Rad54 (and/or Rdh54) assists 1D sliding by binding to the Rad51 nucleoprotein filament, and translocating on the encountered dsDNA. However, it should be noted that other models might also explain reduced homology search without Rad54, such as a function of Rad54 in chromatin remodeling and chromatin mobility during the homology-probing event. Nevertheless, the observed 1D sliding *in vitro* likely plays an important role *in vivo* to facilitate the speed of homology search.

Homology search has been additionally proposed to be facilitated by a process called intersegmental transfer⁹⁰. The concept of intersegmental transfer proposes that the Rad51 nucleoprotein filament does not only probe one region for homology, but can probe multiple regions in parallel by different parts of the Rad51 nucleoprotein filament (Figure 32). If one imagines a nucleoprotein filament track at the DSB of 1 kb length, and assumes that 250 bp of homology are sufficient for efficient recombination¹⁶⁵, parallel intersegmental homology probing might be possible and might facilitate the speed of homology search. However, so far intersegmental transfer has only been observed *in vitro*, and the extend of intersegmental homology probing *in vivo* remains to be tested.

Homology search might also be facilitated by induced chromatin mobility. Recently, fluorescent imaging of single DSBs in *S. cerevisiae* revealed an induction of chromatin mobility of sequences around the DSB in comparison to the intact sequence^{105,106,107,109}. An induced movement of chromatin intuitively suggests that the likelihood of random encounter between distant homologous sequences is increased¹⁰⁹, thus facilitating homology search¹⁰⁸. Moreover, it should also be noted that proximity between the broken and the intact homologous sequence is likely not only mediated by the broken sequence itself but also by the intact homologous sequence. In other words, do the DSB-associated Rad51 filaments search for the

homologous sequence, or vice versa. If homology search is based on a random encounter, likely both contribute to homology search. Along this line, one study observed not only an induced movement of the DSB itself, but also of other chromosomes¹⁰⁵, which might additionally facilitate homology search. However, whether induced chromatin mobility is indeed directly linked to the efficiency of homology search remains to be tested¹⁰⁹.

Taken together, we propose that these additional contributions to the efficiency of long-range homology search (1D sliding, parallel intersegmental homology probing and induced chromatin mobility) significantly decrease the time required to randomly probe large parts of the genome in *S. cerevisiae*. If one additionally considers that ectopic recombination has been often studied by end-point assays (measuring completion of repair)³⁷ – which allow the cells a longer time for repair than the previously assumed 2 hours⁹⁷ – it appears rather likely that ectopic recombination between many different locations in the small genome of *S. cerevisiae* will happen at some point in a certain number of cells, explaining why homology search has been proposed to scan efficiently the entire genome¹⁰⁴. However, it should be noted that - even if these described mechanisms facilitate the speed of homology search – homology still probes with the highest frequency in proximity, and far distant sequences will only be encountered infrequently. Evidently, this predicts that in cells with larger genomes, homology search is not able to encounter every genomic sequence, e.g. the nuclear volume of *S. cerevisiae* in comparison to mammalian cells is only one-thousandth, whereas chromatin mobility is comparable¹⁴⁶. Moreover, such a model would also balance between the need for search and the potential harmful outcome of unwanted recombination between repeated sequences such as transposons.

In summary, chromatin-immunoprecipitation of the recombinase Rad51 monitors nuclear homology search for the first time, and also has a predictive value of recombination rates. This substantially shed light onto the previously enigmatic mechanism of homology search. Moreover, this greatly enables to study the process of homology search in the context of the nuclear organization in further detail, e.g. to study the further components and requirements of homology search, and to study how homology search can proceed in the context of chromatinized DNA.

6 Materials and Methods

For all described protocols, sterile flasks and solutions were used, and basic microbiological and biochemical techniques followed standard protocols^{166,167} or manufacturers instructions. General reagents were purchased from Difco, Invitrogen, Merck, Roth, Sigma and Quiagen. For molecular biology, deoxynucleotide triphosphates (dNTPs) and enzymes were purchased from NEB, and DNA oligonucleotides were custom-made by Eurofins MWG. Taq-Polymerase was generated by the MPI of Biochemistry.

6.1 Microbiology

6.1.1 Escherichia Coli Techniques

E. coli strains were cultivated at 37°C, either in liquid LB media or on LB agar plates. Culture density in liquid media was determined photometrically.

***E. Coli* Strains**

Strain name	Genotype	Source
XL1-Blue	hsd R17 rec A1 end A1 gyrA46 thi-1 sup E44 relA1 lac [F' pro AB lacI ^q ZΔ M15 Tn10 (Tet ^r)]	Stratagene

***E. Coli* Media & Buffer**

LB-media	1 % trypton 0,5 % yeast extracts 1 % NaCl 1,5 % agar (for plates) sterilized by autoclaving
----------	---

Competent *E. Coli* Cells

Transformation of DNA plasmids into *E. coli* cells was achieved by electroporation. For the preparation of electro-competent *E. coli* cells, liquid LB medium was inoculated from a single bacterial colony, finally grown in 1 l of liquid LB medium to an OD₆₀₀ of 0.6 – 0.8. Subsequently, the culture flask was incubated on ice for 30 min, and cells were harvested by centrifugation (10 min, 5000 g, 4 °C). The pelleted cells were carefully resuspended and washed with ice-cold water, centrifuged again and washed twice with 0.5 l ice-cold 10% (v/v) glycerol solution. Upon final washing with 50 ml ice-cold 10 % (v/v) glycerol solution, cells were carefully resuspended in 3 ml ice-cold 10 % (v/v) glycerol solution. Subsequently, 50 µl aliquots were generated from this solution, frozen in liquid nitrogen and stored at -80 °C.

Transformation of *E. Coli*

For Transformation of DNA plasmids into *E. coli* cells, electro-competent *E. coli* cells were thaw on ice and mixed with 2 µl of dialysed ligation samples (for the origin of ligation samples, see paragraph “Ligation of DNA Fragments”). Upon transfer of this suspension into a pre-cooled 0.2 cm gene pulser cuvettes (Biorad), electroporation was carried out by applying a pulse of 1.8 kv, 25 µF and with a resistance of 200 Ω. Subsequently, 1 ml liquid LB medium was added to the cuvettes, carefully mixed, and the suspension was transferred to a fresh culture tube and incubated for 1 hour at 37 °C on a shaker (800 rpm). Thereafter, selection of transformants was achieved by plating the cells on LB agar plates containing the antibiotic whose resistance was encoded on the transformed DNA (mostly ampicillin). Upon incubation over night at 37 °C, single bacterial colonies were inoculated in liquid LB media, and plasmid DNA was isolated (see paragraph “Isolation of Plasmid DNA from *E. coli*”).

6.1.2 *Saccharomyces Cerevisiae* Techniques

Saccharomyces Cerevisiae Strains

All yeast strains were isogenic to either JKM179, JKM161, JKM139 or W303. Strain YCL26 was obtained by crossing YCZ173¹¹⁵ with W303 *MATα* (Claudio Lademann).

Strain	Genotype	References
JKM179	<i>Δhml::ADE1, MATα, Δhmr::ADE1, ade1-100, leu2-3,112 lys5, trp1::hisG', ura3-52, ade3::GAL-HO</i>	111
JKM139	<i>Δhml::ADE1 MATa Δhmr::ADE1, ade1-100, leu2-3,112 lys5, trp1::hisG', ura3-52, ade3::GAL-HO</i>	111
JKM161	<i>HMLα, MATa, Δhmr::ADE1, ade1-100, leu2-3,112, lys5 trp1::hisG', ura3-52, ade3::GAL-HO</i>	111
YXW3	<i>HMLα, MATa, Δhmr::ADE1, ade1-100, leu2-3,112, lys5 trp1::hisG', ura3-52, ade3::GAL-HO, rfa1-t11 (K45E)</i>	126
MK205	<i>MATa-inc, ura3-HOcs, ade3::GAL-HO, ade2-1, leu2-3,112, his3-11,15, trp1-1, can1-100</i>	97
SB368	<i>JKM179, Δrad51::natNT2</i>	Steven Bergink
JOR09	<i>JKM179, Δrad52::kanMX6</i>	This study
JOR24	<i>JKM179, Δrad55::kanMX6</i>	This study
JOR25	<i>JKM179, Δrad57::kanMX6</i>	This study
JOR03	<i>JKM179, Δrad54::kanMX6</i>	This study
JOR05	<i>JKM179, Δrdh54::natNT2</i>	This study
JOR34	<i>JKM179, Δrad54::kanMX6, Δrdh54::natNT2</i>	This study
JOR134	<i>JKM179, rad51-II3A(R188A, K361A, K371A)::kanMX6</i>	This study
JOR07	<i>JKM139, ΔRE::kanMX6</i>	This study
JOR37	<i>JKM161, ΔRE::kanMX6</i>	This study
JOR91	<i>JKM139, ΔRE::kanMX6, ChrV at 24kb::RE-natNT2</i>	This study

JOR15	JKM179, $\Delta Ty170kb(ChrIII)::natNT2$	This study
IP224	JKM179, $rfa1^{9myc}::natNT2$	Ivan Psakhye
JOR51	JKM139, $rfa1^{9myc}::natNT2$	This study
JOR84	JKM139, $rfa1^{9myc}::natNT2$, $\Delta rad51::hphNT1$	This study
JOR85	JKM139, $rfa1^{9myc}::natNT2$, $\Delta rad55::kanMX6$	This study
JOR67	JKM179, $hta1-S129A-tADH::hphNT1$, $hta2-S129A-tADH::kanMX6$	This study
JOR77	W303, $MAT\alpha$, $leu2-3,112$, $ade2-1$, $can1-100$, $his3-11,15$ $ura3-1$, $trp1-1$, $ChrIV_{720kb}::Scel$ (recognition site)- $kanMX6$	This study
JOR87	W303, $MAT\alpha$, $leu2-3,112$, $ade2-1$, $can1-100$, $his3-11,15$ $ura3-1$, $trp1-1$, $ChrIV_{491kb}::Scel$ (recognition site)- $kanMX6$	This study
JOR93	W303, $MAT\alpha$, $leu2-3,112$, $ade2-1$, $can1-100$, $his3-11,15$ $ura3-1$, $trp1-1$, $ChrV_{24kb}::Scel$ (recognition site)- $kanMX6$	This study
JOR94	W303, $MAT\alpha$, $leu2-3,112$, $ade2-1$, $can1-100$, $his3-11,15$ $ura3-1$, $trp1-1$, $ChrXII_{136kb}::Scel$ (recognition site)- $kanMX6$	This study
JOR88	W303, $MAT\alpha$, $leu2-3,112$, $ade2-1$, $can1-100$, $his3-11,15$ $ura3-1$, $trp1-1$, $ChrXII_{394kb}::Scel$ (recognition site)- $kanMX6$	This study
YCL26	W303, $MATa$, $leu2-3,112$, $ade2-1$, $can1-100$, $his3-11,15$ $ura3-1$, $trp1-1$, $ade3::P_{GAL}-HO$, $hml\Delta::pRS-1$, $hmr\Delta::pRS-2$, $mathOcs\Delta::pBR-1$	Claudio Lademann
JOR97	YCL26, $ChrIV_{491kb}::HOcs-hphNT1$,	This study
JOR99	YCL26, $ChrIV_{491kb}::HOcs-hphNT1$, $rfa1^{9myc}::kanMX6$	This study
JOR133	YCL26, $ChrIV_{491kb}::HOcs-hphNT1$, $\Delta RE::kanMX6$	This study
JOR102	YCL26, $ChrI_{120kb}::HOcs-hphNT1$	This study

***Saccharomyces Cerevisiae* Plasmids**

Plasmid name	Description	Source
pWJ1320	Scel expression plasmid (<i>Scel</i> gene placed under <i>GAL</i> promoter); ADE and AmpR selection markers	Michael Lisby; Ref 170

***Saccharomyces Cerevisiae* Media and Buffers**

YPD / YP-Gal /YP-Raf	1 % yeast extract 2 % bacto-peptone 2 % carbon source (glucose, raffinose or galactose) 2 % agar (only for plates) sterilized by autoclaving
YP-Lactate	1 % yeast extract 2 % bacto-peptone 3 % lactic acid adjust pH to 5.5 with NaOH (ca. 12 g/l final) sterilized by autoclaving
YPD G418/NAT/HPH plates	after autoclaving, YPD medium with 2 % agar was cooled to 50 °C, and 200 mg/l G418 (geneticine disulphate, PAA Laboratories), 100 mg/l NAT (nourseothricin, HK Jena) or 500 mg/l Hph (hygromycin B, PAA Laboratories) was added.
SC-media	0.67 % yeast nitrogen base 0.2 % amino acid drop out mix 2 % carbon source (glucose, raffinose or galactose) 2 % agar (for plates) sterilized by autoclaving
SC-lactate	0.67 % yeast nitrogen base 0.2 % amino acid drop out mix 3 % lactic acid adjust pH to 5.5 with NaOH (ca. 12 g/l final) sterilized by autoclaving
Drop out amino acid mix	20 mg Ade, Ura, Trp, His 30 mg Arg, Tyr, Leu, Lys 50 mg Phe 100 mg Glu, Asp 150 mg Val 200 mg Thr 400 mg Ser
SORB	100 mM LiOAc 10 mM Tris-HCl, pH 8.0 1 mM EDTA, pH 8.0 1 M sorbitol sterilized by filtration
PEG	100 mM LiOAc 10 mM Tris-HCl, pH 8 1 mM EDTA, pH 8.0 40 % (w/v) PEG-3350 sterilized by filtration stored at 4 °C

Cultivation and Storage of *Saccharomyces Cerevisiae*

Cultures streaked on agar plates were used for short-term storage (1-2 weeks), whereas cultures were frozen in 15 % (v/v) glycerol at -80 °C for long-term storage. Single yeast colonies on freshly streaked plates were used to inoculate liquid cultures, which were subsequently grown overnight at 30 °C on a shaking platform (150-220 rpm). From this pre-culture the main culture was inoculated to an OD₆₀₀ of 0.1 (or lower) and incubated in baffled flasks (size ≥ 5x liquid culture volume) on a shaking platform (150-220 rpm) at 30°C until mid-log phase growth had been reached (equals OD₆₀₀ of 0.6-0.9), then experiments were performed. The culture density was determined photometrically (OD₆₀₀ of 1 is equal to 1.5x10⁷ cells/ml).

Competent *S. Cerevisiae* Cells

S. cerevisiae cells were grown to mid-log phase, and harvested by centrifugation (5 min, 500 g, RT). Washing was performed once with 25 ml sterile water and once with 10 ml SORB solution. Subsequently, cells were resuspended in 360 µl SORB and 40 µl carrier DNA (salmon sperm DNA, 10 mg/ml, Invitrogen), and stored in 50 µl aliquots at -80°C.

Transformation of *S. Cerevisiae* Cells

Transformation of *S. cerevisiae* cells with linearized plasmid DNA or PCR products was performed by using approximately 2 µg of the respective linearized plasmid DNA or PCR product, and 50 µl of the respective competent cells (see above), both mixed with 6 volumes of PEG and incubated for 30 min at room temperature. Subsequently, DMSO was added (to a final concentration of 10 %), and cells were heat shocked at 42 °C for 10 min. Thereafter, cells were centrifuged, resuspended in 3 ml YPD, incubated for 3 hours at 30 °C and streaked out onto plates containing the respective selective media. After two days of incubation at 30 °C, transformants were replica plated onto the respective selection plate to reduce the rate of false-positive transformants. Correct integration was subsequently tested by yeast colony PCR (see paragraph “PCR Screening of Genomic Recombination Events”). If possible, successful gene knockout or epitope tagging was additionally confirmed by Western blot analysis (see paragraph “Protein Methods”).

Genetic Manipulation of *Saccharomyces Cerevisiae*

Chromosomally tagged strains, mutants and knockouts were constructed by a PCR-based strategy^{168,169} (see paragraph “Amplification of Targeting Cassettes”), using the protocols for competent *S. cerevisiae* cells and transformation described above. Briefly, PCR products used for transformation contained the selection marker (kanMX6, natNT2 or hphNT1) and for chromosomal tagging the epitope tag (Rfa-9myc). For integration, the PCR product is flanked on both sides by genomic targeting sequences. Integration of the PCR products to the correct

chromosomal locations was confirmed by yeast colony PCR using specific primers¹⁶⁸ (see paragraph “PCR Screening of Genomic Recombination Events”).

Mutation of serine-129 to alanine of H2A was targeted to both endogenous alleles of H2A (*hta1* and *hta2*), integrating an *ADH1* terminator. Correct integration and presence of genomic *hta1* and *hta2* mutation was confirmed by yeast colony PCR and sequencing (see below).

The 30 bp specific *SceI* recognition sequence (5'-ttacgctagggataacagggtaatatagcg-3'¹⁷⁰) was cloned next to a selection marker, subsequently genomically integrated at the designated position (ChrIV:491 kb, in-between *YDR024W* and *YDR025W*; ChrV:24 kb, in between *YEL069C* and *YEL068C*; ChrIV:720 kb, in-between *YDR132C* and *YDR133C*; ChrXII:136 kb, in between *YLL007C* and *YLL006W-A*; ChrXII:394 kb, in between *YLR125W* and *YLR126C*), and the presence of the integrated genomic *SceI* recognition sequence was confirmed by sequencing. Similarly, a 36 bp *HO* recognition sequence (5'-agtttcagctttccgcaacagtataattttataaac-3')¹⁷¹ was cloned next to a selection marker and integrated at the designated position (ChrIV:491 kb, in-between *YDR024W* and *YDR025W*; ChrI:120 kb, in-between *YAL018C* and *YAL017W*), and the presence of the integrated genomic *HO*-recognition sequence was confirmed by yeast colony PCR and sequencing.

RE was deleted by deleting 800 bp of the *RE*, which has been shown to be the main element for *RE* function³⁶. Moreover, this deletion does not interfere with neighboring gene function, but retains a mild *RE* activity³⁶. A similar region of the *RE* was cloned next to a selection marker and integrated at the designated position (ChrV:24 kb, in-between *YEL069C* and *YEL068C*), confirmed by yeast colony PCR and sequencing.

To integrate the *rad51-II3A* mutation¹¹⁷ into the JKM179 strain, a PCR product was generated from a *rad51-II3A* mutant (with a *kanMX6* selection marker next to it) bearing strain (3687; kindly provided by D. Bishop). This PCR product (containing the *kanMX6* selection marker and the *RAD51* ORF with the mutations *R188A*, *K361A*, *K371A*) was integrated into the endogenous *Rad51* locus, and the correct integration and presence of genomic mutations (*R188A*, *K361A*, *K371A*) was confirmed by yeast colony PCR and sequencing.

The *rfa1-t11* (K45E) mutant strain was kindly provided by J. Haber¹²⁶.

Phenotypic Analysis of *Saccharomyces Cerevisiae* Strains

To analyze and compare growth of WT and mutant derivative *S. cerevisiae* strains, equal amounts of cells were spotted onto solid media with or without DNA damage inducing drugs (such as zeocin; Invitrogen). Specifically, yeast overnight cultures were harvested and resuspended in 1 ml sterile water. Upon dilution to an OD₆₀₀ of 1, five-fold serial dilutes were prepared and spotted onto the respective solid media plates. Growth was compared after incubation for 2 and 3 days at 30 °C.

6.2 Molecular Biological Techniques

Isolation of Plasmid DNA from *E. Coli*

Single *E. coli* colonies (derived from transformation of plasmid DNA) were inoculated in 5 ml liquid LB medium and growth overnight at 37 °C. Subsequently, DNA plasmids were isolated using a commercially available kit (AccuPrep Plasmid Mini Extraction Kit, Bioneer) according to the manufacturer's instructions.

Isolation of Yeast Genomic DNA

Isolation of yeast genomic DNA (e.g. as a template for the amplification of specific genes or chromosomal elements by PCR) was performed from a 10 ml saturated yeast culture. Upon centrifugation (1000 g, 5 min, RT), cells were resuspended in 0.5 ml and centrifuged again. Thereafter, 200 µl detergent lysis buffer (2 % (v/v) Triton X 100, 1 % (v/v) SDS, 100 mM NaCl, 10 mM Tris-Cl pH 8, 1 mM EDTA), 200 µl phenol/chloroform/isoamyl alcohol (25:24:1 v/v/v; Roth) and approximately 0.3 g glass beads (Ø 425-600 µm; Sigma) were added and the solution was vortexed for 3 min to achieve efficient cell lysis. Subsequently, 200 µl TE pH 8 was added and the resulting mixture was centrifuged (13000 rpm, 5 min, RT). The aqueous layer was transferred to a new microcentrifuge tube, 1 ml 100 % EtOH was added to precipitate DNA, and the suspension was mixed by inversion. Upon centrifugation (13000 rpm, 5 min, 4 °C), the pellet was resuspended in 400 µl TE pH 8. Additionally, 3 µl DNase-free RNase (10 mg/ml) was added to degrade RNA contamination, and incubated for 5 min at 37 °C. Thereafter, DNA was precipitated by the addition of 1 ml 100 % EtOH and 10 µl 4 M ammonium acetate (mixed by inversion). Upon centrifugation (13000 rpm, 5 min, 4°C), the supernatant was discarded and the pellet was air-dried. Finally, the air-dry pellet was resuspended in 50 µl TE pH 8.

Determining DNA Concentration

DNA concentration was determined photometrically (using NanoDrop ND-1000 spectrophotometer (PeqLab)) by measuring the absorbance at a wavelength of 260 nm (OD_{260}). An OD_{260} of 1 is equal to a concentration of 50 µg/ml double-stranded DNA.

6.2.1 Polymerase Chain Reaction (PCR)

PCR was used to amplify DNA fragments from genomic DNA for cloning, to amplify targeting cassettes for chromosomal gene disruption and epitope tagging, to test for genomic recombination events, and to analyze ChIP experiments by quantitative real-time PCR. Generally, all PCR reactions were prepared on ice.

Amplification of Genomic DNA Fragments

Amplification of genomic DNA fragments for subsequent cloning was performed from genomic DNA using the highly accurate *Phusion*TM DNA polymerase (Finnzymes).

PCR mix	μl	98 °C	1 min
5x HF buffer	10	then 25 cycles	
Primer 1 (10 μM)	3	98 °C	20 s
Primer 2 (10 μM)	3	60 °C	20 s
dNTPs (10 mM each)	1	72 °C	90 s (or longer depending on size)
template (gen. DNA)	1		
H ₂ O	31.5		
Phusion polymerase	0.5	72 °C	7 min
		4 °C	∞

Amplification of Targeting Cassettes

Chromosomally tagged strains, mutants and knockouts were constructed by a PCR-based strategy^{168,169}, based on PCR products flanked on both sides by genomic targeting sequences. Upon PCR, a small amount of the PCR sample was analyzed for correct size and for quality. Subsequently, the remaining PCR sample was purified using the PCR purification kit from Qiagen according to the manufacturer's instructions. This purified PCR product was then used for Yeast transformation (see paragraph "Transformation of *S. Cerevisiae* Cells")

PCR mix	μl	Thermocycler	
Long PCR buffer	10	95 °C	5 min
DNA plasmid template	0.65	then 10 cycles	
Primer 1 (10 μM)	6.4	95 °C	30 s
Primer 2 (10 μM)	6.4	54 °C	30 s
dNTPs (10 mM each)	3.5	68 °C	2 min 40 s
MgCl ₂ (50 mM)	1	then 20 cycles	
Vent polymerase	0.7	95 °C	30 s
Taq polymerase	0.8	54 °C	30 s
H ₂ O	12.9	68 °C	2 min 40 s
			+ 20s/cycle
		68 °C	5 min
		4 °C	∞

PCR Screening of Genomic Recombination Events ("Colony PCR")

Yeast colony PCR was performed according to Knop et al¹⁶⁸ and Janke et al¹⁶⁹ to confirm integration of the PCR products to the correct chromosomal locations. Briefly, a yeast colony was swirled into 20 μl of 0,02 M NaOH, and upon addition of glass beads (425-600nm; Sigma) incubated for 5 min at 99 °C with 1400 rpm shaking. Subsequently, the sample was centrifuged for 1 min at 14000 rpm, and 1,6 μl of the supernatant were used as template for PCR using the following protocol:

PCR mix		Thermocycler	
	μl	94 °C	5 min
10x ThermoPol buffer	2	then 30 cycles	
Primer 1 (10 μM)	1.3	94 °C	30 s
Primer 2 (10 μM)	1.3	55 °C	30 s
dNTPs (10 mM each)	0.7	72 °C	1 min
Taq polymerase	0.2	72 °C	5 min
H ₂ O	12.9	4 °C	∞

6.2.2 Molecular Cloning

Digestion of DNA using Restriction Enzymes

Digestion of DNA using site-specific restriction enzymes was performed according to instructions of the manufacturer (New England Biolabs). Briefly, reaction samples were incubated in recommended buffers at the recommended temperature. To avoid re-ligation of plasmid DNA, the 5' end of the plasmid DNA was dephosphorylated by incubation with calf intestinal phosphatase (CIP; New England Biolabs) at 37 °C for 1 hour.

Separation of DNA using Gel Electrophoresis

Size separation and analysis of DNA was performed by gel electrophoresis. Briefly, DNA samples were mixed with 5x DNA loading buffer (0.5 ml 10 % SDS, 0.5 ml 0.5 M EDTA, 2.9 ml 86 % Glycerin, 6.1 ml H₂O, BromphenolBlue, Xylene cyanol FF) and subjected to electrophoresis in agarose gels (mostly 1 % agarose gels; depending on the size of the respective DNA) containing 0.5 $\mu\text{g/ml}$ ethidium bromide at 120 V in TBE buffer. Upon electrophoresis, DNA was visualized using an UV transilluminator (324 nm). Size of the respective DNA was estimated by comparison to standard size markers (1 kb DNA ladder, Invitrogen)

Isolation of DNA fragments from Agarose Gels

If suitable, DNA fragments were excised from agarose gels upon gel electrophoresis, using a sterile razor blade. Then, DNA was extracted from the agarose block by a kit from Qiagen (QIAquick Gel Extraction Kit) according to manufacturer's instructions.

Ligation of DNA Fragments

DNA ligases are used to insert DNA fragments into plasmid vectors. Purified, digested and dephosphorylated vector DNA, insert DNA, Quick ligase and Quick ligase buffer are mixed. The ratio of insert to plasmid is adjusted to 3 to 1 ($\text{Insert} = (\text{bp Insert}/\text{bp plasmid}) \times 300 \text{ ng}$). Ligations were carried out for 10 min at RT, followed by 5 min on ice.

For short inserts (like the HO and SclI recognition sequences), single-stranded primers were annealed to form dsDNA, which then was ligated into a plasmid ("primer ligation"). Specifically, complementary oligonucleotides harboring ends that mimic overhangs resulted from specific restriction endonucleases were ordered and dissolved at a concentration of 100 μ M in linker buffer (50 mM Tris-HCl pH 8, 100 mM NaCl, 1mM EDTA). The complementary oligonucleotides were mixed, denaturated at 95 °C, and slowly cooled (1 °C per minute) until 4 °C. Then, the resulting linker was phosphorylated by incubation with T4 PNK in T4 ligase buffer for 30 min at 37 °C, gel purified and used for ligation.

DNA Sequencing

All sequencing reactions were performed by the MPIB core facility, using an ABI 3730 sequencer, ABI Big Dye 3.1 sequencing chemistry, 300 ng dsDNA template and 5 pmol primer.

6.3 Biochemistry and Cell Biology Techniques

6.3.1 Protein Methods

General Buffers and Solutions

HU sample buffer	200 mM Tris, pH 6.8 8 M urea 5 % (w/v) SDS 1 mM EDTA 1.5 % (w/v) DTT 0.1 % (w/v) bromophenol blue
MOPS running buffer	50 mM MOPS 50 mM Tris base 3.5 mM SDS 1 mM EDTA
Blotting buffer	250 mM Tris base 1.92 M glycine 0.1 % (w/v) SDS 20 % (v/v) methanol
TBST	25 mM Tris-HCl, pH 7.5 137 mM NaCl 2.6 mM KCl 0.1 % (v/v) Tween 20
Stripping buffer	4 % (w/v) SDS 100 mM β -mercaptoethanol 62.5 mM Tris/HCl, pH 6.8

TCA Precipitations

Small-scale cell extracts were prepared by trichloroacetic acid (TCA) precipitation for analytical purposes. 1OD of yeast culture were harvested by centrifugation and resuspended in 1 ml ice-cold water. 150 μ l 1.85 M NaOH/7.5 % β -mercaptoethanol were added and incubated for 15 min on ice to lyse cells. Proteins were precipitated by addition of 150 μ l 55 % TCA and incubation for 10 min on ice. Upon centrifugation (20000 g, 10 min, 4 °C), pelleted precipitated proteins were resuspended in 50 μ l HU sample buffer.

SDS-Polyacrylamide Gel Electrophoresis (PAGE)

Proteins samples in HU sample buffer derived from TCA precipitations were denatured by heating to 65 °C for 10 min and loaded on pre-cast 4-12 % NuPage Bis-Tris gels (Invitrogen, Carlsbad, USA). Gel electrophoresis was performed in MOPS buffer at a constant voltage of 140V. Protein size was estimated by comparison to the standard size marker Precision Plus Protein All Blue Standard (Bio-Rad Laboratories GmbH, Hercules, USA).

Western Blot Analysis

Proteins separated by PAGE were transferred to polyvinylidene fluoride (PVDF) membranes (Millipore, Billerica, USA) for western blot analysis, using wet blotting in an electric tank blotter. This was performed in transfer buffer at a constant voltage of 70 V at 4 °C for 90 min. Thereafter, membranes were blocked for at least 10 min in TBS-T + 5 % milk powder at room temperature, and incubated over night at 4 °C with a primary antibody diluted in TBS-T + 5 % milk powder. Subsequently, the membrane was washed with TBS-T for 4 times (for at least 10 min each) at room temperature, incubated with a horse radish peroxidase (HRP)-coupled secondary antibody (Dianova, Hamburg, Germany), and washed again with TBS-T for 4 times (for at least 10 min each) at room temperature. Signals were obtained by chemiluminescence reactions using ECL, ECL-plus or ECL advanced kits (Amersham/GE Healthcare, Little Chalfont, UK) following manufacturer's instructions. Signals were detected by exposure of the membrane to a chemiluminescence film (Amersham Hyperfilm ECL, GE Healthcare) with variable exposure times and subsequent automated film development, or alternatively by using a LAS-3000 imaging system (Fujifilm Europe GmbH, Düsseldorf, Germany) equipped with a CCD camera.

Stripping of immunoblot membranes was performed for sequential incubation of the same membrane with different primary antibodies. Bound immunoglobulins were removed by incubation of the membrane in stripping buffer for 30 min. Subsequently, the membrane was washed twice with TBS-T, and blocked and probed with a primary antibody as described above.

Antibodies

Specificity	Type	Source
α -Dpm1	mouse, primary antibody	Invitrogen
α -HA	primary antibody	Santa Cruz
α -Myc (9E10)	primary antibody	Sigma
α -Pgk1	primary antibody	Molecular Probes
α -Rad51 (polyclonal)	primary antibody	Santa Cruz
α -Rad52 (polyclonal)	primary antibody	Ref 78
HRP-coupled α -rabbit IgG	secondary antibody	Dianova
HRP-coupled α -mouse IgG	secondary antibody	Dianova

6.3.2 Induction of Single DSBs *in vivo*

To induce a single specific DSB by HO-endonuclease, the *HO* gene is placed under *GAL* promoter expression as originally described^{76,111}. For HO expression, the respective yeast strains were grown in YP-lactate (1 % Bacto Yeast Extract, 2 % Bacto Peptone, 3 % lactic acid, pH 5.5) to avoid glucose repression. HO expression was induced by the addition of galactose to a final concentration of 2 %. In experiments in which a homology is present to allow repair (donor-proficient strains), 2 % glucose (final concentration) was added after 1 hour to shut off HO expression. For *SceI*-based DSB induction, the respective yeast strains were transformed with the *SceI* expression plasmid pWJ1320 (kindly provided by M. Lisby), encoding *SCEI* placed under *GAL* promoter control, and subsequently grown in SC-ADE lactate. *SceI* expression was induced as for HO by the addition of galactose to a final concentration of 2 %.

6.3.3 Chromatin-Immunoprecipitations (ChIP)

General Buffers and Solutions

FA lysis buffer	50 mM HEPES 150 mM NaCl 1 mM EDTA 1 % Triton X-100 0.1 % Deoxycholic acid, Na-salt 0.1 % SDS
FA lysis buffer 5 mM NaCl	50 mM HEPES 500 mM NaCl 1 mM EDTA 1 % Triton X-100 0.1 % Deoxycholic acid, Na-salt 0.1 % SDS
ChIP wash buffer	10 mM Tris HCl pH 8 250 mM LiCl 1 mM EDTA 0.5 % NP-40 0.5 % Deoxycholic acid, Na-salt

ChIP elution buffer	50 mM Tris pH 7.5 10 mM EDTA 1% SDS
TE	10 mM Tris pH 8 1 mM EDTA
Quenching solution	2.5 M glycine Sterilized by autoclaving

Chromatin-Immunoprecipitation

Chromatin immunoprecipitation (ChIP) time-course experiments were performed similarly as described previously^{172,76}. 200 ml cultures of every time point were cross-linked by the addition of 1 % (final concentration) formaldehyde for 16 min (if suitable, 1OD was harvested from each time point directly before crosslinking, and used for Western blot analysis), and subsequent quenching with 375 mM (final concentration) glycine for at least 10 min. 160 OD of crosslinked cells were then pelleted by centrifugation (5500 g, 5 min, 4°C), washed one with ice-cold PBS and transferred to a 2 ml Eppendorf tube. Cells were frozen in liquid N₂, and generally stored overnight (or for some days) at -80°C.

For chromatin preparation, cells were thaw on ice and 800 µl FA lysis buffer (freshly complemented with 1 mg/ml Pefabloc SC (Roche) and EDTA-free complete cocktail (Roche)) was added. Cells were lysed by the addition of zirconia/silica beads (BioSpec Inc., Bartlesville, USA) and the usage of a multi-tube bead-beater (MM301 from Retsch GmbH, Haan, Germany) for 6 times for 3 minutes (30/s frequency) with 3 min cooling intervals (to allow cooling, the bead-beater was continuously placed in a 4 °C cold-room). Upon cell lysis, samples were transferred (piggyback method to separate the sample from the beads) to a 15 ml Falcon tube. Upon additional transfer to a fresh 2 ml Eppendorf tube, chromatin was separated from the soluble fraction by centrifugation (20000 g, 15 min, 4 °C). Subsequently, the chromatin pellet was resuspended in 2 ml ice-cold FA lysis buffer (complemented with 1 mg/ml Pefabloc SC and EDTA-free complete cocktail) and transferred to hard plastic Sumilon 15 ml centrifuge tubes (Sumitomo Bakelite Co., Japan). Then, chromatin was sheared by water/ice bath sonification in Bioruptor UCD-200 instruments (Diagenode sa, Liège, Belgium). Generally, 30 times 30 s cycles (with 30 s breaks in between) at an output of 200 W were performed with the aim to shear the DNA to an average length of 250-500 bp. As the efficiency of the Bioruptor UCD-200 instruments decreased over time the number of cycles was increased meanwhile to 40.

The sheared and thus solubilized chromatin was purified from unbroken cells and cell debris by centrifugation (20000 g, 30 min, 4 °C). Subsequently, 20 µl of the supernatant was removed as “input” samples, and 800 µl of the supernatant was used for immunoprecipitation (IP). For IP, the respective antibody (Anti-c-myc (SIGMA, 9E10), anti-γH2A (phospho-ser129,

Upstate), anti-RPA (Agrisera), anti-Rad51 (Santa Cruz), and anti-Rad52⁷⁸) was added to the chromatin solution and incubated for 90 min at 23 °C with head-over-tail rotation. Thereafter, 25 µl pre-swollen Protein A Sepharose CL-4B 50/50 slurry (GE Healthcare, Little Chalfont, UK) was added and incubated for 30 min at 23 °C with head-over-tail rotation. Beads were then washed three times with 400 µl FA lysis buffer, once with 400 µl FA lysis buffer containing 0.5 M NaCl, once with 400 µl ChIP wash buffer and once with TE pH 8 (with centrifugation in between each step; 150 g, 3 min, RT). 110 µl ChIP elution buffer was added and incubated at 65 °C for 15 min (shaking at 1400 rpm) to elute bound protein-DNA complexes. Upon centrifugation, 100 µl of the supernatant was removed as “ChIP” sample.

Input and ChIP samples were digested by Proteinase K for 2 hours at 42 °C and decrosslinked for 6 hours at 65 °C. Subsequently, the Input and ChIP DNA samples were purified using the QIAquick PCR purification kit (Quiagen, Hilden, Germany), and thereafter either used for RT-qPCR (see paragraph “Quantitative Real-Time PCR for ChIP Analysis”) or ChIP-on-chip analysis (see paragraph “ChIP-on-chip analysis”).

Quantitative Real-Time PCR for ChIP Analysis

Quantitative Real-Time PCR (RT-qPCR) analysis on ChIP samples was performed using the LightCycler 480 SYBR Green I Master hot-start reaction mix (Roche Diagnostics GmbH, Mannheim, Germany) and the LightCycler 480 System. 2 µl of either ChIP sample (undiluted) or input sample (1:10 dilution) were mixed with 18 µl master mix (see below) in triplicates in 384-well LightCycler plates. Pipetting was performed by a CAS-1200 PCR setup robot (Corbett Lifescience/Quiagen, Hilden, Germany).

RT-qPCR mix

	µl
SYBR Green I Master Mix	10
Primer 1 (10 µM)	1.2
Primer 2 (10 µM)	1.2
H ₂ O	5.6
Sample	2

LightCycler

95 °C	10 min
then 45 cycles	
95 °C	10 s
57 °C	10 s
72 °C	16 s
Melting curve analysis	
4 °C	∞

To quantify template DNA concentration, for each primer pair a dilution series was generated from one input samples (1:5, 1:50, 1:500, 1:5000) and the LightCycler PCR amplification curves were quantified from their second derivative maximum. Moreover, melting curve analysis was performed as a quality control for primer specificity (only a single PCR product should be amplified per reaction).

Generally, RT-qPCR ChIP data was normalized to a control locus and to 1 before DSB induction. Normalization to a control locus (*YJL112W/Mdv1*) was calculated by ((IP[test]/input[test])/(IP[control]/input[control])).

Monitoring Mating-type Switching by quantitative Real-Time PCR

Recombination between *MAT* and *HML* loci was monitored by RT-qPCR, using unique primers pA and pB that prime distal to *MAT* and within *HML*¹¹². Thus, only upon recombination a PCR product can be generated. RT-qPCR was performed on ChIP Input samples.

Primers used for Real-Time PCR

Name	Sequence	Chr. Location	Source
JOR001 for	GCAACTGTCACAGTTGTTAGCCG	Chr. III, 253 kb	This study
JOR002 rev	ATTTCCCTCGGGAACCTTCTT	Chr. III, 253 kb	This study
JOR053 for	CCCAAGCTCACAAATTAATATGGC	Chr. III, 275 kb	This study
JOR053 rev	GCATCTGTAGTACCACTGCTCTTTG	Chr. III, 275 kb	This study
JOR138 for	CTTTTCGTGTTCTAGCGTGTTAC	Chr. III, 29 kb	This study
JOR139 rev	CTATCCAAAACCCTGGGCAA	Chr. III, 29 kb	This study
JOR140 for	CATGGCACTTACTGTGTTACCTTG	Chr. III, 23 kb	This study
JOR141 rev	GCGTGTGTTCTAGATTTAGTCGAAG	Chr. III, 23 kb	This study
JOR161 for	CGCCATTTGGGTGTAAAATCG	Chr. III, 28 kb	This study
JOR161 rev	GGAAACCTGGTTTGGAGATCAATC	Chr. III, 28 kb	This study
JOR254 for	AACGACGTGCTGTTTACCTGAT	Chr. V, 30 kb	This study
JOR255 rev	TGTGCACTAATGGGATATTCGG	Chr. V, 30 kb	This study
JOR256 for	AACGCAGACTCGGCTTTATCTA	Chr. V, 55 kb	This study
JOR257 rev	GACCATCTGACAGACTATTCCACAA	Chr. V, 55 kb	This study
JOR258 for	TATGGGTACCTATATGAAGCCCTG	Chr. V, 20 kb	This study
JOR259 rev	GACAACGGGACATTGATCTTTG	Chr. V, 20 kb	This study
JOR330 for	AGGGCCAACACCTAGTCCAA	Chr. IV, 496 kb	This study
JOR331 rev	AGGCGAAGTTAGTGCTGAACA	Chr. IV, 496 kb	This study
CterYJL112Win	GCGTGCCTGGTCACAGGTTTCATACGAC	Chr. X, 207 kb	76
CterYJL112Wre	TCATACGGCCCAAATATTTACGTCCC	Chr. X, 207 kb	76
HO -100check	GAGCATATTACTCACAGTTTGGCTC	Chr. III, 200 kb	76
HO +190re	GGATAGCTATACTGACAACATTCAG	Chr. III, 200 kb	76
HO +0,2 kb in	CCTGGTTTTTGGTTTTGTAGAGTGG	Chr. III, 201 kb	111
HO +0,2 kb	GAGCAAGACGATGGGGAGTTTC	Chr. III, 201 kb	111
HO +5,7 kb in	ACCAGCAGTAATAAGTCGTCCTGA	Chr. III, 206 kb	111
HO +5,7 kb re	CCAAGGAATAATGATCTAAGCACA	Chr. III, 206 kb	111
pA (<i>MAT</i> distal)	GCAGCACGGAATATGGGACT	switched <i>MAT</i>	112
pB (<i>Yα</i>)	ATGTGAACCGCATGGGCAGT	switched <i>MAT</i>	112
p <i>HML</i> for	TCCCCATCGTCTTGCTCT	Chr. III, 14 kb	111
p <i>HML</i> rev	CCC AAGGCTTAGTATACACATCC	Chr. III, 14 kb	111

6.3.4 ChIP-on-chip Analysis

ChIP-chip was performed as described previously⁷⁶. Briefly, samples were processed as for ChIP. After RNase (DNase-free RNase) treatment and ligation of linker oligonucleotides, DNA was amplified two times for 14 PCR cycles (using the GenomePlex Whole Genome Amplification (WGA) and reamplification kits (Sigma)), as described in the Farnham Lab protocol for WGA amplification of DNA¹⁷³. Subsequent labeling of input and IP samples (either Cy3 or Cy5), hybridization to custom-made high-density whole *S. cerevisiae* genome NimbleGen arrays, array scanning and raw data extraction was performed by SourceBioSource (former imaGenes; NimbleGen ChIP-chip service). Two different kinds of

NimbleGen arrays were used in this study. Whereas for Figure 12A (Rfa1-9myc and Rad52) “array type 1” (NimbleGen CA4214-00-01 with 32 bp median genomic probe spacing) has been used, for all other data “array type 2 (12plex NimbleGen custom array with 84 bp median genomic probe spacing and only unique oligonucleotides) has been used. Quality controls, normalization and data analysis was performed using R/Bioconductor (www.Rproject.org; www.bioconductor.org) as described (¹⁷⁴ and Tobias Straub Epigenome project PROT43, <http://www.epigenesys.eu/>). Briefly, despite array normalization and mean of two independent experiments, data depicted in all figures represent raw data. Consequently, single spikes in the ChIP-chip data correspond to single oligonucleotides, and are hybridization artifacts. All ChIP-chip data are normalized to the input. The depicted data in Figures 10, 12A, 13A-C, 15A, 20, 23A-D, 24, and 26A-D were additionally normalized to the corresponding 0 hr data set.

6.4 Computer-aided Analysis

Literature review was performed using databases integrated into the National Center of Biotechnology Information (www.ncbi.nlm.nih.gov) and Papers2 (<http://support.mekentosj.com/kb>). For *S. cerevisiae* genomic sequence and protein information the Saccharomyces Genome Database (www.yeastgenome.org) was used. Sequence analysis (DNA restriction enzyme maps, DNA sequencing analysis) was performed using DNA-Star software (DNA Star Inc.). Data statistics and representation were performed by GraphPad Prism (www.graphpad.com/scientific-software/prism/), ChIP-on-chip data representation was performed by the Integrated Genome Browser (<http://bioviz.org/igb/>). ChIP-on-chip quality controls, normalization and data analysis was performed using R/Bioconductor (www.Rproject.org; www.bioconductor.org). Matlab was used to segment ChIP-on-chip data into 20 kb windows, centered to the respective centromere position. Figures were labeled and illustrations were created using Adobe Illustrator software (Adobe Systems Inc.). For text and table generation, the Microsoft Office software package (Microsoft Corp.) was used.

6.5 Statistical Analysis

All ChIP data are depicted on a log₂-scale and as the mean \pm SEM (standard error of the mean) of 3 independent ChIP experiments, despite Figures 23E and 23F, in which 4 independent experiments were performed to allow statistical analysis via Kruskal–Wallis one-way analysis of variance. All ChIP-chip data are depicted on a log₂-scale and as the mean of two independent experiments (which includes a labeling dye swap to exclude labeling artifacts), despite Figures 21B, 22A, 22B and 24, which depict experiments that were only performed once.

7 References

1. Branzei, D. & Foiani, M. Maintaining genome stability at the replication fork. *Nat Rev Mol Cell Biol* **11**, 208–219 (2010).
2. Kim, N. & Jinks-Robertson, S. Transcription as a source of genome instability. *Nat Rev Genet* **13**, 204–214 (2012).
3. Mitchell, J. R., Hoeijmakers, J. H. & Niedernhofer, L. J. Divide and conquer: nucleotide excision repair battles cancer and ageing. *Current Opinion in Cell Biology* **15**, 232–240 (2003).
4. Aguilera, A. & Gómez-González, B. Genome instability: a mechanistic view of its causes and consequences. *Nat Rev Genet* **9**, 204–217 (2008).
5. Thompson, L. H. & Schild, D. Recombinational DNA repair and human disease. *Mutat. Res.* **509**, 49–78 (2002).
6. Vijg, J. & Suh, Y. Genome Instability and Aging. *Annu. Rev. Physiol.* **75**, 645–668 (2013).
7. Lichten, M. Meiotic recombination: Breaking the genome to save it. *Current Biology* **11**, R253–R256 (2001).
8. Schatz, D. G. & Ji, Y. Recombination centres and the orchestration of V(D)J recombination. *Nat Rev Immunol* **11**, 251–263 (2011).
9. Symington, L. S. & Gautier, J. Double-strand break end resection and repair pathway choice. *Annu. Rev. Genet.* **45**, 247–271 (2011).
10. Chapman, J. R., Taylor, M. R. G. & Boulton, S. J. Playing the end game: DNA double-strand break repair pathway choice. *Molecular Cell* **47**, 497–510 (2012).
11. Lieber, M. R. The mechanism of double-strand DNA break repair by the nonhomologous DNA end-joining pathway. *Annu. Rev. Biochem.* **79**, 181–211 (2010).
12. Daley, J. M., Palmbo, P. L., Wu, D. & Wilson, T. E. Nonhomologous end joining in yeast. *Annu. Rev. Genet.* **39**, 431–451 (2005).
13. Heyer, W.-D., Ehmsen, K. T. & Liu, J. Regulation of homologous recombination in eukaryotes. *Annu. Rev. Genet.* **44**, 113–139 (2010).
14. Malkova, A. & Haber, J. E. Mutations arising during repair of chromosome breaks. *Annu. Rev. Genet.* **46**, 455–473 (2012).
15. Hicks, W. M., Kim, M. & Haber, J. E. Increased Mutagenesis and Unique Mutation Signature Associated with Mitotic Gene Conversion. *Science* **329**, 82–85 (2010).
16. Stracker, T. H. & Petrini, J. H. J. The MRE11 complex: starting from the ends. *Nat Rev Mol Cell Biol* **12**, 90–103 (2011).
17. Garcia, V., Phelps, S. E. L., Gray, S. & Neale, M. J. Bidirectional resection of DNA double-strand breaks by Mre11 and Exo1. *Nature* **479**, 241–244 (2011).
18. Huertas, P. DNA resection in eukaryotes: deciding how to fix the break. *Nat Struct Mol Biol* **17**, 11–16 (2010).
19. Longhese, M. P., Bonetti, D., Manfrini, N. & Clerici, M. Mechanisms and regulation of DNA end resection. *EMBO J* **29**, 2864–2874 (2010).
20. Papamichos-Chronakis, M. & Peterson, C. L. Chromatin and the genome integrity network. *Nat Rev Genet* **14**, 62–75 (2012).
21. Mazón, G., Mimitou, E. P. & Symington, L. S. SnapShot: Homologous recombination in DNA double-strand break repair. *Cell* **142**, 646–646.e1 (2010).

22. Bell, J. C., Plank, J. L., Dombrowski, C. C. & Kowalczykowski, S. C. Direct imaging of RecA nucleation and growth on single molecules of SSB-coated ssDNA. *Nature* **491**, 274–278 (2012).
23. Barzel, A. & Kupiec, M. Finding a match: how do homologous sequences get together for recombination? *Nat Rev Genet* **9**, 27–37 (2008).
24. Weiner, A., Zauberman, N. & Minsky, A. Recombinational DNA repair in a cellular context: a search for the homology search. *Nat. Rev. Microbiol.* **7**, 748–755 (2009).
25. San Filippo, J., Sung, P. & Klein, H. Mechanism of eukaryotic homologous recombination. *Annu. Rev. Biochem.* **77**, 229–257 (2008).
26. Llorente, B., Smith, C. E. & Symington, L. S. Break-induced replication: what is it and what is it for? *Cell Cycle* **7**, 859–864 (2008).
27. Li, X., Stith, C. M., Burgers, P. M. & Heyer, W.-D. PCNA Is Required for Initiation of Recombination-Associated DNA Synthesis by DNA Polymerase δ . *Molecular Cell* **36**, 704–713 (2009).
28. Haber, J. E. Lucky breaks: analysis of recombination in *Saccharomyces*. *Mutat. Res.* **451**, 53–69 (2000).
29. Strathern, J. N. *et al.* Homothallic switching of yeast mating type cassettes is initiated by a double-stranded cut in the MAT locus. *Cell* **31**, 183–192 (1982).
30. Kostriken, R. & Heffron, F. The product of the HO gene is a nuclease: purification and characterization of the enzyme. *Cold Spring Harb Symp Quant Biol* **49**, 89–96 (1984).
31. Jensen, R. E. & Herskowitz, I. Directionality and regulation of cassette substitution in yeast. *Cold Spring Harb Symp Quant Biol* **49**, 97–104 (1984).
32. Sugawara, N. & Haber, J. E. *Methods in Enzymology*. **408**, 416–429 (Elsevier, 2006).
33. Haber, J. E. Mating-type gene switching in *Saccharomyces cerevisiae*. *Annu. Rev. Genet.* **32**, 561–599 (1998).
34. Klar, A. J., Hicks, J. B. & Strathern, J. N. Directionality of yeast mating-type interconversion. *Cell* **28**, 551–561 (1982).
35. Wu, X. & Haber, J. E. MATa donor preference in yeast mating-type switching: activation of a large chromosomal region for recombination. *Genes & Development* **9**, 1922–1932 (1995).
36. Wu, X. & Haber, J. E. A 700 bp cis-acting region controls mating-type dependent recombination along the entire left arm of yeast chromosome III. *Cell* **87**, 277–285 (1996).
37. Coïc, E., Richard, G.-F. & Haber, J. E. *Saccharomyces cerevisiae* donor preference during mating-type switching is dependent on chromosome architecture and organization. *Genetics* **173**, 1197–1206 (2006).
38. Li, J. *et al.* Regulation of budding yeast mating-type switching donor preference by the FHA domain of Fkh1. *PLoS Genet.* **8**, e1002630 (2012).
39. Sun, K., Coïc, E., Zhou, Z., Durrens, P. & Haber, J. E. *Saccharomyces* forkhead protein Fkh1 regulates donor preference during mating-type switching through the recombination enhancer. *Genes & Development* **16**, 2085–2096 (2002).
40. Wu, C. *et al.* Mcm1 regulates donor preference controlled by the recombination enhancer in *Saccharomyces* mating-type switching. *Genes & Development* **12**, 1726–1737 (1998).
41. West, S. C. Molecular views of recombination proteins and their control. *Nat Rev Mol Cell Biol* **4**, 435–445 (2003).
42. Holthausen, J. T., Wyman, C. & Kanaar, R. Regulation of DNA strand exchange in homologous recombination. *DNA Repair* **9**, 1264–1272 (2010).

43. Mortensen, U. H., Lisby, M. & Rothstein, R. Rad52. *Curr. Biol.* **19**, R676–7 (2009).
44. Holloman, W. K. Unraveling the mechanism of BRCA2 in homologous recombination. *Nat Struct Mol Biol* **18**, 748–754 (2011).
45. Loveday, C. *et al.* Germline RAD51C mutations confer susceptibility to ovarian cancer. *Nat Genet* **44**, 475–476 (2012).
46. Liu, J. *et al.* Rad51 paralogues Rad55–Rad57 balance the antirecombinase Srs2 in Rad51 filament formation. *Nature* **479**, 245–248 (2011).
47. Harrison, J. C. & Haber, J. E. Surviving the breakup: the DNA damage checkpoint. *Annu. Rev. Genet.* **40**, 209–235 (2006).
48. Harper, J. W. & Elledge, S. J. The DNA Damage Response: Ten Years After. *Molecular Cell* **28**, 739–745 (2007).
49. Flott, S. *et al.* Regulation of Rad51 function by phosphorylation. *EMBO Rep.* **12**, 833–839 (2011).
50. Yata, K. *et al.* Plk1 and CK2 Act in Concert to Regulate Rad51 during DNA Double Strand Break Repair. *Molecular Cell* **45**, 371–383 (2012).
51. Miller, K. M. & Jackson, S. P. Histone marks: repairing DNA breaks within the context of chromatin. *Biochem. Soc. Trans.* **40**, 370–376 (2012).
52. Ström, L. *et al.* Postreplicative formation of cohesion is required for repair and induced by a single DNA break. *Science* **317**, 242–245 (2007).
53. Kim, J. A., Kruhlak, M., Dotiwala, F., Nussenzweig, A. & Haber, J. E. Heterochromatin is refractory to γ -H2AX modification in yeast and mammals. *The Journal of Cell Biology* **178**, 209–218 (2007).
54. Iacovoni, J. S. *et al.* High-resolution profiling of γ H2AX around DNA double strand breaks in the mammalian genome. *EMBO J* **29**, 1446–1457 (2010).
55. van Attikum, H., Fritsch, O., Hohn, B. & Gasser, S. M. Recruitment of the INO80 Complex by H2A Phosphorylation Links ATP-Dependent Chromatin Remodeling with DNA Double-Strand Break Repair. *Cell* **119**, 777–788 (2004).
56. Morrison, A. J. *et al.* INO80 and gamma-H2AX interaction links ATP-dependent chromatin remodeling to DNA damage repair. *Cell* **119**, 767–775 (2004).
57. van Attikum, H., Fritsch, O. & Gasser, S. M. Distinct roles for SWR1 and INO80 chromatin remodeling complexes at chromosomal double-strand breaks. *EMBO J* **26**, 4113–4125 (2007).
58. Chai, B., Huang, J., Cairns, B. R. & Laurent, B. C. Distinct roles for the RSC and Swi/Snf ATP-dependent chromatin remodelers in DNA double-strand break repair. *Genes & Development* **19**, 1656–1661 (2005).
59. Shim, E. Y. *et al.* RSC mobilizes nucleosomes to improve accessibility of repair machinery to the damaged chromatin. *Molecular and Cellular Biology* **27**, 1602–1613 (2007).
60. Kent, N. A., Chambers, A. L. & Downs, J. A. Dual Chromatin Remodeling Roles for RSC during DNA Double Strand Break Induction and Repair at the Yeast MAT Locus. *Journal of Biological Chemistry* **282**, 27693–27701 (2007).
61. Costelloe, T. *et al.* The yeast Fun30 and human SMARCD1 chromatin remodellers promote DNA end resection. *Nature* **489**, 581–584 (2012).
62. Chen, X. *et al.* The Fun30 nucleosome remodeler promotes resection of DNA double-strand break ends. *Nature* **489**, 576–580 (2012).
63. Eapen, V. V., Sugawara, N., Tsabar, M., Wu, W.-H. & Haber, J. E. The *Saccharomyces cerevisiae* Chromatin Remodeler Fun30 Regulates DNA End Resection and Checkpoint Deactivation. *Molecular and Cellular Biology*

- 32**, 4727–4740 (2012).
64. Smeenk, G. & van Attikum, H. The chromatin response to DNA breaks: leaving a mark on genome integrity. *Annu. Rev. Biochem.* **82**, 55–80 (2013).
 65. Bergink, S. & Jentsch, S. Principles of ubiquitin and SUMO modifications in DNA repair. *Nature* **458**, 461–467 (2009).
 66. Bekker-Jensen, S. & Mailand, N. The ubiquitin- and SUMO-dependent signaling response to DNA double-strand breaks. *FEBS Lett.* **585**, 2914–2919 (2011).
 67. Dou, H., Huang, C., Van Nguyen, T., Lu, L.-S. & Yeh, E. T. H. SUMOylation and de-SUMOylation in response to DNA damage. *FEBS Lett.* **585**, 2891–2896 (2011).
 68. Jentsch, S. & Müller, S. Regulatory Functions of Ubiquitin and SUMO in DNA Repair Pathways. *Subcell. Biochem.* **54**, 184–194 (2010).
 69. Jackson, S. P. & Durocher, D. Regulation of DNA damage responses by ubiquitin and SUMO. *Molecular Cell* **49**, 795–807 (2013).
 70. Lukas, J., Lukas, C. & Bartek, J. More than just a focus: The chromatin response to DNA damage and its role in genome integrity maintenance. *Nat. Cell Biol.* **13**, 1161–1169 (2011).
 71. Huen, M. S. Y. *et al.* RNF8 Transduces the DNA-Damage Signal via Histone Ubiquitylation and Checkpoint Protein Assembly. *Cell* **131**, 901–914 (2007).
 72. Kolas, N. K. *et al.* Orchestration of the DNA-damage response by the RNF8 ubiquitin ligase. *Science* **318**, 1637–1640 (2007).
 73. Mailand, N. *et al.* RNF8 ubiquitylates histones at DNA double-strand breaks and promotes assembly of repair proteins. *Cell* **131**, 887–900 (2007).
 74. Bekker-Jensen, S. *et al.* HERC2 coordinates ubiquitin-dependent assembly of DNA repair factors on damaged chromosomes. *Nat. Cell Biol.* **12**, 80–6; sup pp 1–12 (2009).
 75. Doil, C. *et al.* RNF168 binds and amplifies ubiquitin conjugates on damaged chromosomes to allow accumulation of repair proteins. *Cell* **136**, 435–446 (2009).
 76. Kalocsay, M., Hiller, N. J. & Jentsch, S. Chromosome-wide Rad51 spreading and SUMO-H2A.Z-dependent chromosome fixation in response to a persistent DNA double-strand break. *Molecular Cell* **33**, 335–343 (2009).
 77. Torres-Rosell, J. *et al.* The Smc5-Smc6 complex and SUMO modification of Rad52 regulates recombinational repair at the ribosomal gene locus. *Nat. Cell Biol.* **9**, 923–931 (2007).
 78. Sacher, M., Pfander, B., Hoege, C. & Jentsch, S. Control of Rad52 recombination activity by double-strand break-induced SUMO modification. *Nat. Cell Biol.* **8**, 1284–1290 (2006).
 79. Danielsen, J. R. *et al.* DNA damage-inducible SUMOylation of HERC2 promotes RNF8 binding via a novel SUMO-binding Zinc finger. *The Journal of Cell Biology* **197**, 179–187 (2012).
 80. McAleenan, A. *et al.* SUMOylation of the α -Kleisin Subunit of Cohesin Is Required for DNA Damage-Induced Cohesion. *Current Biology* **22**, 1564–1575 (2012).
 81. Altmannova, V. *et al.* Rad52 SUMOylation affects the efficiency of the DNA repair. *Nucleic Acids Research* **40**, 3775–3775 (2012).
 82. Dou, H., Huang, C., Singh, M., Carpenter, P. B. & Yeh, E. T. H. Regulation of DNA repair through deSUMOylation and SUMOylation of replication protein A complex. *Molecular Cell* **39**, 333–345 (2010).
 83. Psakhye, I. & Jentsch, S. Protein Group Modification and Synergy in the SUMO Pathway as Exemplified in DNA Repair. *Cell* **151**, 807–820 (2012).

84. Cremona, C. A. *et al.* Extensive DNA damage-induced sumoylation contributes to replication and repair and acts in addition to the mec1 checkpoint. *Molecular Cell* **45**, 422–432 (2012).
85. Branzei, D. *et al.* Ubc9- and Mms21-Mediated Sumoylation Counteracts Recombinogenic Events at Damaged Replication Forks. *Cell* **127**, 509–522 (2006).
86. Galanty, Y. *et al.* Mammalian SUMO E3-ligases PIAS1 and PIAS4 promote responses to DNA double-strand breaks. *Nature* **462**, 935–939 (2009).
87. Morris, J. R. *et al.* The SUMO modification pathway is involved in the BRCA1 response to genotoxic stress. *Nature* **462**, 886–890 (2009).
88. Sinha, M. & Peterson, C. L. A Rad51 Presynaptic Filament Is Sufficient to Capture Nucleosomal Homology during Recombinational Repair of a DNA Double-Strand Break. *Molecular Cell* **30**, 803–810 (2008).
89. Sinha, M., Watanabe, S., Johnson, A., Moazed, D. & Peterson, C. L. Recombinational repair within heterochromatin requires ATP-dependent chromatin remodeling. *Cell* **138**, 1109–1121 (2009).
90. Forget, A. L. & Kowalczykowski, S. C. Single-molecule imaging of DNA pairing by RecA reveals a three-dimensional homology search. *Nature* **482**, 423–427 (2012).
91. Adzuma, K. No sliding during homology search by RecA protein. *J. Biol. Chem.* **273**, 31565–31573 (1998).
92. Ragunathan, K., Liu, C. & Ha, T. RecA filament sliding on DNA facilitates homology search. *Elife* **1**, e00067 (2012).
93. Savir, Y. & Tlusty, T. RecA-mediated homology search as a nearly optimal signal detection system. *Molecular Cell* **40**, 388–396 (2010).
94. De Vlaminc, I. *et al.* Mechanism of homology recognition in DNA recombination from dual-molecule experiments. *Molecular Cell* **46**, 616–624 (2012).
95. Bressan, D. A., Vazquez, J. & Haber, J. E. Mating type-dependent constraints on the mobility of the left arm of yeast chromosome III. *The Journal of Cell Biology* **164**, 361–371 (2004).
96. Inbar, O. & Kupiec, M. Homology search and choice of homologous partner during mitotic recombination. *Molecular and Cellular Biology* **19**, 4134–4142 (1999).
97. Aylon, Y., Liefshitz, B., Bitan-Banin, G. & Kupiec, M. Molecular dissection of mitotic recombination in the yeast *Saccharomyces cerevisiae*. *Molecular and Cellular Biology* **23**, 1403–1417 (2003).
98. Haber, J. E. & Leung, W. Y. Lack of chromosome territoriality in yeast: promiscuous rejoining of broken chromosome ends. *Proc. Natl. Acad. Sci. U.S.A.* **93**, 13949–13954 (1996).
99. Lichten, M. & Haber, J. E. Position effects in ectopic and allelic mitotic recombination in *Saccharomyces cerevisiae*. *Genetics* **123**, 261–268 (1989).
100. Burgess, S. M. & Kleckner, N. Collisions between yeast chromosomal loci in vivo are governed by three layers of organization. *Genes & Development* **13**, 1871–1883 (1999).
101. Ira, G., Malkova, A., Liberi, G., Foiani, M. & Haber, J. E. Srs2 and Sgs1–Top3 Suppress Crossovers during Double-Strand Break Repair in Yeast. *Cell* **115**, 401–411 (2003).
102. Agmon, N., Pur, S., Liefshitz, B. & Kupiec, M. Analysis of repair mechanism choice during homologous recombination. *Nucleic Acids Research* **37**, 5081–5092 (2009).
103. Coïc, E. *et al.* Dynamics of homology searching during gene conversion in

- Saccharomyces cerevisiae revealed by donor competition. *Genetics* **189**, 1225–1233 (2011).
104. Aylon, Y. & Kupiec, M. DSB repair: the yeast paradigm. *DNA Repair* **3**, 797–815 (2004).
105. Miné-Hattab, J. & Rothstein, R. Increased chromosome mobility facilitates homology search during recombination. *Nat. Cell Biol.* **14**, 510–517 (2012).
106. Dion, V., Kalck, V., Horigome, C., Towbin, B. D. & Gasser, S. M. Increased mobility of double-strand breaks requires Mec1, Rad9 and the homologous recombination machinery. *Nat. Cell Biol.* **14**, 502–509 (2012).
107. Neumann, F. R. *et al.* Targeted INO80 enhances subnuclear chromatin movement and ectopic homologous recombination. *Genes & Development* **26**, 369–383 (2012).
108. Gehlen, L. R., Gasser, S. M. & Dion, V. How Broken DNA Finds Its Template for Repair: A Computational Approach. *Progress of Theoretical Physics Supplement* 20–29
109. Dion, V. & Gasser, S. M. Chromatin Movement in the Maintenance of Genome Stability. *Cell* **152**, 1355–1364 (2013).
110. Wolner, B., van Komen, S., Sung, P. & Peterson, C. L. Recruitment of the recombinational repair machinery to a DNA double-strand break in yeast. *Molecular Cell* **12**, 221–232 (2003).
111. Sugawara, N., Wang, X. & Haber, J. E. In vivo roles of Rad52, Rad54, and Rad55 proteins in Rad51-mediated recombination. *Molecular Cell* **12**, 209–219 (2003).
112. White, C. I. & Haber, J. E. Intermediates of recombination during mating type switching in *Saccharomyces cerevisiae*. *EMBO J* **9**, 663–673 (1990).
113. Oakley, G. G. & Patrick, S. M. Replication protein A: directing traffic at the intersection of replication and repair. *Front. Biosci.* **15**, 883–900 (2010).
114. Yamane, A. *et al.* RPA Accumulation during Class Switch Recombination Represents 5′–3′ DNA-End Resection during the S–G2/M Phase of the Cell Cycle. *Cell Reports* **3**, 138–147 (2013).
115. Zierhut, C. & Diffley, J. F. X. Break dosage, cell cycle stage and DNA replication influence DNA double strand break response. *EMBO J* **27**, 1875–1885 (2008).
116. Müller, B., Koller, T. & Stasiak, A. Characterization of the DNA binding activity of stable RecA-DNA complexes. Interaction between the two DNA binding sites within RecA helical filaments. *Journal of Molecular Biology* **212**, 97–112 (1990).
117. Cloud, V., Chan, Y. L., Grubb, J., Budke, B. & Bishop, D. K. Rad51 Is an Accessory Factor for Dmc1-Mediated Joint Molecule Formation During Meiosis. *Science* **337**, 1222–1225 (2012).
118. Jin, Q. W., Fuchs, J. & Loidl, J. Centromere clustering is a major determinant of yeast interphase nuclear organization. *Journal of Cell Science* **113** (Pt 11), 1903–1912 (2000).
119. Duan, Z. *et al.* A three-dimensional model of the yeast genome. *Nature* **465**, 363–367 (2010).
120. O'Sullivan, J. M. Yeast chromosomal interactions and nuclear architecture. *Current Opinion in Cell Biology* **22**, 298–304 (2010).
121. Zimmer, C. & Fabre, E. Principles of chromosomal organization: lessons from yeast. *The Journal of Cell Biology* **192**, 723–733 (2011).
122. Bystricky, K., Laroche, T., Van Houwe, G., Blaszczyk, M. & Gasser, S. M. Chromosome looping in yeast: telomere pairing and coordinated movement reflect anchoring efficiency and territorial organization. *The Journal of Cell*

- Biology* **168**, 375–387 (2005).
123. Therizols, P., Duong, T., Dujon, B., Zimmer, C. & Fabre, E. Chromosome arm length and nuclear constraints determine the dynamic relationship of yeast subtelomeres. *Proc. Natl. Acad. Sci. U.S.A.* **107**, 2025–2030 (2010).
124. Taddei, A., Hediger, F., Neumann, F. R., Bauer, C. & Gasser, S. M. Separation of silencing from perinuclear anchoring functions in yeast Ku80, Sir4 and Esc1 proteins. *EMBO J* **23**, 1301–1312 (2004).
125. Schober, H. *et al.* Controlled exchange of chromosomal arms reveals principles driving telomere interactions in yeast. *Genome Res.* **18**, 261–271 (2008).
126. Wang, X. & Haber, J. E. Role of Saccharomyces Single-Stranded DNA-Binding Protein RPA in the Strand Invasion Step of Double-Strand Break Repair. *Plos Biol* **2**, e21 (2004).
127. Heyer, W.-D., Li, X., Rolfsmeier, M. & Zhang, X.-P. Rad54: the Swiss Army knife of homologous recombination? *Nucleic Acids Research* **34**, 4115–4125 (2006).
128. Heyer, W.-D., Li, X., Rolfsmeier, M. & Zhang, X.-P. Functions of the Snf2/Swi2 family Rad54 motor protein in homologous recombination. *Biochim. Biophys. Acta* **1809**, 4115–4125 (2011).
129. Mazin, A. V., Mazina, O. M., Bugreev, D. V. & Rossi, M. J. Rad54, the motor of homologous recombination. *DNA Repair* **9**, 286–302 (2010).
130. Sung, P., Petukhova, G. & Stratton, S. Catalysis of homologous DNA pairing by yeast Rad51 and Rad54 proteins. *Nature* **393**, 91–94 (1998).
131. Bugreev, D. V., Mazina, O. M. & Mazin, A. V. Rad54 protein promotes branch migration of Holliday junctions. *Nature* **442**, 590–593 (2006).
132. Solinger, J. A., Kiiianitsa, K. & Heyer, W.-D. Rad54, a Swi2/Snf2-like recombinational repair protein, disassembles Rad51:dsDNA filaments. *Molecular Cell* **10**, 1175–1188 (2002).
133. Nimonkar, A. V. *et al.* Saccharomyces cerevisiae Dmc1 and Rad51 Proteins Preferentially Function with Tid1 and Rad54 Proteins, Respectively, to Promote DNA Strand Invasion during Genetic Recombination. *Journal of Biological Chemistry* **287**, 28727–28737 (2012).
134. Shah, P. P. *et al.* Swi2/Snf2-Related Translocases Prevent Accumulation of Toxic Rad51 Complexes during Mitotic Growth. *Molecular Cell* **39**, 862–872 (2010).
135. Shroff, R. *et al.* Distribution and Dynamics of Chromatin Modification Induced by a Defined DNA Double-Strand Break. *Current Biology* **14**, 1703–1711 (2004).
136. Szilard, R. K. *et al.* Systematic identification of fragile sites via genome-wide location analysis of gamma-H2AX. *Nat Struct Mol Biol* **17**, 299–305 (2010).
137. Gonda, D. K. & Radding, C. M. By searching processively RecA protein pairs DNA molecules that share a limited stretch of homology. *Cell* **34**, 647–654 (1983).
138. Yancey-Wrona, J. E. & Camerini-Otero, R. D. The search for DNA homology does not limit stable homologous pairing promoted by RecA protein. *Current Biology* **5**, 1149–1158 (1995).
139. Pâques, F. & Haber, J. E. Multiple pathways of recombination induced by double-strand breaks in Saccharomyces cerevisiae. *Microbiology and Molecular Biology Reviews : MMBR* **63**, 349–404 (1999).
140. Krogh, B. O. & Symington, L. S. RECOMBINATION PROTEINS IN YEAST. *Annu. Rev. Genet.* **38**, 233–271 (2004).
141. Marshall, W. F. *et al.* Interphase chromosomes undergo constrained

- diffusional motion in living cells. *Curr. Biol.* **7**, 930–939 (1997).
142. Misteli, T. & Phair, R. D. High mobility of proteins in the mammalian cell nucleus. *Nature* **404**, 604–609 (2000).
143. Heun, P. Chromosome Dynamics in the Yeast Interphase Nucleus. *Science* **294**, 2181–2186 (2001).
144. Elf, J., Li, G. W. & Xie, X. S. Probing Transcription Factor Dynamics at the Single-Molecule Level in a Living Cell. *Science* **316**, 1191–1194 (2007).
145. Lanctôt, C., Cheutin, T., Cremer, M., Cavalli, G. & Cremer, T. Dynamic genome architecture in the nuclear space: regulation of gene expression in three dimensions. *Nat Rev Genet* **8**, 104–115 (2007).
146. Misteli, T. & Soutoglou, E. The emerging role of nuclear architecture in DNA repair and genome maintenance. *Nat Rev Mol Cell Biol* **10**, 243–254 (2009).
147. Nasmyth, K. & Haering, C. H. Cohesin: its roles and mechanisms. *Annu. Rev. Genet.* **43**, 525–558 (2009).
148. Simon, P., Houston, P. & Broach, J. Directional bias during mating type switching in *Saccharomyces* is independent of chromosomal architecture. *EMBO J* **21**, 2282–2291 (2002).
149. Bystricky, K. *et al.* Regulation of Nuclear Positioning and Dynamics of the Silent Mating Type Loci by the Yeast Ku70/Ku80 Complex. *Molecular and Cellular Biology* **29**, 835–848 (2009).
150. Dekker, J., Rippe, K., Dekker, M. & Kleckner, N. Capturing chromosome conformation. *Science* **295**, 1306–1311 (2002).
151. van Steensel, B. & Dekker, J. Genomics tools for unraveling chromosome architecture. *Nat Biotechnol* **28**, 1089–1095 (2010).
152. Cremer, T. *et al.* Chromosome territories – a functional nuclear landscape. *Current Opinion in Cell Biology* **18**, 307–316 (2006).
153. Gibcus, J. H. & Dekker, J. The Hierarchy of the 3D Genome. *Molecular Cell* **49**, 773–782 (2013).
154. Cavalli, G. & Misteli, T. Functional implications of genome topology. *Nat Struct Mol Biol* **20**, 290–299 (2013).
155. Cremer, T. & Cremer, M. Chromosome territories. *Cold Spring Harb Perspect Biol* **2**, a003889 (2010).
156. Berger, A. B. *et al.* High-resolution statistical mapping reveals gene territories in live yeast. *Nature Methods* **5**, 1031–1037 (2008).
157. Dorn, J. F. *et al.* Yeast kinetochore microtubule dynamics analyzed by high-resolution three-dimensional microscopy. *Biophys. J.* **89**, 2835–2854 (2005).
158. Wong, H. *et al.* A Predictive Computational Model of the Dynamic 3D Interphase Yeast Nucleus. *Current Biology* **22**, 1881–1890 (2012).
159. Tjong, H., Gong, K., Chen, L. & Alber, F. Physical tethering and volume exclusion determine higher-order genome organization in budding yeast. *Genome Res.* **22**, 1295–1305 (2012).
160. Witten, D. M. & Noble, W. S. On the assessment of statistical significance of three-dimensional colocalization of sets of genomic elements. *Nucleic Acids Research* **40**, 3849–3855 (2012).
161. Ben-Elazar, S., Yakhini, Z. & Yanai, I. Spatial localization of co-regulated genes exceeds genomic gene clustering in the *Saccharomyces cerevisiae* genome. *Nucleic Acids Research* **41**, 2191–2201 (2013).
162. Wilson, J. H., Leung, W. Y., Bosco, G., Dieu, D. & Haber, J. E. The frequency of gene targeting in yeast depends on the number of target copies. *Proc. Natl. Acad. Sci. U.S.A.* **91**, 177–181 (1994).
163. Hoang, M. L. *et al.* Competitive repair by naturally dispersed repetitive DNA during non-allelic homologous recombination. *PLoS Genet.* **6**, e1001228

- (2010).
164. Nimonkar, A. V., Amitani, I., Baskin, R. J. & Kowalczykowski, S. C. Single Molecule Imaging of Tid1/Rdh54, a Rad54 Homolog That Translocates on Duplex DNA and Can Disrupt Joint Molecules. *Journal of Biological Chemistry* **282**, 30776–30784 (2007).
 165. Jinks-Robertson, S., Michelitch, M. & Ramcharan, S. Substrate length requirements for efficient mitotic recombination in *Saccharomyces cerevisiae*. *Molecular and Cellular Biology* **13**, 3937–3950 (1993).
 166. Ausubel, F. M. *et al.* *Current Protocols in Molecular Biology*. (Current Protocols, 1988).
 167. Sambrook, J., Fritsch, E. F. & Maniatis, T. *Molecular Cloning. Vol 2*. (Cold Spring Harbor, N.Y., Cold Spring Harbor Laboratory Press, 1989).
 168. Knop, M. *et al.* Epitope tagging of yeast genes using a PCR-based strategy: more tags and improved practical routines. *Yeast* **15**, 963–972 (1999).
 169. Janke, C. *et al.* A versatile toolbox for PCR-based tagging of yeast genes: new fluorescent proteins, more markers and promoter substitution cassettes. *Yeast* **21**, 947–962 (2004).
 170. Lisby, M., Mortensen, U. H. & Rothstein, R. Colocalization of multiple DNA double-strand breaks at a single Rad52 repair centre. *Nat. Cell Biol.* **5**, 572–577 (2003).
 171. Pâques, F. & Haber, J. E. Two pathways for removal of nonhomologous DNA ends during double-strand break repair in *Saccharomyces cerevisiae*. *Molecular and Cellular Biology* **17**, 6765–6771 (1997).
 172. Aparicio, O. *et al.* Chromatin immunoprecipitation for determining the association of proteins with specific genomic sequences in vivo. *Curr Protoc Mol Biol* **Chapter 21**, Unit 21.3 (2005).
 173. O'Geen, H., Nicolet, C. M., Blahnik, K., Green, R. & Farnham, P. J. Comparison of sample preparation methods for ChIP-chip assays. *BioTechniques* **41**, 577–580 (2006).
 174. Prestel, M., Feller, C., Straub, T., Mitlöhner, H. & Becker, P. B. The Activation Potential of MOF Is Constrained for Dosage Compensation. *Molecular Cell* **38**, 815–826 (2010).

8 Abbreviations

1D	One-dimensional	<i>MATα</i>	<i>MAT</i> locus containing α information
3D	Three-dimensional	<i>MATα</i>	<i>MAT</i> locus containing α information
Amp	Ampicilin	Min	Minute
ARS	Autonomously replicating sequences	Mito	Mitochondrion
BIR	Break-induced replication	MRX	MRX complex consisting of Rad50, Mre 11 and Xrs2
Bp	Base-pairs	Myc	Epitope derived from c-myc
BRCA2	Breast cancer tumor suppressor 2	N	Number of independent experiments
CEN	Centromere	Nat	Noursethricin
ChIP	Chromatin immunoprecipitation	<i>NatNT2</i>	Gene conferring resistance to noursethricin
ChIP-chip	ChIP analyzed by genome-wide tiling arrays	NHEJ	Non-homologous end-joining
Chr	Chromosome	Ns	Not significant
dHJ	Double-Holliday junction	ORF	Open reading frame
DNA	Deoxyribonucleic acid	P	Primer
dNTP	Desoxynucleoside triphosphate	PCR	Polymerase chain reaction
D-loop	Displaced strand loop	RPA	Replication protein A
DSB	DNA double-strand break	R	Arginine
dsDNA	Double-stranded DNA	Rad	Radiation
E	Glutamate	Raf	Raffinose
FISH	Fluorescent in situ hybridization	rDNA	DNA coding for ribosomal RNA
Fkh1	Forkhead transcription factor1	<i>RE</i>	Recombination enhancer element
G418	Geneticine disulfate	RNA	Ribonucleic acid
Gal	Galactose	RT	Room temperature
GFP	Green fluorescent protein	RT-qPCR	Real-time quantitative PCR
H2A	Histone 2 A	<i>Scel</i>	<i>Scel</i> endonuclease
H2A.X	Histone 2 A variant X	<i>Scel</i> -cs	<i>Scel</i> endonuclease DNA cleavage site
H3	Histone 3	<i>S. cerevisiae</i>	<i>Saccharomyces cerevisiae</i>
<i>HML</i>	Hidden <i>MAT</i> left, silent mating-type locus	SC media	Synthetic complete media
<i>HMR</i>	Hidden <i>MAT</i> right, silent mating-type locus	SDS	Sodium dodecylsulfate
HO	HO (homothallic switching) endonuclease	SDSA	Synthesis-dependent strand annealing
HO-cs	HO endonuclease DNA cleavage site	SEM	Standard error of the mean
<i>HphNT1</i>	Gene conferring resistance to hygromycin	SIM	SUMO-interacting motif
HR	Homologous recombination	SPB	Spindle pole body
Hr	Hour	ssDNA	Single-stranded DNA
IP	Immunoprecipitation	SUMO	Small ubiquitin-like modifier
IN	Input	TCA	Trichloroacetic acid
INO80	Inositol requiring 80	Tel	Telomere
K	Lysine	VDJ	Variable, diversity and joining genes
Kan	Kanamycin	WT	Wild-type
<i>KanMX6</i>	Gene conferring resistance to G418	γ H2A	Histone 2A phosphorylated on Serine 129 (<i>S. cerevisiae</i>) or H2A.X phosphorylated on Serine 139 in mammalian cells
Kb	Kilobase pairs	YPD	Yeast bactopectone dextrose
Log	Logarithmic		
<i>MAT</i>	Mating-type locus		

9 Figure Index

Figure 1. The core pathway of homologous recombination.	6
Figure 2. The <i>S. cerevisiae</i> mating-type system.	8
Figure 3. The recombinase Rad51 - a central protein in homologous recombination.	11
Figure 4. Regulation of homologous recombination.	13
Figure 5. Analysis of homology recognition and homology search.	16
Figure 6. DSB-distant Rad51 signals upon a single DSB cover almost the entire DSB-harboring chromosome.	21
Figure 7. Model for a correlation between Rad51 ChIP signals and homology search.	22
Figure 8. DSB-distant Rad51 signals can be detected by Rad51-directed ChIP analyzed by RT-qPCR.	23
Figure 9. The DSB-distant Rad51 signals depend on the Rad51 mediators Rad52 and Rad55/Rad57.	25
Figure 10. The DSB-distant Rad51 ChIP signals are a mating-type independent phenomenon upon a single DSB.	26
Figure 11. RPA- and Rad52-directed ChIP experiments upon induction of a single DSB.	29
Figure 12. DSB-distant Rad51 ChIP signals exceed the area of resection.	31
Figure 13. The DSB-distant Rad51 ChIP signals correlate with donor preference in the mating-type system.	34
Figure 14. The DSB-distant Rad51 ChIP signals can be detected during ongoing repair.	36
Figure 15. The DSB-distant Rad51 ChIP signals can be detected during ongoing repair.	37
Figure 16. DSB-distant Rad51 ChIP signals depend on the second DNA-binding site of Rad51.	39
Figure 17. The <i>RE</i> element can guide homology search in <i>trans</i> from <i>MAT</i> to chromosome V.	42
Figure 18. The <i>RE</i> element can guide homology search <i>in trans</i> from an HO-cleavage site to another chromosome.	43
Figure 19. Rad51 ChIP signals can be detected at and around all centromeres upon formation of a centromere-proximal DSB.	46
Figure 20. Rad51 ChIP signals around centromeres require a centromere-proximal DSB.	47
Figure 21. Homology search upon DSB induction at a telomere-proximal location.	50
Figure 22. Homology search upon DSB formation at an rDNA repeat-proximal location.	52
Figure 23. The single-strand binding protein RPA has a potential role during homology search.	54
Figure 24. The Snf2/Swi2 family motor protein Rad54 is required for efficient homology search.	56
Figure 25. Specificity of γ H2A-directed ChIP experiments.	58
Figure 26. γ H2A ChIP signals follow homology search in the mating-type system.	59
Figure 27. γ H2A ChIP signals also follow homology search on <i>MAT</i> -independent chromosomes.	60
Figure 28. The γ H2A ChIP profile follows homology search according to nuclear organization.	61

Figure 29. γ H2A ChIP signals follow homology search.	63
Figure 30. “Efficient genome-wide” versus “absence of long-range” homology search models.	67
Figure 31. Nuclear organization in <i>S. cerevisiae</i>	70
Figure 32. Facilitated 3D/1D homology search model.	75

10 Acknowledgements

I would like to thank Stefan Jentsch, my PhD supervisor, for his great support, his scientific creativity, and his sense for ideas/findings bearing major implications. Stefan, I would also like to thank you for the scientific freedom and possibilities that one has in your lab, allowing and stimulating own scientific ideas and the own scientific development. I am also very grateful for your support and understanding to finish experiments for a paper derived from my master thesis and to write a review on that topic in parallel to performing my PhD in your group. Moreover, I would like to thank you for interesting and insightful personal talks and discussions, and for the overall great time in your group!

I am also especially grateful for the excellent technical assistance from Sven. Thank you Sven for your help with numerous experiments, your work was always highly accurate and reproducible. Next to your great technical assistance, I would also like to thank you personally for our great time together in the lab!

Thank you Claudio for inspiring discussions and superb shared and continued experimental work on homology search! Same thanks to Benjamin, further continuing and supporting discussions and experiments on homology search. Thank you both for your good company and fun in the lab, which was further stimulated by Sean! The same holds true for Kenji and Dirk when I was starting my PhD, thank you both for that. Moreover, I would like to thank all other members of the Jentsch Department for insightful discussions and a great time, especially highlighting Max, Jochen, Julian, Irina, Alex, Flo, Ivan, Christian, Tim and Steven. Further thanks to my internship and bachelor students Ilker and Christoph for a nice time in the lab. Additionally, I would like to thank Max, Benjamin and Claudio for critical reading of this thesis.

Thanks also to Max and Klaus for scientific discussions, coffee breaks in the MPI cafeteria and for overall friendship.

I would also like to thank Peter Becker for continuous support during my PhD thesis, particularly for co-refereeing my PhD thesis, and for constructive criticism and fruitful discussion as part my thesis advisory committee (TAC). The same thanks to Michael Sixt, also part of my TAC, for great discussion and support. Moreover, I would like to thank Tobias Straub for having taken the time to substantially support on the establishment of ChIP-chip analysis.

Moreover, I would like to thank the Boehringer Ingelheim Fonds (BIF) for the PhD scholarship, exceptionally supporting this thesis and my personal development. Next to financial support, the BIF fellowship enabled me stunning scientific and personal discussions during Hirschegg and Lautrach seminars. Thank you Claudia, Anja and all other BIF team members! Similar thanks apply also to the IMPRS coordination office, thank you Hans-Jörg, Maxi und Ingrid for your excellent support to all IMPRS-LS PhD students!

A great and warm thanks to my family, especially to my parents who always supported me in my life. I greatly appreciate how you care for me and at the same time leave me the freedom to find my own way in life. Moreover, I would also like to thank the family of my wife Kristine, Trudi, Philip, Reiner, Ingrid and Jan, for joyful distraction and support.

Success and happiness during my PhD would have also not been possible without my wife Kristine and our son Jonas. Thank you for your love, patience, understanding, support and everything else!

11 Curriculum Vitae

Personal Data

Name	Jörg Renkawitz
Date / Place of Birth	February 15, 1983, Heidelberg, Germany
Marital status	Married, 1 son (born 12.08.2011)
Address	Max Planck Institute of Biochemistry Am Klopferspitz 18 82152, Martinsried, Germany E-Mail: renkawit@biochem.mpg.de

Academic Education

Since 12/2008	PhD studies: <i>Homology search during DNA double-strand break repair.</i> Supervisor: Prof. Dr. S. Jentsch (MPI of Biochemistry, Martinsried).
March-October 2008	Master Thesis: <i>Dynamic characterization of the cytoskeleton during dendritic cell migration.</i> Supervisor: Dr. M. Sixt (MPI of Biochemistry, Martinsried). Grade 1.0
2006-2008	Master of Science in Biochemistry, Ludwig-Maximilians University Munich. Final grade 1.09
April-July 2006	Bachelor Thesis: <i>Methods to identify new substrates of protein tyrosine phosphatase 1B - RNAi mediated gene silencing, in vitro/ in vivo 'substrate-trapping' and quantitative mass spectrometry approaches.</i> Supervisor: Dr. H. Daub (MPI of Biochemistry, Martinsried). Grade 1.0
2003-2006	Bachelor of Science in Biochemistry, Technical University Munich. Final grade 1.5
2002	High school diploma, Martin Luther Schule Marburg. Final grade 1.8

Research Internships

August-October 2007	<i>Characterization of the transcription factor Nrf2 in mouse skin epidermis.</i> Supervisor: Prof. S. Werner (ETH Zurich, Switzerland)
May-June 2007	<i>Development of a 'sleeping beauty' transposase-based transposon.</i> Supervisor: Dr. Z. Ruzsics (Max-von-Pettenkofer Institute, Munich)
February-April 2007	<i>Histidin-Biotin-Tag introduction into Rpb1 and purification of S. cerevisiae 12 subunit RNA polymerase II.</i>

Supervisor: Dr. M. Kashlev (National Cancer Institute, NIH, Frederick, USA)

August-Sept. 2005 *Protein engineering, protein purification and attempts of crystallization of the RNA polymerase I subunits A14/A43 of S. cerevisiae.*
Supervisor: Prof. P. Cramer (Gene Center, Munich)

Professional Experience and other Engagements

2009-2011 Organization of the Graduate Program/Distinguished Visitor Lecture Series of the MPI of Biochemistry (Speaker selection, invitation, coordination)

2006-2008 Actively contributing member of the „Biotechnologische Studenteninitiative (btS)“, a German nation-wide organization to build an interface between academia and industry (e.g. organization of the company contact fair “ScieCon München 2007”)

2002-2003 Community service, geriatric care center (Altenhilfezentrum Stiftung St.Jakob, Marburg)

Awards/Fellowships

MPIB Junior Research Award 2013, PhD fellowship of the Boehringer-Ingelheim-Fonds (BIF) (2009-2012), International Max Planck Research School (IMPRS) (2008-2013)

Publications

Renkawitz J., Lademann C.A., Kalocsay M. and Jentsch S. (2013). Monitoring homology search during DNA double-strand break repair in vivo. *Mol. Cell* **50**, 261-272, 2013

Renkawitz J., Schumann K., Weber M., Lämmermann T., Pflücke H., Piel M., Polleux J., Spatz J.P. and Sixt M. (2009). Adaptive force transmission in amoeboid cell migration. *Nat. Cell Biol.* **11**, 1438-1443

Lämmermann T., **Renkawitz J.**, Wu X., Hirsch K., Brakebusch C. and Sixt M. (2009). Cdc42-dependent leading edge coordination is essential for interstitial dendritic cell migration, *Blood* **113**, 5703-5710

Mertins P., Eberl C., **Renkawitz J.**, Olsen J.V., Tremblay M.L., Mann M., Ullrich A. and Daub H. (2008). Investigation of protein tyrosine phosphatase 1B function by quantitative proteomics. *Mol. Cell Proteomics* **7**, 1763-1777

Geiger S.R., Kuhn C.D., Leidig C., **Renkawitz J.** and Cramer P. (2008). Crystallization of RNA polymerase I subcomplex A14/A43 by iterative prediction, probing and removal of flexible regions. *Acta Crystallogr. Sect. F. Struct. Biol. Cryst. Commun.* **F64**, 413-418.

Reviews/Editorials

Renkawitz, J., Lademann, C.A., and Jentsch, S. Mechanisms and principles of homology search during recombination. *Nat. Rev. Mol. Cell Biol.* Commissioned review in preparation.

Renkawitz, J., Lademann, C.A., and Jentsch, S. γ H2AX spreading linked to homology search. *Cell Cycle*. Editorial feature, in press.

Renkawitz J. and Sixt M. Mechanisms of force generation and force transmission during interstitial leukocyte migration. (2010). *EMBO Rep.* **11**, 744-750